The Brain's Intrinsic Spatiotemporal Structure
and its Potential Application in Artificial Intelligence

Mehrshad Golesorkhi

Thesis submitted to the University of Ottawa
in partial fulfillment of the requirements for the
Doctorate in Philosophy in Electrical and Computer Engineering

School of Electrical Engineering and Computer Science
Faculty of Engineering
University of Ottawa

© Mehrshad Golesorkhi, Ottawa, Canada, 2021

Abstract

Neuroscience focuses largely on how the brain mediates perception and cognition. However, this leaves open the basic organization and hierarchies of the brain's neural activity by itself prior to and independent of its role in cognition. A recent model characterizes the brain's intrinsic features in terms of temporo-spatial dynamical (rather than cognitive) terms – the brain's spatiotemporal hierarchies shape what is called 'brain's intrinsicality'. The brain's intrinsicality may provide potential applications in designing artificial intelligence (AI). In this dissertation, I explore 'intrinsic neural timescales' and their spatial topography as one main building block of the brain's intrinsicality. First, I present empirical investigation of temporal hierarchy and information flux as two basic facets of brain's intrinsicality using magnetoencephalography (MEG) and functional magnetic resonance imaging (fMRI) data. That is complemented by introducing the notion of intrinsicality through intrinsic neural timescales and how they shape input processing in the brain. Then, I propose a model for input processing through intrinsic neural timescales and provide some notes on how that model can be implemented in an artificial agent. I conclude that the spatiotemporal dynamics of the brain's intrinsicality provides potential key insights for Artificial General Intelligence (AGI).

Acknowledgements

I would like to thank all people who helped me during my PhD studies for their advice, guidance, and supports. I owe sincere thankfulness to my supervisors, Professors Georg Northoff and Mustapha C. E. Yagoub, the comprehensive and proposal examiners, and the defense committee.

Last but not least, I owe to express my appreciative feeling to my family for all of their supports and motivations. They may be far away, but they are always in my thoughts.

Table of Contents

List of Figures

List of Tables

Chapter 1 Introduction

1.1 Motivation

1.1.1 Spatiotemporal dynamics: the common currency between neural and mental features

How can the brain bring forth the various mental features that characterize our experience? Recent investigations have demonstrated regions, networks, and/or frequencies involved in mental features like self [1]–[6], consciousness [7]–[18], mind wandering [19], episodic simulation [20], empathy [21], free will [22], and emotion [23]. Various mechanisms like integration [15], higher-order cognitive functions [24], predictive coding [25], non-linearity and criticality [26]–[28], operational space-time [29], [30], and global neuronal workspace [8], [31], have been put forward as underlying substrates of mental features (as well as several others not mentioned here). The main problem is to demonstrate the connection of neuronal and mental features, that is, what features in the brain's neuronal activity provide the connection to mental activity. The question of the connecting mechanism focuses more on an underlying commonly shared feature than on the differences between neuronal and mental features. Any connection of neuronal into mental features must presuppose some deeper underlying shared feature, a so-called "common currency" [32], [33].

What exactly is meant by "common currency"? Consider economic trade by way of analogy. Global trading between different countries is possible only on the basis of a shared currency, a "common currency" like the US dollar in our days. Imagine, if we could only observe the global trading without knowing that the US dollar (or any other currency, for that matter) provides the "common currency". We would then be puzzled about the sheer amount of trading between the different countries and wonder why and how they can be so closely connected and exchange so freely their goods.

The quest and assumption of a "common currency" can be conceived an empirical hypothesis about the relationship between neuronal and mental features, that is, those mechanisms that allow for neuronal activity to transform into mental features. Focusing on the brain itself and how its mechanisms transform neuronal into mental activity, the "common currency" is an explicitly empirical hypothesis that connects neuroscience to contemporary physics with especially the latter's view of time and space [34]. Presupposing a "construction view" of time and space, as in contemporary physics, Northoff et al. [32] focus on various spatiotemporal mechanisms of how the brain constructs its "inner time and space".

The spatiotemporal characterization requires a "spatiotemporal approach" to brain and mind, for which reason Northoff et al.[32] speak of "Spatiotemporal Neuroscience". Spatiotemporal Neuroscience defines the brain's neuronal activity in terms of its spatiotemporal dynamics rather than by functions (cognitive, social, sensory, motor, affective, etc.). The spatiotemporal or dynamics-based approach to the brain allows Spatiotemporal Neuroscience to link the brain's spatiotemporal dynamics to the spatiotemporal dynamics of mental features. Spatiotemporal dynamics are thus shared by both neuronal and mental features for which reason they provide their "common currency": in short, neural dynamics are mental dynamics. This entails a transformative, intrinsic, and non-causal relationship of neuronal and mental features.

In conclusion, Northoff el al. [32] proposes a novel empirical view of neuro-mental relationship. Neuronal and mental features are here conceived as derivatives and conjugate pairs of a commonly shared underlying feature, spatiotemporal dynamics, which provides their "common currency". Importantly, such definition aligns neuroscience with contemporary physics as hallmarked by its construction view of time and space. Such alignment with physics, in turn, opens novel doors and methodological tools to investigate the brain in neuroscience. Picking up these threads, the main focus in the present work is on the brain's intrinsic temporo-spatial organization, i.e. brain's intrinsicality. Specifically, I am raising the question how the brain itself constructs its own "inner time and space" [35], that is, its dynamics and topography. This, as I will point out later, carries major implications for Artificial Intelligence as the brain's "inner time and space", that is its intrinsically, may show promising applications in designing artificial agents. My focus in this thesis is on the brain's spatial and temporal intrinsicality which I consider as stepping stone for implementing and designing artificial agents in the future.

1.1.2 Brain-based Artificial Intelligence

The development of AI agents with near-human or super-human performance on some tasks has so far been driven by the paradigms of reinforcement learning [36], [37] and deep learning [38]. Even models of an artificial self; i.e., self-consciousness, have been proposed and implemented by, for instance, Prescott [39], [40] and Tani [41].

Prescott proposes a computational architecture, whereby different selves like ecological, agential, extended, interpersonal, conceptual and private self are associated with different operating modules [40]. Each module in his artificial agent is supposed to be in charge of each of these different selves, including their respective abilities and capacities. Yet another architecture is the combination of top-down (providing the agent's inner input) and bottom-up (providing the agent's outer input) layers that Tani uses in his compelling model of an artificial agent [41]. However, despite all this progress, we are still lacking the kind of artificial agents that augment human selves in their decision making, as in moral dilemmas, or in their alignment to – and prediction of – catastrophic events in the environment, or in psychotherapeutic practice.

It is assumed the agent's relation and alignment to the environment is crucial. The term environment is here meant to include cultural, social, natural, ecological, and geological/geographic contexts (as well as various others). Alignment signifying adaptation to – and shaping by – the environment then includes the long-term experience-dependence of the agent's inner structure on her respective cultural and evolutionary context [42]–[44].

Such environmental shaping remains to be modelled as it is the case in the brain where, for instance, early traumatic life events strongly shape the brain's organization in adulthood. Therefore, recent calls have been made from both within [36] and without [45] AI, to improve the artificial agent's interface with their respective environmental contexts. A dynamic and continuously adaptative interface with the environment (including its social, cultural, ecological, geographical, evolutionary, and other features) is missing in AI at its current state.

Thus, improving the agent's adaptive interface with the environment can be one main focus of AI. That would not only allow for developing artificial agents that could augment the capacities of human agents but would also be 'trustworthy'[38]. In other words, it can be claimed that, despite the brain's cognitive shortcomings as exposed by recent AI [38], we can nevertheless learn important lessons from it. Specifically, we can take inspiration from the principles by which the brain aligns itself to its continuously changing both social and ecological environments. In particular, recent neuroscience has brought to the fore two such principles - free energy principle [46] and spatiotemporal dynamics [35]. Future AI methodologies may benefit from modelling its artificial agents along the lines of those principles.

The key observations about the brain that drive this suggestion are as follows: The brain stands in a temporally continuous interface with the environment, described in terms of the free energy principle (FEP). At the core of the FEP is Variational Free Energy, which underwrites spatiotemporal dynamics of two systems: in this case the agent and its environment. Crucially, the brain's spatiotemporal dynamics is organized in hierarchical manner, that is, according to growing time- and space- scales, which are adaptively determined and finely nested. Finally, this spatiotemporal hierarchy has been associated with neuro-mental connection for both self and consciousness [32], [47]–[50].

Taken together, conjoining the hierarchical dynamics of FEP and spatiotemporal dynamics in artificial agents will allow novel, expressive and explainable ways for artificial agents to adapt to different environmental contexts – contexts that are constituted by human selves and non-human factors. This will prove crucial in the proposed augmentation which could cover diagnosis and prognosis in mental health, economic forecasting, environmental disaster prediction – and other spheres that rest on the central role of the mind and its moral decision making.

1.1.3 Spatial Intrinsicality: core-periphery structure

Does the brain exhibit an intrinsic spatial organization or topography as it is put in neuroscience? This means that such spatial intrinsicality should be shared by all subjects independent of their state like rest or task. Moreover, it means that such spatial intrinsicality determines the brain as brain. Different models, relying on distinct principles, have been suggested for the cortical organization [51]. Being based strongly on anatomical grounds, medial-lateral and especially rostral-caudal models as well as modular models [39] have been proposed for the human brain [52]. The rostral-caudal model suggests an anatomical gradient from more unimodal subcortical and sensory regions to more heteromodal prefrontal regions, which can be distinguished by their micro- and macro-structural/architectonic features [27], [28], [52]. However, more recent, functionally oriented, investigations question the primacy of such rostral-caudal organization.

Margulies et al.[52] (see also refs. [53], [54]) suggest rather an onion-like model of the human brain. Such onion-like model is featured by different, i.e., inner, middle, and outer layers. Inner layers mediate transmodal functions like self [1], episodic simulation [20] and mind-wandering [19], which indicate the default-mode network (DMN) that is situated at the core in the brain's overall spatial organization [54]. In contrast, more modal functions like motor and various sensory modalities implicate sensorimotor cortices that represent the outer layers; e.g., the periphery [55]. The onion-like model entails the distinction between a core, e.g., the most inner layer, and a periphery, i.e., the outer layers. This

amounts to what has been described as 'core-periphery model' in social science [56] and the centripetal hierarchies proposed by Mesulam in neurobiology [57].

A core-periphery architecture can be characterized by a core that shares nodes with strong interconnections among each other. These core-core connections are much stronger than the connections of the core to the periphery; i.e., core-periphery connections, and also the connections among the nodes within the periphery itself, i.e., periphery-periphery connections [56]. Such a core-periphery model has been applied to the brain where it has recently garnered much support; especially on temporal and, more generally, dynamic grounds of the brain's resting state and task-evoked activity [27], [28], [53], [58], [59] (see also related spatial models of brain like "rich club" [60] and "dynamic core" [61]).

However, these studies leave open how the brain's spatial organization is linked to its temporal dynamic. Does the brain's spatial topography converge with its temporal dynamical organization? That convergence, if present, will be key in my thesis as I consider it instrumental in designing artificial agents as we are here confronted with the question of linking their inner spatial organization with their temporal scales. For that reason, we now shift to the brain's intrinsic temporality.

1.1.4 Temporal Intrinsicality: neural time scales and temporal hierarchy

How about the brain's intrinsic features on the temporal side? This leads us to the temporal organization of the brain. One of the leading authors here is Hasson who conducted a series of fMRI studies of the encoding of external stimulus sequences (music, movies, etc.), where stimuli (words, sentences, paragraphs, etc.) had different durations [62]–[64]. Using inter-subjective correlation of task-evoked fMRI data, they associated stimulus duration with responses in different regions. This enabled them to infer that the different regions exhibit different temporal integration for encoding and receiving external stimuli –cast in terms of "temporal receptive windows" (TRW) [63], [65].

Specifically, they observed that words (1s -/+ 0.5s) elicited activation in primary sensory regions like visual (when presented visually) or auditory (when presented auditorily) cortex. Sentences, lasting longer, (8 +/- 3s) were associated with higher regions like medial temporal and parietal cortex, while whole paragraphs lasting about 38 +/- 17s) were associated with fluctuations in the DMN [62], [64]. Together, these data show that different regions exhibit different durations in their TRW's, which map onto a temporal hierarchy of the brain's functional anatomy.

These data show that the brain's timescales are directly related to the timescales of stimulus bound responses, thus entailing some form of temporal correspondence of neuronal dynamics and the sensorium. Most interestingly, a more or less analogous hierarchy of timescales can be observed not only during evoked activity but also in the brain's spontaneous or intrinsic activity [27], [28], [66]–[68]. Measured by the correlation between different time points of neural activity, i.e., the autocorrelation window (ACW), these studies demonstrate diverse correlation lengths, (i.e., ACW), in different regions, in the resting state.

The different timescales and implicit temporal hierarchy operate across the functional anatomy described above. The regions in the core show rather long ACW and thus more extended intrinsic neuronal timescales than the periphery, where the ACW is relatively shorter. Specifically, Gollo and colleagues [27] show that core regions like DMN and the insula evince predominantly slow timescales, with stronger power in infra-slow (0.01 to 0.1Hz) and slower (0.1 to 1Hz) and relatively weaker power in faster frequencies (1-180Hz) (see also [47], [48], [69], [70] for supportive evidence on the regional-systemic level).

In contrast to the DMN as core, sensorimotor regions in the outer periphery exhibit relatively less power in the infra-slow and slow frequency ranges – and relatively more power in the faster ranges (1-180Hz) [47], [48], [69], [70]. Together, this amounts to an intricate temporal or dynamic hierarchy; i.e., a chronoarchitecture within which each region – as featured by its "natural frequency" or "intrinsic neural time scale" [28], [64].

How is the brain's intrinsic temporal hierarchy related to its intrinsic spatial topography? We currently do not know. The convergence of temporal and spatial hierarchies in the brain is the core of my thesis. Both of my major empirical works are targeted towards showing the convergence of spatial and temporal hierarchies in the brain; this will serve as stepping stone for designing analogous spatiotemporal hierarchical convergence in artificial agents which these currently lack.

1.2 Questions

The aim of this research is to investigate the spatiotemporal dynamics of the brain's spontaneous activity and how it is affected in the presence of stimuli in order to address the intrinsic properties of the brain. That serves as basis for a future artificial agent – what is intrinsic to the brain, that is, its spatiotemporal dynamics, may need to be implemented in artificial agents as their intrinsic design to make them more adaptive, better performing and extending their capacities. The focus in this PhD is therefore on the intrinsic spatiotemporal dynamics of the brain.

Three major facets of spatiotemporal dynamics are being addressed in this work. First, we investigate the topography of intrinsic neural timescales and how stimuli may affect them using empirical data, machine learning, and simulation. In the second step, considering the importance of infraslow frequencies, we investigate the information flux of the intrinsic neural timescales in the infraslow frequencies using human fMRI data, and algorithms from signal processing and computer science. Lastly, input processing is explored through the intrinsic neural timescales as the building blocks of the brain's intrinsicality. Based on that previous literature, we explore different aspects of input processing and propose a model for its underlying mechanism is the brain. Later, that model is extended to cover artificial agents.

1.3 Main Contributions

This dissertation has three main contributions. First, we empirically showed that brain's intrinsic neural timescales has core-periphery hierarchy (see [71] for other definitions of hierarchy) with an increase the length of timescales from periphery to core. We also showed the consistency of this hierarchy between resting and task states which, after

controlling for resting state, suggests carry-over effect from resting to task state. Moreover, using machine learning we suggested that longer timescales, compared to shorter ones, are better at inter-individual differentiation and are also better at predicting whether a region belongs to core or periphery.

Considering the importance of longer timescales (slower frequencies), secondly, the network-specificity (along the lower- and higher-order networks) and task-specificity of brain's complexity was empirically shown in slower frequencies. This was accompanied by the median frequency (MF) to get a sense of the speed of the brain signal which revelead a unique relationship between complexity and MF suggesting that the change in the complexity of a region is partially mediated by MF of that region during resting state.

The third contribution of this thesis is two-fold. First, we investigated input processing with respect to intrinsic neural timescales and discussed input sharing and input matching (with the environment) as two major aspects of input processing. Second, we discussed temporal segregation, temporal integration and temporal sampling as the important mechanisms involved in input processing through intrinsic neural timescales. Finally, we propose the potential applications of this approach for Artificial Intelligence.

1.4 Outline of the thesis

This thesis is presented in form of three articles. In chapter two (first article), we empirically investigate the temporal hierarchy of intrinsic neural timescales including their convergence with the brain's spatial intrinsicality during resting and different task states using human data, machine learning and simulation. In chapter three (second article), we take a step toward infraslow information processing in the brain as a manifestation of its spatiotemporal intrinsicality. This is achieved empirically via using human fMRI data and simulation. Chapter 4 (third article) opens with a review of the literature on the intrinsicality in the brain with intrinsic neural timescales. Then, we explore different facets of intrinsic neural timescales and propose a model for input processing in the brain achieved through intrinsicality. Finally, we close chapter 4 by suggesting the different applications of this model specially in building the next generation of artificial general intelligence. We close the dissertation in chapter 5 with a conclusion and suggestions for future works.

Chapter 2 Temporal hierarchy of intrinsic neural timescales converges with spatial core-periphery organization

2.1 Abstract

The human cortex exhibits intrinsic neural timescales that shape a temporal hierarchy. Whether this temporal hierarchy follows the spatial hierarchy of its topography namely the core-periphery organization remains an open issue. Using Magnetoencephalography data, we investigate intrinsic neural timescales during rest and task states; we measure the autocorrelation window in short (ACW-50) and, introducing a novel variant, long (ACW-0) windows. We demonstrate longer ACW-50 and ACW-0 in networks located at the core compared to those at the periphery with rest and task states showing a high ACW correlation. Calculating rest-task differences, i.e., subtracting the shared core-periphery organization, reveals task-specific ACW changes in distinct networks. Finally, employing kernel density estimation, machine learning, and simulation, we demonstrate that ACW-0 exhibits better prediction in classifying a region's time window as core or periphery. Overall, our findings provide fundamental insight into how the human cortex's temporal hierarchy converges with its spatial core-periphery hierarchy.

2.2 Introduction

The brain shows a complex temporal structure during both resting and task states. Recent findings demonstrate intrinsic neural timescales in resting state with shorter timescales in unimodal sensory regions and longer ones in transmodal regions of the default-mode (DMN) and fronto-parietal (FPN) networks [72]–[75]. At the same time, there is increasing evidence that task states structure information in temporal terms as described by "temporal receptive fields" [76] or "temporal receptive windows" [63]. Specifically, short segments like single words are processed mainly in unimodal lower-order sensory regions like the visual or auditory cortex while longer segments, integrating different stimuli, are processed in higher-order regions like DMN and FPN [63], [64], [77]–[80]. How such temporal structuring during task states is related to the resting state's intrinsic neural timescales remains yet unclear, though. One goal of our paper is, therefore, to investigate whether the resting state's intrinsic neural timescales are preserved and/or changed during the transition from rest to task.

Analogous to the temporal hierarchy of intrinsic neural timescales, the hierarchical organization has also been observed on the spatial side, that is, its topographic organization. Converging evidence shows micro- and macro-scale hierarchical organization in the human cortex following what has been described as 'core-periphery' [27], [28], [52], [54], [81]–[84]. A core-periphery (CP) architecture [56] can be characterized by a core that includes nodes with strong functional connectivity (FC) among each other (i.e. core-core connections or 'rich club' [58]–[61]). These core-core connections can be observed among regions included in the default-mode (DMN), fronto-parietal (FPC), and cingulo opercular networks [27], [28], [52], [54], [81], [84]. These networks constituting the core have been distinguished from those at the opposite end of the core-periphery gradient, that is, sensory networks like visual, auditory, and somatomotor networks [27], [28], [52], [54], [81], [84]. The spatial hierarchy of CP has been mainly observed in functional magnetic resonance

imaging (fMRI) measuring infraslow frequency ranges (0.01 to 0.1Hz). This leaves open whether CP organization is also present in the faster frequency (1.3 - 50Hz) as measured in MEG/EEG where, so far, an anterior-posterior hierarchy has been demonstrated [85]. Therefore, our goal was to probe whether the core-periphery hierarchy is also present in the faster frequency range (1.3 - 50Hz) while controlling for anterior-posterior hierarchy.

How are temporal and spatial hierarchies related to each other? Recent studies demonstrate that the intrinsic neural timescales within specific regions strongly correlate with their FC [72], [74]. Given this relationship between FC and ACW, the FC-based spatial-topographic core-periphery organization may converge with the temporal hierarchy of the intrinsic neural timescales during both rest and task states. This touches upon the more general question about the relationship and potential convergence of temporal and spatial hierarchies in the brain, and whether such convergence is carried over from rest to task states. Investigating the convergence of spatial and temporal hierarchies of the brain is the overarching aim of our study. Insight into such possible convergent temporo-spatial core-periphery hierarchy is of importance to understand the brain's organization which, in turn, is important for mental features like self and consciousness as they have neurally been characterized by temporo-spatial dynamics [32], [35], [47], [48], [50], [70], [86], [87].

2.2.1 Aims and hypotheses

The general aim of our study is to probe whether the temporal hierarchy of intrinsic neural timescales during both resting and task states follows the spatial topography of the core-periphery (CP) hierarchy (see Figure 2.1 for a general overview). To this end, we used MEG rest and task data from the Human Connectome Project's (HCP) dataset. To operationalize core-periphery organization, we used three different definitions of CP including Schaeffer/Margulies (SCP) [52], Ji/Ito (JCP) [72], and restricted Ji/Ito (RCP). We determined the autocorrelation window (see below) of the regions/networks in the three different CP definitions to probe whether the hierarchical distribution of intrinsic neural timescales follows the spatial core-periphery organization. Data analyses including rest-task correlation and rest-task differences were complemented by kernel density estimation, machine learning, and simulation for a more precise differentiation of core and periphery regions on temporal grounds, i.e., their intrinsic neural timescales.

Intrinsic neural timescales can be measured by the autocorrelation window (ACW), which measures repeating patterns in a signal and enables testing for correlation in neural activity patterns at different points in time [75]. The ACW has been determined at the cellular level [75], [76], [88] as well as systems-level (using fMRI [72], [74] and EEG/MEG [48], [64], [89]). Therefore, we here use ACW to measure the spatial CP organization in the faster frequency range of MEG. To account for different window sizes, we, in addition to the standard measurement of autocorrelation decline at 50% (ACW-50), also used a longer window size where ACW was defined as the length of time at the first instance where the Pearson correlation reaches zero (ACW-0) (See methods for details and differences between the two measures). Employing short (ACW-50) and long (ACW-0) window sizes enabled us to probe a more fine-grained temporal organization, that is, whether core and periphery regions can be differentiated by differences in the shorter and longer temporal windows within the faster frequency range of MEG (1.3-50Hz).

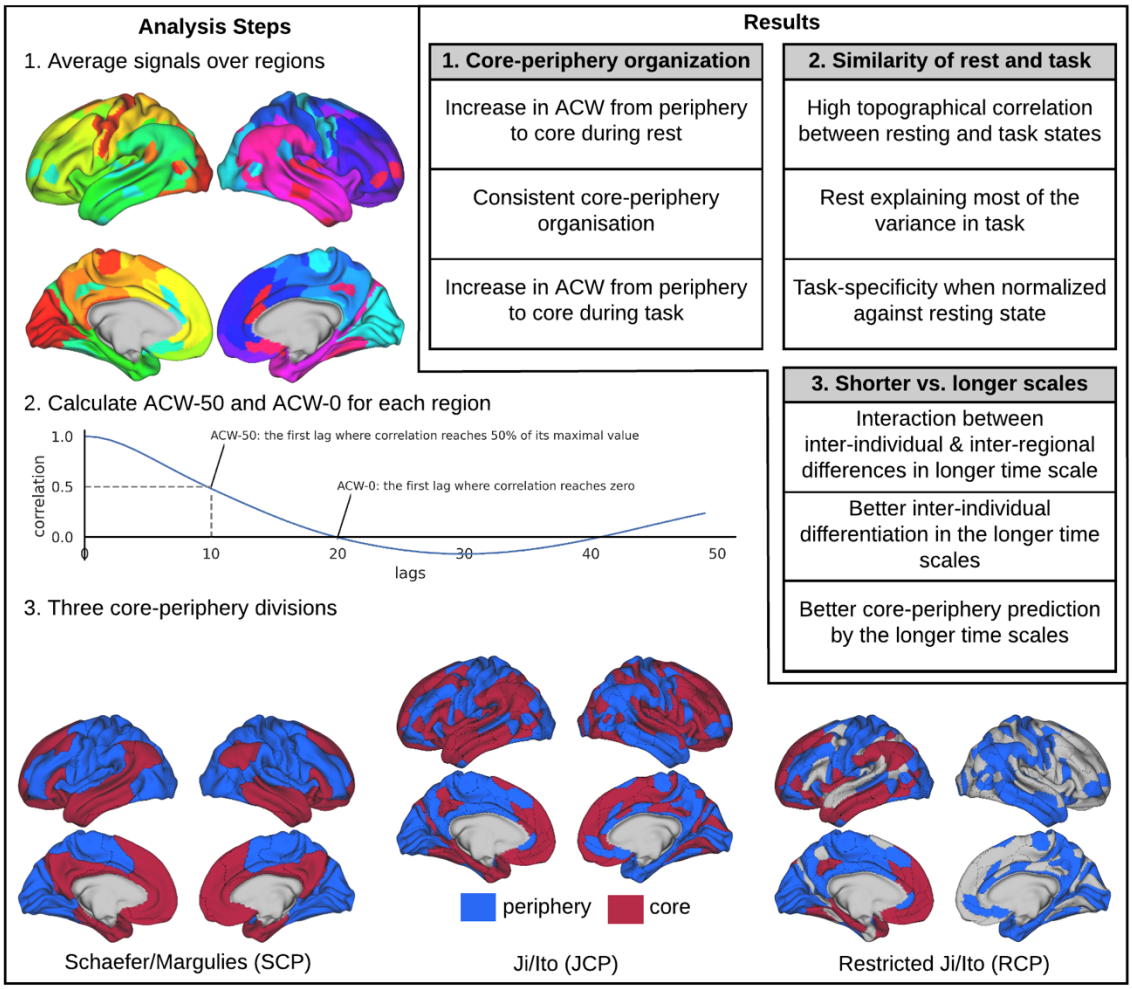

Figure 2.1: Schema of the paper. Represents the primary analysis conducted in this study. First, the time-series were averaged over cortical brain regions (1). Then, ACF was calculated for each region and from that ACW-50 and ACW-0 were extracted (2). Three different core-periphery divisions were defined based on the Schaefer and Ji templates (3). In Schaefer/Margulies (SCP) core-periphery division, cortical regions/networks are defined based on the Schaefer template 40 and then divided into core or periphery based on the first principal gradient introduced in ref. 14. The regions/networks in Ji/Ito (JCP) are from Ji template 41 and each region is labelled core or periphery based on unimodal/transmodal definition in ref. 1. The periphery definition in Restricted Ji/Ito (RCP) is similar to JCP, but only the regions in cingulo opercular, frontoparietal and default-mode networks are assigned to the core division, and the rest of the regions are ignored.

Our first specific aim focuses on the resting state as to investigate whether the temporal hierarchy of intrinsic neural timescales follows the spatial hierarchy of core-periphery organization. fMRI (0.01 to 0.1Hz) resting state studies of intrinsic neural timescales demonstrate short ACW in unimodal sensory regions and long ACW in transmodal regions [72]–[74] which suggests a CP organization. Extending these results to the faster frequency range (1.3-50Hz), we hypothesize that the topographical distribution of the resting state's intrinsic neural timescales, i.e., ACW-50 and ACW-0, converges with the spatial CP organization – this would imply a truly temporo-spatial core-periphery hierarchy.

The second specific aim is to investigate the intrinsic neural timescales during different task states including their relation to resting state, i.e., rest-task correlation and rest-task differences. This is based on the findings, that rest and task data by themselves show strong hierarchical similarities in intrinsic neural timescales [63], [64], [72], [74], [80] as well as previous data showing that the core-periphery organization holds during task states [53], [82]. Together, these findings suggest carry-over of temporal and spatial hierarchies from rest to task states which we measure by rest-task correlation

and rest-task differences. Taken together, we hypothesize that the convergence of temporal hierarchy with the spatial core-periphery organization also holds during task states as being carried over from rest to task; we, therefore, hypothesize a high correlation of the resting state's spatial topography of the intrinsic neural timescales with the one during task states.

The third specific aim consists of probing whether core and periphery regions differ from each other by the length of the windows of their intrinsic neural timescales as measured by the different window sizes of ACW-50 (shorter window) and ACW-0 (longer window). This is based on the observation that, compared to the periphery, core regions/networks exhibit stronger slow frequencies [69], [90] which leads to longer time windows [64], [91] as measured with especially the ACW-0 (rather than the ACW-50). We, therefore, hypothesized that the ACW-0, probing longer time windows, allows differentiating core and periphery regions better than the shorter time window of ACW-50. To support the empirical data, we also use machine learning and simulation to verify this hypothesis that the longer time window of ACW-0 allows for more precise characterization of core region relative to periphery regions when compared to the shorter ACW-50.

2.3 Methods

Experimental model and subject details. The analyses involved magnetoencephalography (MEG) data of 89 subjects from the Human Connectome Project (HCP) WU-Minn HCP 1200 subjects data release [92]. Resting state MEG data were acquired in runs of approximately 6 minutes. During the scan, the subjects were instructed to relax with eyes open and maintain fixation on a red crosshair. ECG and EOG recordings were also performed. Following the completion of resting state MEG, subjects were asked to complete three tasks of language processing (story vs. math, StoryM), motor (Motort) and working memory (Wrkmem). Task MEG data were acquired with the same parameters as the rest. Each task was approximately 7, 14 and 10 minutes for StoryM, Motort and Wrkmem, respectively. The sampling frequency was 2034.5 Hz.

Task paradigms. The tasks were all block-design paradigms. In the working memory task, participants were instructed to retain images in their visual working memory and compare them with subsequently presented images. The language processing task consisted of 7 blocks of a story task interleaved with 15 blocks of a math task. The story blocks presented participants with brief auditory stories. Motor processing was assessed using a task in which participants were presented with visual cues instructing the movement of either the right hand, left hand, right foot, or left foot. The paradigm of each task is extensively discussed in the WU-Minn HCP 1200 Subjects data release manual.

Preprocessing. The HCP released preprocessed data. It included the following steps: removal of artifacts, bad channels, and bad segments based on HCP quality assurance standards [93], down-sample to 508.62 Hz, bandpass (1.3–150 Hz) and notch (59–61 Hz, 119–121 Hz) filtering, and removal of non-brain components through independent component analysis (ICA).

Source reconstruction was conducted similar to a recent article by Demirtaş et al.[94], which used the same HCP data. Briefly, reconstruction was done for 8004 vertices (8k space) on the cortical surface using Fieldtrip and software provided by HCP. First, we applied a low-pass filter (50 Hz) on the sensor data, which was projected on to source space by synthetic aperture magnetometry. The details of the projection are provided in Demirtaş et al.[94]. After source reconstruction, time courses were parcellated using two well-known templates provided by Schaefer et al. [95] (Schaefer) and Ji et al. [96] (Ji). The Schaefer and Ji templates consist of 200 and 360 regions cortical areas, respectively. The regions Schaefer template were divided into 7 networks including Visual, Somatomotor, Dorsal Attention, Salience, Limbic, FPC (frontoparietal), and DMN (default-mode). Moreover, the Ji template consisted of 12 networks of Visual1, Visual2, Auditory, Somatomotor, Dorsal Attention, Posterior Multimodal, Ventral Multimodal, Orbito Affective, Language, Cingulo Opercular, FPC, and DMN. The templates were resampled to 8K space using resampling tools available in the HCP workbench software. Finally, the time courses were averaged over runs resulting in four conditions of Rest (resting state MEG), StoryM, Motort, and Wrkmem (task states MEG).

Calculation of the metrics. In the next step, autocorrelation (ACF) of the regions' time courses were calculated within the statsmodel library [97] using the fast Fourier transform algorithm. From that, two ACW values were extracted per autocorrelation function: the first lag (in milliseconds) where the autocorrelation decays to 50% of its maximum (ACW-50) and the first instance where the autocorrelation reaches zero (ACW-0).

Core-periphery division. To analyze the core-periphery (CP) hypothesis, the regional data was divided into two categories of periphery and core base on the network they belonged to. Three different core-periphery divisions were defined. 1) Core-periphery based on the Schaefer template and the principal gradient in the Margulies et al. article[52] (Schaefer/Margulies or SCP) in which the regions in the Visual, Somatomotor, Dorsal Attention and Salience networks were labelled as periphery and the regions in the Limbic, FPC, and DMN networks as the core. 2) Core-periphery based on the Ji template and the unimodal-transmodal definition in Ito et al.[72] (Ji/Ito or JCP) in which periphery is defined as the regions in Visual1, Visual2, Auditory, and Somatomotor networks and core as the regions in Dorsal Attention, Posterior Multimodal, Ventral Multimodal, Orbito Affective, Language, Cingulo Opercular, FPC, and DMN. 3) Restricted core-periphery based on the Ji template and a restricted version of core from JCP definition (RCP) in which the periphery is similar to JCP, but the core is defined as only the regions in Cingulo Opercular, FPC, and DMN. This definition of CP ignores the rest of the regions.

Anterior-posterior regression. The core-periphery organization of ACW was validated by removing the probable effect of the anterior-posterior organization from both ACW-50 and ACW-0. From the HCP released data, the averaged T_1-weighted structural MRI was used to extract the y-coordinate of each region defined in both Schaefer and Ji templates. The ACW values for all regions and their corresponding y-coordinates were fed into a linear regression model as

dependent and independent variables, respectively. The residual of the model was used in the CP analysis as the residual ACW.

Rest-task similarity. The similarity between resting and task states was addressed using spatial correlation, linear regression and regional correlation. The spatial correlation was calculated as a single Pearson correlation coefficient between resting and a task condition (e.g. Rest vs. StoryM) over brain regions after averaging over subjects (thus creating a single brain per condition, illustrated in the box of Figure 2.4a). The spatial similarity was further investigated using linear regression. The regional ACW values were averaged over subjects. Then, task state ACW was modelled as a function of resting state for each task condition. The regional correlation was used to measure the regional similarity between resting and task states. This correlation was calculated for each region across subjects between a pair of conditions (illustrated in the box of Figure 2.4b).

Rest-task difference. The difference between rest and task state was calculated as a percentage of change per region per subject. Each region's rest and task (e.g. StoryM) values were put in the $\frac{REST - TASK}{REST} \times 100$ formula to both measures the change from the rest to the task and normalize against the rest at the same time. The percentage of change was averaged across subjects and used in the analysis of the core-periphery organization.

Density estimation. To observe the relationship between ACW-50 and ACW-0, we estimated the probability distribution of the data, by removing all the labels (e.g. region and network), by averaging over regions, and by averaging over subjects. Removing all the labels means that for each scale (whether 50 or 0) all the data from all tasks, regions, and subjects were put together and fed to the estimation algorithm. Estimation was performed using the statsmodel's kernel density estimator (KDEUnivariate) using the Gaussian kernel and expectation-maximization algorithm.

Inter-individual effects. To investigate the impact of inter-individual differences on ACW scales, we used logistic regression. A binary classification using logistic regression was designed. First, all ACW values were averaged over regions. Then, each subject was labelled either 'high variability' and 'low variability' (actual labels) based on their resting state ACW value. High variability refers to those subjects whose averaged ACW value (averaged over regions) is above the median of ACW values. Logistic regression was incorporated to determine the label for each subject during each task state. Then the predicted labels were compared to actual ones. The area under the Receiver Operating Characteristic (ROC) curve was computed based on the predicted and actual labels. ROC is a well-known metric for diagnostic test evaluation. In a ROC curve, the true positive rate is plotted as a function of the false positive rate for different cut-off points of a parameter (ACW-50 or ACW-0). The area under the ROC curve (AUROC) tells how much the model is capable of distinguishing between two diagnostic groups (low variability subjects compared to high variability ones). The higher the area under the curve, the better the model at correctly predicting the true label.

Core-periphery Classification and feature selection. To investigate which ACW scale is better at discriminating core from periphery regions, a 2-class classification problem was used with the logistic function as the classifier. Each region's signal was labelled either core (class 1) or periphery (class 2). All the other labels were removed from the data (i.e. condition, subject, network, and region). For each region, the ACW values were used as features. Thus, each sample in the model had a 1-D feature vector containing either ACW-50 or ACW-0 value and a label (whether core or periphery). To increase the reliability of the results, we used the k-fold cross-validation method with 20 folds. Three different models were created. Model 1 used both ACW values as features (each sample had two features), Model 2 used only ACW-50 and the third model used only ACW-0. The training and testing were conducted using the K-fold cross-validation algorithm with 20 folds. Accuracy, precision, recall, and the area under the AUC curve was calculated as efficiency metrics.

All of the classification steps were implemented using the scikit-learn library of Python programming language. For validation purposes, the same procedure was reused with a support vector machine (SVM) classifier using the radial basis function (RBF) kernel. Furthermore, mutual information [98] was used as a univariate feature selection method to determine which of the two scales is better if it was required to choose between the two. Mutual information is a data-driven method capable of capturing any kind of statistical dependency between the target class variable and the feature. It is equal to zero if the two are independent and the more they are dependent the more mutual information approaches 1. For that, we used the" SelectKBest" function with the "mutual_info_classif" scoring function from the scikit-learn library.

Simulated Signals. The relationship between ACW-50 and ACW-0 was investigated using simulation analysis. 20000 pseudo-aleatory signals within four different categories (5000 each) were simulated. The autocorrelation function of each signal was calculated and from that ACW scales were extracted. The categories included (I) pink noise, (II) sine wave, and linear combinations of (III) pink noise and sine wave, and (IV) pink noise, white noise and sine wave. Uniformly distributed random weights were used for the linear combinations and the frequency of the sine waves. The frequency range and the sampling rate was fixed to be equal to our real data. Pink noise was chosen to model the scale-free behaviour, white noise for pure randomness and sine wave for oscillation. For each category two density functions were calculated (one for each ACW scale) and compared to the density functions of our real data.

Statistics and Reproducibility. All statistical analyses were performed in the statsmodel library [97] and R v.3.6 and all p-values were corrected for multiple comparisons using the FDR correction method. Student's t-test, One- and two-way analysis of variance (ANOVA) were used to determine the difference in ACW during resting and task states. For significant results, post-hoc analysis using Tukey's HSD method was conducted to show the within factor differences. The steps for each analysis are described in their designated section both in results and method.

Software. All steps of the data processing were performed with in-house scripts written in Python programming language using NumPy, SciPy, cifti, joblib, matplotlib, and seaborn libraries. The source code and the figures are freely available at www.georgnorthoff.com/codes/. For brain map visualization purposes, wb_view (part of Connectome Workbench software, https://www.humanconnectome.org/software/connectome-workbench) was used.

2.4 Results

In this paper, our main aim was to investigate whether the temporal hierarchy of intrinsic neural timescales of the faster frequency (1-50Hz) of MEG conform to core-periphery (CP) architecture and how they'll be affected in the task state. Preprocessed MEG data of 89 subjects from the Human Connectome Project (HCP) were low-pass filtered at 50 Hz (thus the frequency range was 1.3-50Hz). One resting state (Rest, 6 minutes) and three task conditions of language processing (StoryM, 7 min), motor (Motort, 14 min), and working memory (Wrkmem, 10 min) were recorded from each subject. Sensor signals were projected onto source space by synthetic aperture magnetometry method and then parcellated using two well-known templates provided by Schaefer et al. [95] and Ji et al. [96]. In the first parcellation (Schaefer) the surface-based data were parcellated into 200 regions (7 networks: Visual, Somatomotor, Dorsal Attention, Salience, Limbic, FPC and DMN) and 360 regions in the second (Ji) parcellation (12 networks: Visual1, Visual2, Auditory, Somatomotor, Dorsal Attention, Posterior Multimodal, Ventral Multimodal, Orbito Affective, Language, Cingulo Opercular, FPC and DMN).

Three different core-periphery divisions were defined in this work. 1) Schaefer/Margulies core-periphery (SCP): the regions from the Schaefer template were divided into core and periphery based on the principal gradient introduced in ref. [52] in which regions in the Limbic, FPC and DMN networks were put into the core category and the others in the periphery one. 2) Ji/Ito core-periphery (JCP): the regions from the Ji template were used for this CP definition. They were labelled core or periphery based on the unimodal/transmodal definition of ref. [72] in which regions in Visual1, Visual2, Auditory, and Somatomotor were assigned to the periphery, and the rest of the brain to the core. 3) Restricted Ji/Ito core-periphery (RCP) which was similar to JCP, but with a more restricted core definition. Only the regions of Cingulo Opercular, FPC and DMN networks were put into the core of RCP and the rest of the regions (not in either periphery or core) were ignored. The primary analysis steps are illustrated in Figure 2.1 and the findings are presented in the box of the same figure.

2.4.1 ACW during resting state

In the first analysis, we calculated ACW values for each cortical region in the resting state data. For each region, two ACW scales were calculated, i.e. ACW-50 and ACW-0, as the first lags where autocorrelation function (ACF) reaches half of its maximum value, and zero, respectively. Next, the ACW values were averaged over subjects and were assigned to either core or periphery categories. All three CP divisions (Figure 2.2a for SCP, b for JCP and c for RCP) show an increase in both ACW scales from the periphery to the core. The difference between core and periphery was statistically tested using student's t-test (with Cohen's d for the effect size) which showed significant differences ($p < 0.001$) between the two in SCP (ACW-50: $t = -5.25, d = -0.77$, ACW-0: $t = -5.42, d = -0.78$), JCP (ACW-50: $t =$

$-5.72, d = -0.66$, ACW-0: $t = -11.67, d = -1.33$) and RCP (ACW-50: $t = -6.12, d = -0.75$, ACW-0: $t = -13.58, d = -1.63$).

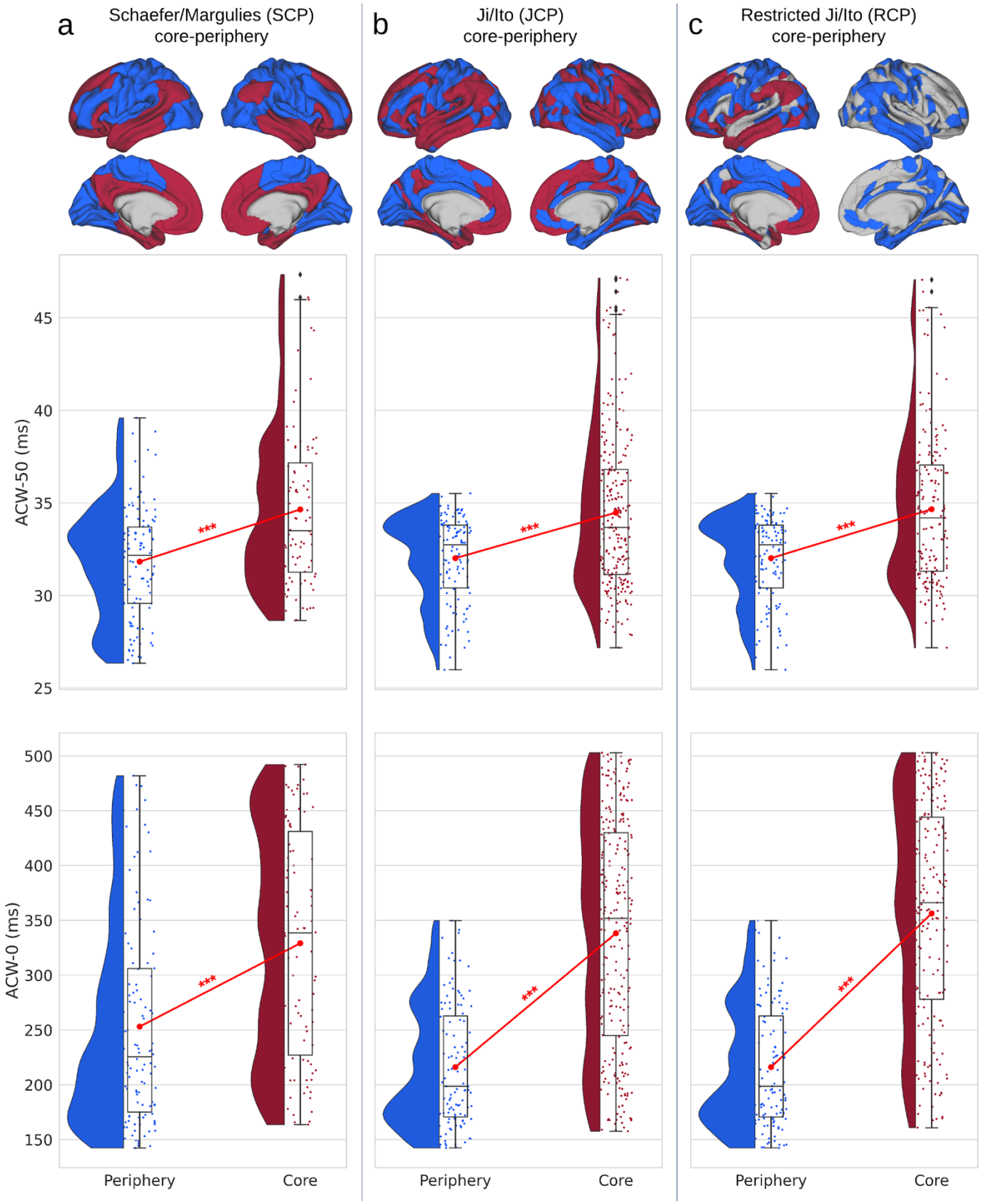

Figure 2.2: Autocorrelation window (ACW) during resting state for the three core-periphery (CP) divisions. Raincloud represent regions. Values are presented in milliseconds. Brain plots show the different CP divisions of the regions. (a) Showing raincloud for the ACW values of core and

*periphery using the Schaefer/Margulies division (SCP). The student's t-test showed a significant difference in ACW-50 (t=-5.25,d=-0.77) and ACW-0 (t= -5.42,d=-0.78). (b) The same analysis as (a), but using the CP definition of the Ji/Ito (JCP). Student's t-test was significant for the difference of both ACW-50 and ACW-0 between core and periphery (t=-5.72,d=-0.66 and t= -11.67,d=-1.33, respectively). (c) The same analysis using the restricted definition of core (RCP) showed a significant statistical difference between core and periphery for both ACW-50 (t=-6.12,d=-0.75) and ACW-0 (t= -13.58,d=-1.63). Stars represent the significance level (*** ≡ α=0.001).*

A recent article [85] argues that the peak frequency of the MEG signal in the range of 3-45 Hz follows the anterior-posterior axis (more details in the discussion). To further validate the core-periphery organization of ACW, we used linear regression to regress out the effect of this axis. An anterior-posterior value was calculated for each region based on the y coordinate of the region in the anatomical surface map (provided by the HCP group). Then, the anterior-posterior axis was used as the independent variable in the linear model of ACW. The residual of the model (residual ACW) is presented in the Supplementary Figure 2.1 for all three CP divisions. SCP (ACW-50: $t = -7.80, d = -1.14$, ACW-0: $t = -7.23, d = -1.04$), JCP (ACW-50: $t = -10.43, d = -1.20$, ACW-0: $t = -11.65, d = -1.33$), and RCP (ACW-50: $t = -11.69, d = -1.43$, ACW-0: $t = -13.51, d = -1.62$) show a significant ($p < 0.001$) difference between core and periphery of residual ACW, thus, validating our previous results.

The topography of ACW during resting state was further explored on a network level using both Schaefer (Supplementary Figure 2.2a) and Ji (Supplementary Figure 2.2b) templates. Plotting these values revealed different spatial patterns among the networks. One-way Analysis of Variance (ANOVA) suggests significant ($p < 0.001$) differences between networks in both ACW-50 (Schaefer: $F(6, 193) = 11.17, \eta^2 = 0.25$, Ji: $F(11, 348) = 24.23, \eta^2 = 0.43$) and ACW-0 (Schaefer: $F(6, 193) = 21.42, \eta^2 = 0.39$, Ji: $F(11, 348) = 215.64, \eta^2 = 0.86$).

2.4.2 Organization of ACW along the principal gradient of core-periphery

Margulies et al. [52] suggest a principal gradient of functional connectivity for the core-periphery organization which captures the transition between different networks (Figure 3c from ref. [52]). To further validate that the topography of ACW follows the core-periphery organization, we projected our results on to the same cutouts provided in Figure 3c of ref. [52] (Figure 2.3). The results suggest a direction of change similar to the principal gradient.

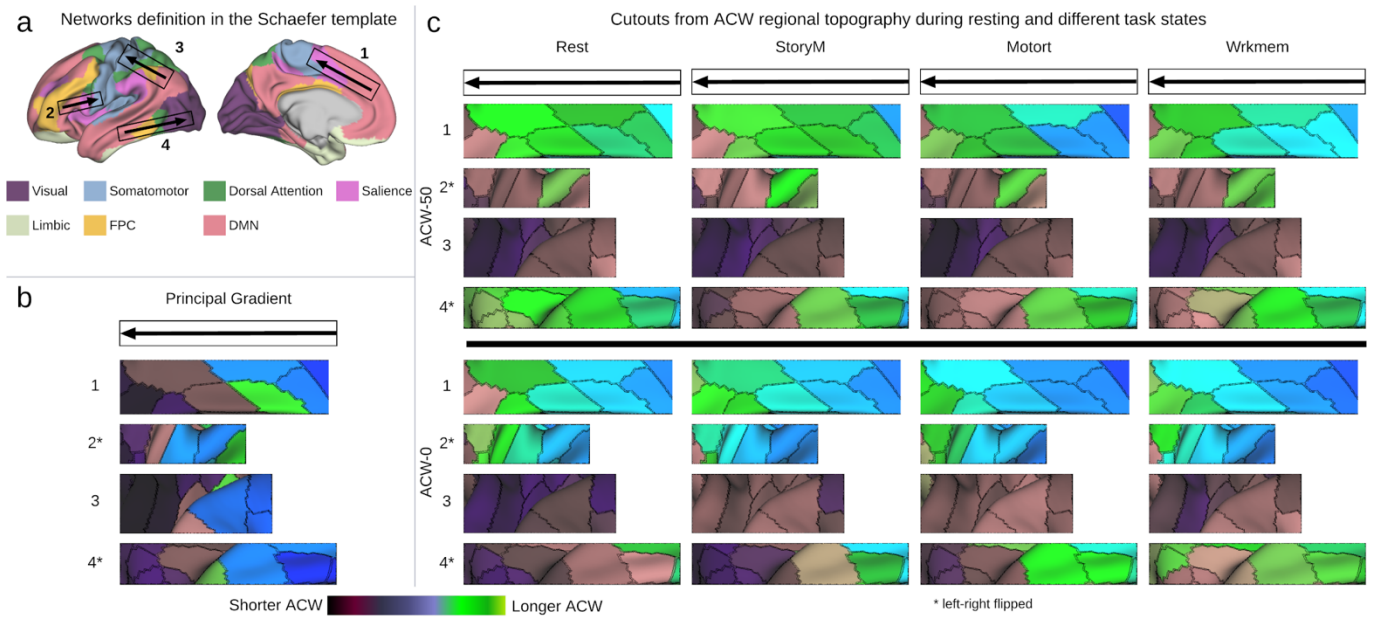

Figure 2.3: ACW cutouts for principal gradient of functional connectivity. The cutouts are similar to Figure 3c of ref. [52]. They suggest that the direction of cross-regional changes in ACW is similar to the principal gradient of functional connectivity defined in ref [52] further validating the presence of the core-periphery organization in ACW. (a) Networks and the cutouts on the brain. (b) The regional principal gradient from the cutouts. (c) regional ACW values from the cutouts.

2.4.3 ACW during task states

To investigate whether the CP organization of ACW is preserved during the task state, we calculated ACW-50 and ACW-0 for the three different task conditions of language processing (StoryM), motor (Motort) and working memory (Wrkmem). An increase in both ACW scales from the periphery to the core in all three task conditions was observed (Figure 2.4). To test that, we used three separate two-way Analysis of Variances (ANOVA) for the three CP organizations (SCP, JCP, and RCP). Both task (3 levels) and core-periphery (2 levels) were used as independent factors in the model. The model shows significant ($p < 0.001$) effect of core-periphery factor for SCP (ACW-50: $F(1, 594) = 57.69, \eta^2 = 0.08$, ACW-0: $F(1, 594) = 70.47, \eta^2 = 0.09$), JCP (ACW-50: $F(1, 1074) = 318.44, \eta^2 = 0.22$, ACW-0: $F(1, 1074) = 464.40, \eta^2 = 0.26$), and RCP (ACW-50: $F(1, 1074) = 311.75, \eta^2 = 0.25$, ACW-0: $F(1, 1074) = 549.90, \eta^2 = 0.33$). Complete result of the ANOVA test is presented in Supplementary Table 2.1. Further post-hoc analysis using Tukey's HSD method reveals that regions in the periphery are significantly different from those in the core in all three CP divisions of all task conditions (Table 2.1). These results align with our resting state findings suggesting that the ACW in both 50 and 0 scales was higher in the core regions during all three tasks thus following a CP regime during task states.

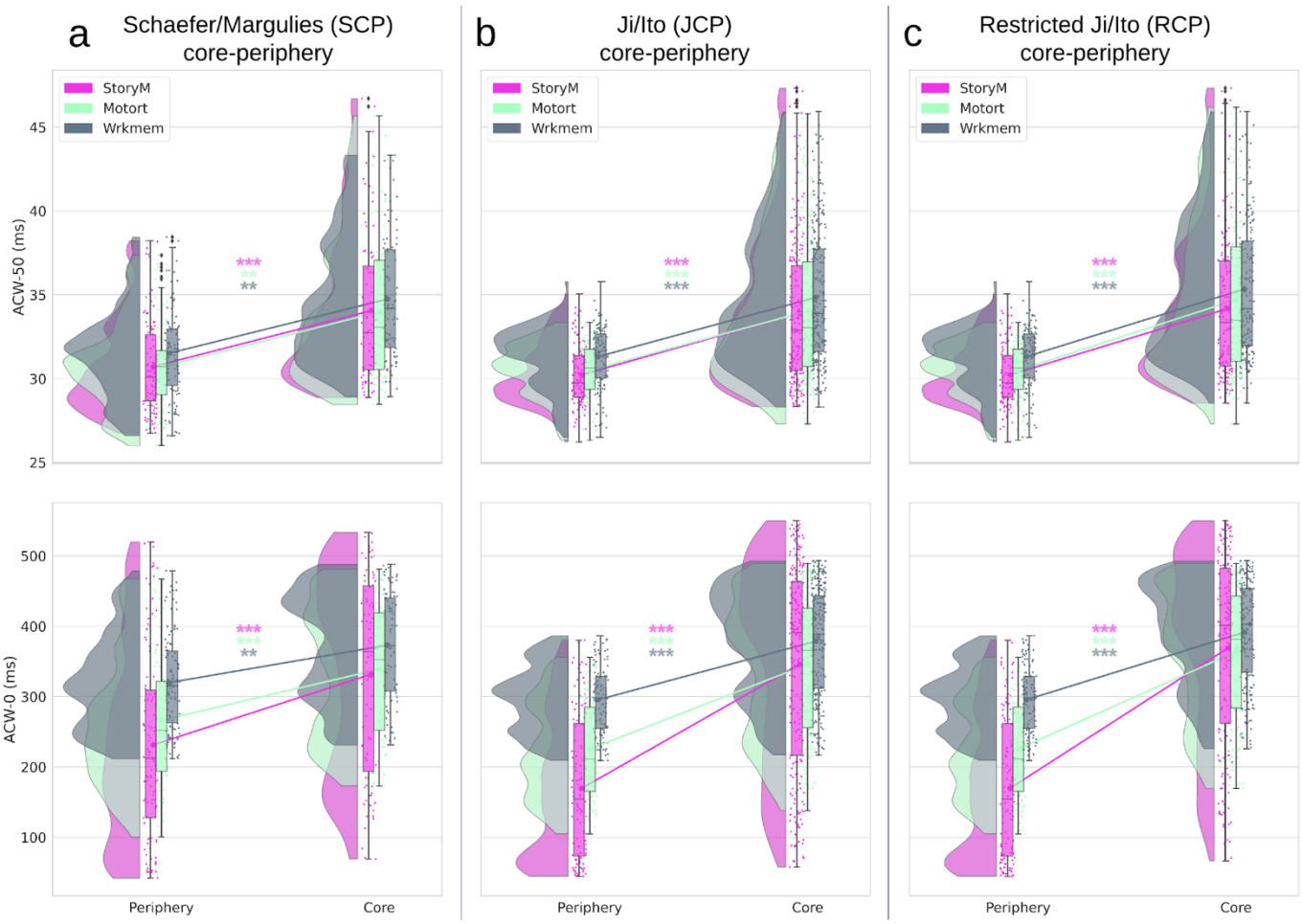

Figure 2.4: ACW during task conditions for different core-periphery divisions. Raincloud represent regions divided into core and periphery. Values are presented in milliseconds. (a) Showing raincloud for the ACW values of core and periphery using the Schaefer/Margulies division (SCP). Two-way analysis of variance (ANOVA) using task condition (3 levels: StoryM, Motort and Wrkmem) and CP (2 levels: core and periphery) as factors showed significant ($p < 0.001$) effect of CP factor on ACW-50 ($F(1,594) = 57.69, \eta^2 = 0.08$) and ACW-0 ($F(1,594) = 70.47, \eta^2 = 0.09$). Complete ANOVA result is presented in Supplementary Table 2.1. (b) Similar analysis as in (a) for the Ji/Ito core-periphery (JCP). Again, two-way ANOVA showed significant ($p < 0.001$) effect of CP factor on ACW-50 ($F(1,1074) = 318.44, \eta^2 = 0.22$) and ACW-0 ($F(1,1074) = 464.40, \eta^2 = 0.26$). (c) Similar to (a) and (b) but using the restricted core-periphery (RCP). Similar to previous results the effect of CP factor was significant ($p < 0.001$) for ACW-50 ($F(1,1074) = 311.75, \eta^2 = 0.25$) and ACW-0 ($F(1,1074) = 549.90, \eta^2 = 0.33$). Similar to the resting state results, an increase in both ACW scales along the different definitions of CP can be observed in all task conditions. Post hoc analysis using the Tukey HSD method revealed significant differences between periphery and core in all task conditions. The post-hoc results are presented in Table 2.1. Stars represent the significance level ($*** \equiv \alpha = 0.001, ** \equiv \alpha = 0.01$).

To extend the resting state results and further validate the CP organization of ACW scales during task conditions, we controlled for the anterior-posterior gradient by regressing out the y coordinate of each region and repeating the aforementioned analysis on the residual ACW values. The y coordinate of all regions was used as the independent variable in a linear regression model (one model per each scale) to estimate the ACW values (ACW values used as dependent variables). Then, the residual of the model was determined as the residual ACW and plotted along the three definitions of CP, i.e. SCP, JCP, and RCP (Supplementary Figure 2.3). Statistical analysis using two-way ANOVA (similar to previous results, complete ANOVA in Supplementary Table 2.2) showed a significant ($p < 0.001$) effect of the core-periphery factor on residual ACW. SCP: ACW-50, $F(1,594) = 152.67, \eta^2 = 0.20$; ACW-0: $F(1,594) = 144.40, \eta^2 = 0.19$). JCP: ACW-50, $F(1,1074) = 514.64, \eta^2 = 0.32$; ACW-0, $F(1,1074) = 518.48, \eta^2 = 0.32$. RCP: ACW-50, $F(1,1074) = 565.43, \eta^2 = 0.38$; ACW-0: $F(1,1074) = 607.97, \eta^2 = 0.40$. Moreover, post-hoc

analysis using Tukey's HSD method revealed that the periphery has significantly lower ACW values compared to the core in the task condition within all three different definitions of CP (Supplementary Table 2.3). These results validate our original results suggesting that ACW during task, similar to rest, follows a core-periphery organization.

Table 2.1: Post-hoc results for periphery vs. core in different task conditions. Tukey HSD method was used to determine the between factor significance of ANOVA on both ACW-50 and ACW-0 along different CP divisions.

		StoryM			Motort			Wrkmem		
		t	d	p	t	d	p	t	d	p
SCP	ACW-50	-5.41	-0.77	***	-3.47	-0.49	**	-3.60	-0.51	**
	ACW-0	-6.48	-0.92	***	-4.71	-0.67	***	-3.43	-0.48	**
JCP	ACW-50	-9.80	-1.11	***	-5.65	-0.64	***	-5.46	-0.61	***
	ACW-0	-15.47	-1.75	***	-10.63	-1.20	***	-7.34	-0.83	***
RCP	ACW-50	-11.24	-1.34	***	-6.36	-0.75	***	-6.02	-0.71	***
	ACW-0	-11.57	-2.03	***	-11.57	-1.42	***	-8.25	-0.98	***
d stands for Cohen's d effect size. The values are represented as periphery vs. core. Stars represent the significance level ($*** \equiv \alpha = 0.001, ** \equiv \alpha = 0.01$).										

Task state ACW was also investigated along the different networks defined by both Schaefer and Ji templates. Both ACW scales were first averaged over subjects and then plotted for different networks (Supplementary Figure 2.4). The effect of networks on the ACW values was tested using ANOVA. First, ACW was modelled with both task (3 levels) and network (6 levels in Schaefer and 12 levels in Ji templates) as independent factors to test if the effect of network is overall significant. Then, a one-way ANOVA with only the network as the independent factor was calculated for each task to determine the effect of network in each task. The results are presented in Supplementary Table 2.4 showing a significant ($p < 0.001$) effect of network in both templates on ACW-50 and ACW-0 during all three task conditions.

2.4.4 The relationship between resting and task states in ACW

The similarity between resting and task states. In this step, we investigated how the resting state's intrinsic neural timescales including their CP-gradient are carried over to task states; for that, we conducted various analyses on rest-task similarities and differences. The rest-task similarity analysis was performed in three steps, spatial correlation, linear regression and regional correlation.

The spatial correlation was calculated to see how similar the spatial distribution of ACW values are between resting and different task states (Figure 2.5a for ACW-50 and b for ACW-0). It was conducted by first averaging each condition (either resting or task) across subjects and then correlating resting state's averaged brain map with each task state's brain map across regions. Pearson correlation showed that all tasks ACW's spatial distributions are highly ($n = 360, p < 0.001$) correlated with the resting state in both ACW scales, i.e. 50 and 0, (values are presented in Figure 2.5) suggesting similar spatial topography between resting and task states.

To extend our spatial correlation results, we also conducted linear regression. ACW during each task state was modelled as a function of the resting state in a linear model (Supplementary Figure 2.5) after averaging all conditions (either resting or task) across subjects (thus, one brain map for each condition). This analysis revealed a significant ($n = 360, p < 0.001$) linear relationship between Rest and all three task conditions in both Schaefer and Ji parcellation templates (R^2 values are presented in Supplementary Figure 2.5) suggesting that rest ACW can explain more than 85% of the variance in task ACW.

Next, the rest-task similarity was further explored using regional correlation. The results were analogous for both ACW-50 (Figure 2.5c) and ACW-0 (Figure 2.5d). In both cases, first, a Pearson correlation coefficient was calculated for each region over different subjects ($n = 89$) between resting and each task state (e.g. Rest vs. StoryM). Then, p-values were corrected for multiple comparisons using the False Discovery Rate (FDR) method at $\alpha = 0.05$ while non-significant coefficients were ignored. The results show a high correlation of resting and task states across subjects suggesting that the similarity between resting and task states is consistent across subjects. Together, the findings show strong rest-task similarity suggesting that the convergence of temporal and spatial hierarchies during the resting state is carried over to task states.

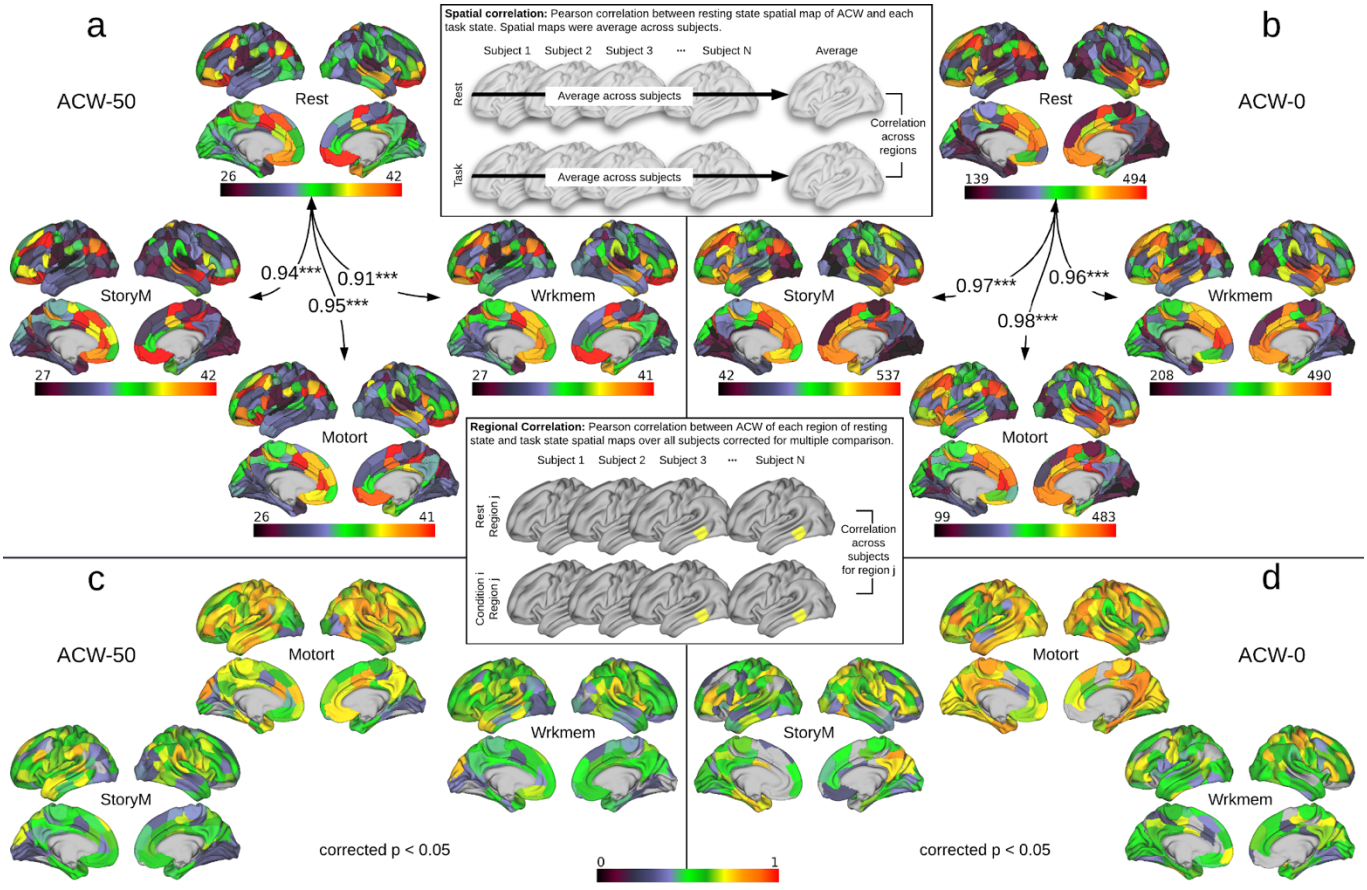

Figure 2.5: The spatial similarity between resting and task states. The similarity was calculated by applying rest-task spatial correlation (a, b) and intra-regional rest-task correlation (c, d). The boxes with the gray brains show how spatial and regional correlation was calculated. The yellow region in the box of Regional Correlation is a sample region chosen only for illustration purpose. (a) and (b) show spatial correlation (numbers on the arrows) between different conditions alongside their spatial distribution over brain regions for ACW-50 and ACW-0, respectively. Each

*value on the arrows is a Pearson correlation coefficient between a pair of conditions across the brain regions (n = 360). All correlation values suggest that different conditions are highly correlated with each other (*** ≡ $\alpha = 0.001$). (c) and (d) show the regional correlation between resting and each task state in ACW-50 and ACW-0, respectively. Pearson correlation coefficients were calculated for each region over different subjects, then corrected for multiple comparisons using the FDR correction method at $\alpha = 0.05$. Only the regions that survived the correction are illustrated.*

Degree of change from resting to task state: This analysis aimed to investigate the degree of task-related changes relative to rest and whether that change also conforms to a CP regime. For that, we calculated the percentage of change from resting to task state. It was calculated per region and per subject in all three task conditions and was normalized against their respective resting state values, i.e., the degree of change from rest to task (see methods for details), in all three CP divisions (SCP, RCP and JCP, Figure 2.6). The percentage of change was then tested for statistical significance using two-way ANOVA similar to previous resting and task state analyzes. Task condition (3 levels) and core-periphery (2 levels) were used as independent factors to investigate their effects on the percentage change of ACW scales from rest to the task. The statistical test (Supplementary Table 2.5) suggests a significant ($p < 0.001$) effect of core-periphery factor on the change in ACW in SCP (ACW-50: $F(1,594) = 10.63, \eta^2 = 0.01$, ACW-0: $F(1,594) = 12.17, \eta^2 = 0.01$), JCP (ACW-50: $F(1,1074) = 99.61, \eta^2 = 0.07$, ACW-0: $F(1,1074) = 26.74, \eta^2 = 0.01$), and RCP (ACW-50: $F(1,1074) = 97.35, \eta^2 = 0.08$, ACW-0: $F(1,1074) = 34.92, \eta^2 = 0.02$). The difference between periphery and core was also investigated using Tukey's HSD method in a post-hoc analysis (Table 2.2). We can see a prominent change in ACW from rest to task. However, the direction of change is not similar among the three conditions (e.g. StoryM and Motort showing opposite directions of change from rest to task in ACW-0). These findings suggest task-specific effects in especially ACW-0 but also in ACW-50. Notably, these task-specific findings were not observed in the task conditions alone, i.e., independent of rest (Figure 2.4); they become only apparent when one subtracts task from rest, i.e., rest-task difference, which subtracts, i.e., eliminates, those features shared by rest and task, e.g., core-periphery organization.

Table 2.2: Post-hoc results for periphery vs. core in the change from resting to task state. Tukey's HSD method was used to determine the between factor significance of ANOVA on both ACW-50 and ACW-0 along different CP divisions.

		StoryM			Motort			Wrkmem		
		t	d	p	t	d		t	d	p
SCP	ACW-50	-6.09	-0.86	***	-0.84	-0.12	0.90	-1.12	-0.16	0.50
	ACW-0	-1.58	-0.22	0.50	2.32	0.33	0.18	6.31	0.90	***
JCP	ACW-50	-11.07	-1.25	***	-2.43	-0.27	0.14	-2.42	-0.27	0.14
	ACW-0	-5.17	-0.58	***	3.09	0.35	*	14.88	1.68	***
RCP	ACW-50	-12.02	-1.43	***	-2.54	-0.30	0.11	-2.45	-0.29	0.13
	ACW-0	-5.26	-0.62	***	3.32	0.39	*	16.28	1.94	***
d stands for Cohen's d effect size. The values are represented as periphery vs. core. Stars represent the significance level (*** ≡ $\alpha = 0.001$, * ≡ $\alpha = 0.05$).										

Taken together, our results, on one hand, suggest a consistent similarity in the organization of ACW between resting and different task states – this is documented by their high similarity in all three statistical rest-task analyses. On the other

hand, when the effect of resting state is removed, i.e., eliminated, as when calculating the rest-task differences, each task shows distinct features in its temporal organization. These results suggest that task-specific effects occur within the framework of the more fundamental core-periphery organization as that is preserved during both rest and task states.

2.4.5 The relationship between different timescales and their predictive power

So far, we have investigated the temporal organization of neural activity using two different scales of ACW, i.e. 50 and 0 which showed more or less similar results for both. The last part of our analysis involves investigating the relationship between ACW-50 and ACW-0 and showing the differential effects of them in determining core-periphery organization in a more fine-grained way. This was done using three methods: kernel density estimation, simulation and machine learning.

Kernel density estimation. First, the density estimation of the ACW data was performed to observe the general density function (DF) over the whole data. We used our Ji-parcellated data (360 regions per subject) and removed all the labels (e.g. task, subject, region) from the ACW values; then the range of each ACW scale (i.e. 50 or 0) was scaled to be between 0 and 1. Based on the histograms of the data, we decided to use the Gaussian kernel with the expectation-maximization algorithm to estimate the two DFs (for ACW-50 and ACW-0). Figure 2.7a left shows the estimated DFs. It can be observed that the range of ACW-0 values is much wider than ACW-50; this suggests a higher variety or range of ACW-0 values in the probability space which may allow for a more fine-grained differentiation between different labels (i.e., condition, subject, or region).

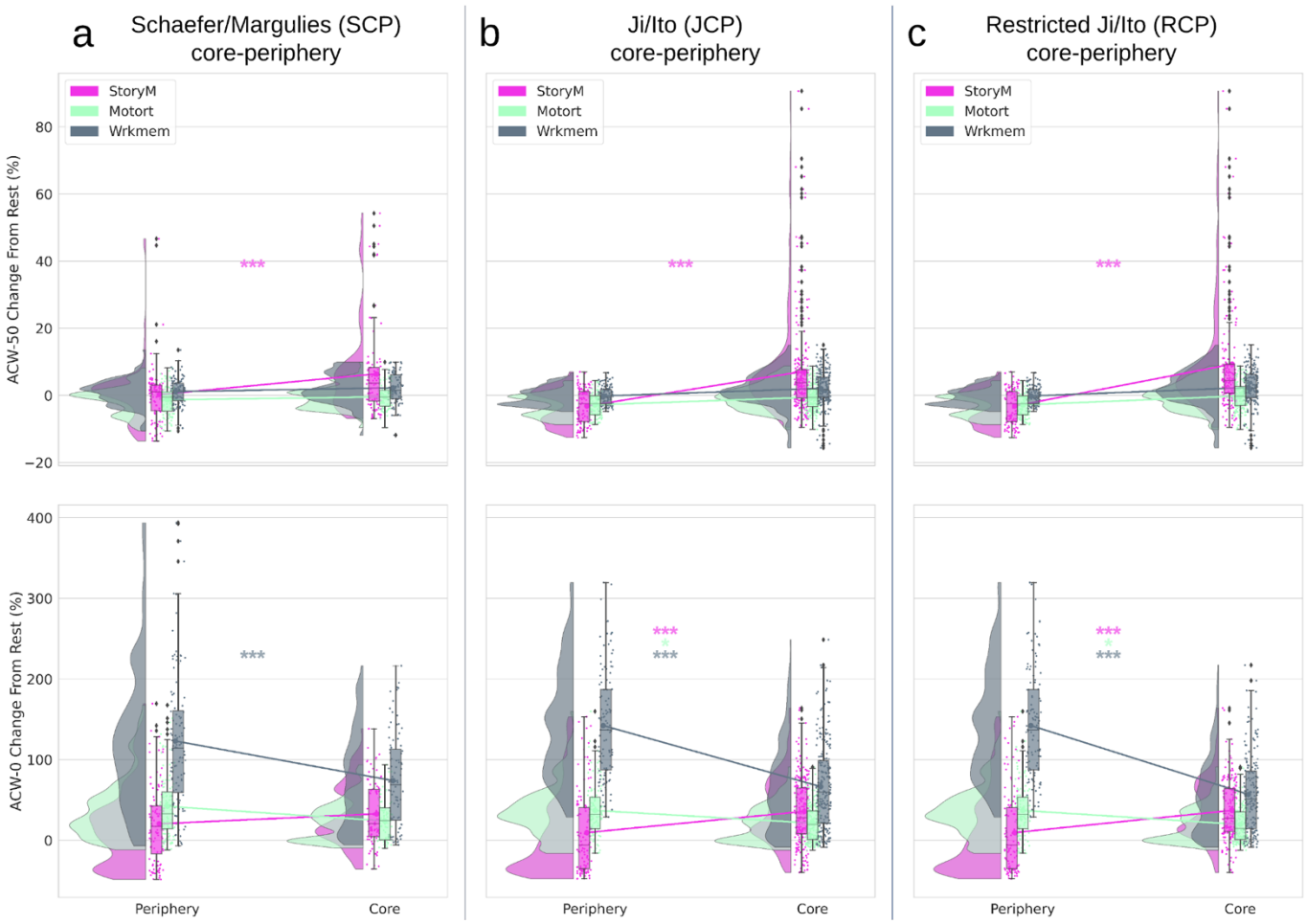

*Figure 2.6: Change in ACW from rest to task states in different CP divisions by calculating rest-task differences. Rainclouds represent regions divided into core and periphery. Values are presented in percentages. Stars represent the significance level (*** ≡ $\alpha = 0.001$,* ≡ $\alpha = 0.05$). (a) Showing rainclouds for the ACW change values of core and periphery using the Schaefer/Margulies division (SCP). A statistical test (Supplementary Table 2.5) was performed with two-way ANOVA using task condition (3 levels: StoryM, Motort and Wrkmem) and CP (2 levels: core and periphery) as independent factors. It showed significant ($p < 0.001$) effect of CP factor on ACW-50 ($F(1, 594) = 10.63, \eta^2 = 0.01$) and ACW-0 ($F(1, 594) = 12.17, \eta^2 = 0.01$). (b) Ji/Ito template (JCP): again, two-way ANOVA showed significant ($p < 0.001$) effect of CP factor on ACW-50 ($F(1, 1074) = 99.61, \eta^2 = 0.07$) and ACW-0 ($F(1, 1074) = 26.74, \eta^2 = 0.01$). (c) Restricted Ji/Ito template (RCP): significant ($p < 0.001$) effect of CP for ACW-50 ($F(1, 1074) = 97.35, \eta^2 = 0.08$) and ACW-0 ($F(1, 1074) = 34.92, \eta^2 = 0.02$). Post-hoc analysis was performed using Tukey's HSD method to determine whether the difference between core and periphery is significant. The results are provided in Table 2.2.*

Importantly, the data suggest that ACW-0 follows two separate Gaussian distributions. To investigate whether these two distributions are related to subjects or/and regions, we repeated the same analysis once averaging the data over the regions to remove the effect of the inter-regional differences (Figure 2.7a middle) and once averaging over the subjects to remove the effect of the inter-individual difference (Figure 2.7a right). This revealed that the two separate DFs of ACW-0 only appear when we take the interaction of inter-individual and inter-regional differences (subject X region interaction) into consideration (the DFs without any label, i.e. Figure 2.7a left). That observation was consistent in all rest and task conditions suggesting that some subjects' regional ACW follows the first DF and some subjects follow the second one. Together, these findings suggest considerable inter-subject variability in specifically the longer timescale, i.e., ACW-0, whereas inter-subject variability was rather minimal in the shorter timescale, i.e., ACW-50.

The impact of inter-individual differences in ACW-50 and ACW-0 was further validated using a binary classification problem. First, ACW values were averaged over regions (one ACW value per subject) and divided into two groups of "low variability" and "high variability". The median of ACW values during resting state was used as the dividing threshold. Thus, the subjects were divided and labeled (actual label) as "low variability" or "high variability" considering only the activity during resting state. Second, a classification analysis was carried out on the activity during different tasks using a logistic regression analysis. For each task, the predicted labels (output of the logistic regression) were compared to actual ones (created from the resting state data in the first step) across all subjects. The area under the Receiver Operating Characteristic (ROC) curve was computed based on the predicted and actual labels (Figure 2.7b). An ROC curve is a graphical plot that illustrates the diagnostic ability of a binary classifier system as its discrimination threshold is varied. The area under the ROC curve (AUROC) tells how much the model is capable of distinguishing between the two classes. The higher the area under the curve, the better the model is at correctly predicting the true label. Results show that all the obtained AUROCs from ACW-0 are higher than those from ACW-50 for the three tasks. This implies that the ACW-0 contains more information than ACW-50 or, in other words, the predictive capability of ACW-0 to discriminate between subjects of high and low variability during the tasks are higher than the ACW-50.

Simulation. In the second analysis, we were interested to see if the double Gaussian distribution of ACW-0 is due to random noise or is indeed related to the brain signal. For that, we simulated random oscillatory and noise signals in distinct frequencies as distinguished by their different kinds of noises. Pink noise and sine waves were used as the basis of our pseudo-aleatory signals. They were simulated in the same frequency range and sampling rate as our original data (1.3-50 Hz) with uniformly distributed random weights. 20000 signals categorized into four distinct categories (5000 each) were used: pure pink noise, pure sine wave, a combination of sine and pink noise, and a combination of sine, pink and white noise. Random uniform coefficients were used to linearly combine signals in the third and fourth categories (see Supplementary Figure 2.6 for a sample signal in each category). Pink noise was utilized to simulate scale-freeness [99], sine wave for oscillation and white noise for pure randomness. Both ACW scales were calculated for the signals and plotted against each other in Supplementary Figure 6. Kernel density of each category was also estimated (Figure 2.7c); however, none of the simulated signals yielded the specific distributions like the ones previously observed in the brain signal suggesting that the two Gaussians observed in ACW-0 is not random, validating our previous results.

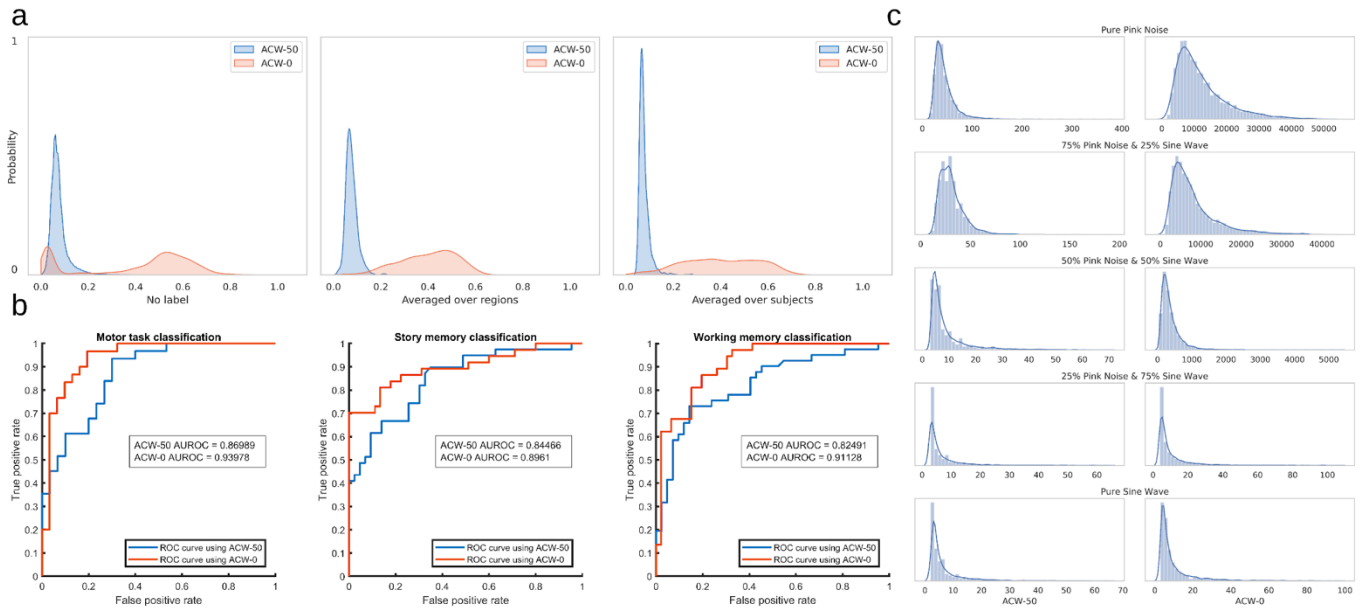

Figure 2.7: Relationship between shorter (ACW-50) and longer (ACW-0) time window measures. (a) The probability density of the data removing all labels (condition, subject or region), averaged over the region and averaged over the subjects. The Ji-parcellated data (360 regions per subject) was used for this analysis. The range of the data is scaled between 0 and 1 separately for ACW-50 and ACW-0. The density estimation with no label suggests a single narrow Gaussian distribution for ACW-50 and two separate Gaussians for ACW-0. When averaged over either regions or subjects, the two Gaussians of ACW-0 disappears. Thus, the double distribution of ACW-0 is only presented when the interaction of inter-individual differences with regional differences is taken into consideration. Moreover, ACW-0 is expanded over a wider range of values compared to ACW-50 suggesting better and more fine-grained differentiation capacity in the probability space. (b) Receiver operating characteristic (ROC) curves for discriminating subjects in different task conditions (StoryM, Motort, and Wrkmem). They suggest that ACW-0 has better discriminative power among subjects than ACW-50. (c) The density estimation of ACW values in simulated signals.

Machine learning. As the third and final analysis, we used machine learning to determine how the two ACW scales differ in predicting whether a region belongs to the core or periphery. To simplify the question without losing generality, we designed a two-class classification problem using a logistic classifier to determine if a signal is from a core (class 1) or periphery (class 2) region. Table 2.3 summarizes the results which show that not only the two scales have different performances, but also ACW-0 is a better predictor than ACW-50. The results were also replicated with a support vector machine (SVM) classifier using the radial basis function (RBF) kernel (Table 2.3).

Table 2.3: The results for the 2-class classification problem. The values are averaged over 20 folds of the K-fold cross-validation algorithm using Logistic regression and support vector machine (SVM) classifiers. The results are presented if each sample has two features (both ACW-50 and ACW-0), or only one feature (either ACW-50 or ACW-0). They suggest better classification power for ACW-0 compared to ACW-50.

Algorithm	Model #	Features	Mean Accuracy (%)	Mean Precision (%)	Mean Recall (%)	Mean AUC of ROC
Logistic Regression	1	ACW-50 & ACW-0	69.14	63.33	46.61	74.12
	2	Only ACW-50	60.55	40.61	6.02	61.10
	3	Only ACW-0	69.08	63.37	46.12	74.45
SVM	1	ACW-50 & ACW-0	69.15	63.14	47.20	73.19
	2	Only ACW-50	61.61	41.21	7.01	48.72
	3	Only ACW-0	69.13	63.12	47.07	70.68

Next, we used a univariate feature selection method to determine which feature (ACW-50 or ACW-0) is better if we were required to choose one of the two. This method works by selecting the best features based on a univariate statistical test. We used mutual information as our scoring function [98] which is a data-driven method capable of capturing any kind of statistical dependency between two variables. It is equal to zero if and only if the class label is independent of the ACW scale (which means the scale is not a good feature) and higher values mean higher dependency between the two. It suggested that ACW-0 (score = 0.5) was a better feature compared to ACW-50 (score = 0.1) when predicting a region's core or periphery association.

2.5 Discussion

We demonstrate that the temporal hierarchy of intrinsic neural timescale measured by shorter and longer ACW, i.e., ACW-50 and ACW-0 follows the spatial topography namely the core-periphery hierarchy. Networks in the core exhibit longer intrinsic timescale, i.e., ACW-50 and ACW-0, than those at the periphery – this holds across both rest and task states as supported by strong rest-task correlation. Comparing rest and task reveals task-specific changes in particular networks only when the core-periphery organization is eliminated by subtraction, i.e., rest-task differences. Finally, we demonstrate that the longer timescale measure, i.e., ACW-0, exhibits higher accuracy in differentially classifying core vs periphery regions when compared to the shorter ACW-50; this suggests a stronger impact of slower frequencies in the core than in periphery regions resulting in their better and more precise differentiation. Together, we demonstrate that the temporal hierarchy of (shorter and longer) intrinsic neural timescales converges with the spatial topography of the core-periphery hierarchy of the human cortex with both providing an intrinsically temporo-spatial hierarchy during rest and task states.

2.5.1 Core-periphery organization – converging spatial and temporal hierarchies

The spatial topography of the core-periphery hierarchy of the human cortex has been observed in resting state [52], [54], [81], [84]. We extend these findings beyond the spatial domain by showing a corresponding temporal hierarchy of intrinsic neural timescale. Animal [75] and modelling [27], [28], [67] studies observed different intrinsic neural timescales in lower- and higher-order regions/networks of the brain. This leaves open whether the human brain exhibits an analogous temporal architecture. Extending the animal and modelling findings to the human cortex, we, in rest states, observed shorter durations in ACW-50 and especially ACW-0 in periphery regions/networks like sensory and motor networks. That was complemented by longer ACW (especially in ACW-0) durations in the core networks like DMN, cingulum operculum, and FPN.

Together, these findings strongly suggest an intrinsic, i.e., network-specific, temporal architecture with different intrinsic neural timescales following the spatial topography, that is, the core-periphery hierarchy. One may consequently want to speak of an integrated spatiotemporal core-periphery hierarchy. Future investigation is needed to establish a more intimate link between temporal and spatial dimensions. For instance, one may raise the question of whether the functional connectivity among the regions of the core, i.e., core-core connectivity, is directly related to the longer intrinsic timescale in these regions as it is suggested by the recent findings of close relation between inter-regional functional connectivity

and intra-regional ACW [72], [74]. Yet another example could be to link the core-periphery hierarchy to other temporal dynamic measures like the peak frequency, which recently has been shown to exhibit anterior-posterior hierarchy[85]. This raises the question, whether the anterior-posterior hierarchy is embedded in the more comprehensive core-periphery hierarchy which, by itself, was not affected when regressing the anterior-posterior gradient (See results).

An analogous temporo-spatial core-periphery hierarchy was observed during task states. Periphery networks showed shorter ACW while core networks exhibited longer ACW during all three task states. These findings suggest that the temporo-spatial core-periphery hierarchy is carried over from rest to task state holding across different tasks. One may consequently assume that the spatiotemporal core-periphery hierarchy may be an intrinsic feature that remains independent of the respective context, i.e., rest or task. That converges well with the observation that spatial core-periphery hierarchy has also been observed during task states [53], [82] which may then be interpreted as simple carry-over from the rest. This remains to be explored in future studies.

Finally, findings on intrinsic neural timescale show higher-order networks like the DMN display the longest temporal receptive windows (based on functional connectivity) during equally complex tasks, i.e., story or movie [63]–[65], [77], [78], [80]. We replicated these findings in terms of ACW during task states and extend it to the rest where an analogous temporal hierarchy was observed. Moreover, when comparing rest and task ACW, i.e., rest-task differences, we observed task-specific effects that no longer followed the core-periphery hierarchy which we assume to be related to the cancelling out of the core-periphery hierarchy commonly shared by rest and task states. That, in turn, opened the door for observing task-specific ACW changes in particular networks. We demonstrate that the probability density of ACW shows a propensity towards longer ACW-0 in specifically the core networks while it remains shorter in periphery networks. This suggests some network-specific effects of longer (ACW-0) and also shorter (ACW-50) intrinsic neural timescale. Specifically, ACW-50 may be ideal to measure differences in shorter durations of intrinsic timescales in the periphery which are lost in the longer time window of ACW-0. Conversely, ACW-0 measuring longer time interval may be better suited to differentiate between regions with longer intrinsic timescales in specifically the core as it is suggested by our probability density function analysis.

2.5.2 Rest shapes task states – intrinsic neural timescales enable temporal integration

Given that a core-periphery organization of intrinsic neural timescales in both rest and task states was observed, we tested for their relationship. We observed a high degree of correlation in the spatial differences for rest ACW-50/ACW-0 with their corresponding values in the three task states as well as among the three task states. That was complemented by high degrees in the correlation of the levels of ACW rest with those during the three task states. Together, these findings strongly support the assumption of an intrinsic temporal architecture in the brain that is preserved across rest and task states thus shaping both – the core-periphery organization is carried over from rest to task states independent of task-specific changes.

Our data suggest an intimate relationship between the intrinsic neural timescales during rest and task. We assume that such intimate relationship consists of temporal integration. The ACW and, more generally, the intrinsic neural timescales allow for temporal integration of stimuli through their temporal summing and pooling [91]. The need for temporal integration is especially relevant in complex stimuli or tasks like the movie: complex sequences of stimuli need to be integrated here to apprehend their meaning. This requires a prolonged autocorrelation window in especially higher-order networks as it is suggested by our rest-task findings. Moreover, complex stimuli like music or movies involve multiple time scales including short and long – a corresponding hierarchy of timescales on the neural side may consequently be best for processing complex inputs [80].

In addition to the temporal integration of the various stimuli within the task itself, the external task-related stimuli need to be temporally integrated also with the spontaneous activity's ongoing internal stimuli as related to internal cognition like mind-wandering [19] and bodily inputs [55], [100]. Such temporal integration may be mediated by the changes in the ACW during the transition from rest to task [55], [101]. This remains speculative at this point though. We currently do not know whether, and if so how, the length of the autocorrelation window in lower- and higher-order networks is related to different degrees of temporal integration of external and internal stimuli (see [91] for first steps in this direction).

2.5.3 Limitations

Several limitations need to be mentioned. We employed a novel measure of time window, the ACW-0. While our findings show rest and task differences of ACW-0 compared to the shorter ACW-50, future studies both imaging and modelling may be necessary to further establish their differences. Yet another question in this respect is whether ACW-50 and ACW-0 mediate different cognitive processes as it is suggested by their association with different regions/networks in the spatial hierarchy, i.e., core and periphery. Modelling studies will be needed to establish a causal relation between rest and task temporo-spatial hierarchies. While employing different measures of rest-task similarity, we were unable to establish a causal rest-task connection in temporo-spatial hierarchies.

2.6 Conclusion

We show the convergence of the brain's temporal hierarchy, i.e., its intrinsic neural timescales, with the spatial topography of the core-periphery hierarchy during both rest and task states. This suggests an intrinsically spatiotemporal core-periphery hierarchy in the human cortex which shapes its cognitive processing during rest and task states. Pointing to its importance, the temporo-spatial nature of the brain's core-periphery organization may be key in understanding mental features like self and consciousness including their temporo-spatial organization in perception [35], [70], [87], [102]–[104]. Specifically, the temporo-spatial core-periphery organization could provide a dynamic feature shared by both neural and mental levels, i.e., a "common currency" [32], requiring what recently has been described as "Spatiotemporal Neuroscience" [33].

2.7 Supplementary Material

2.7.1 Supplementary Figures

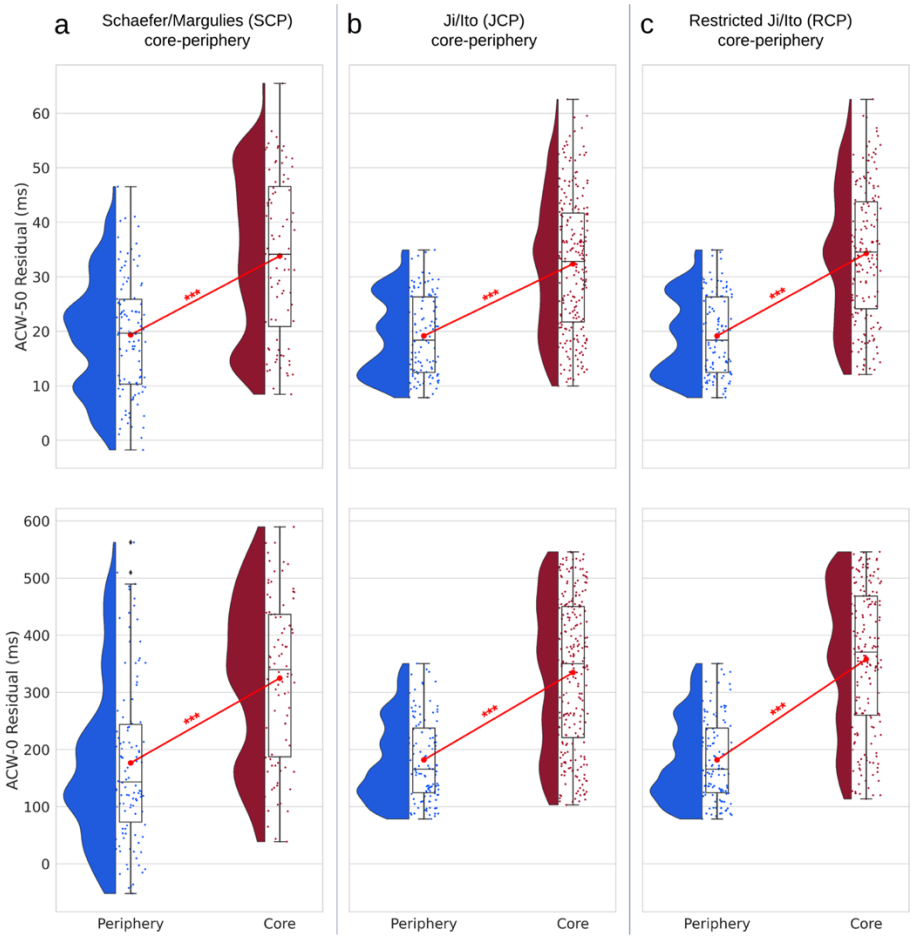

Supplementary Figure 2.1: Residual autocorrelation window (ACW) during resting state for the three core-periphery (CP) divisions after regressing out the anterior-posterior gradient. Raincloud represent regions divided into core and periphery. Values are presented in milliseconds. The y-coordinate of each region's anatomical location was used as its index along the anterior-posterior axis. The y-coordinates were regressed out from ACW values in a linear regression model and then the residual ACW was plotted along the core-periphery division. The results replicate our original results with ACW during resting state. (a) Raincloud for the ACW values of core and periphery using the Schaefer parcellation template (SCP): ACW-50, $t = -7.80, d = -1.14$, *ACW-0,* $t = -7.23, d = -1.04$ *(b) The extended core definition of the Ji parcellation template (JCP): ACW-50,* $t = -10.43, d = -1.20$, *ACW-0,* $t = -11.65, d = -1.33$ *(c) The restricted definition of core (RCP): ACW-50,* $t = -11.69, d = -1.43$, *ACW-0,* $t = -13.51, d = -1.62$. *Stars represent the significance level (*$*** \equiv \alpha = 0.001$*).*

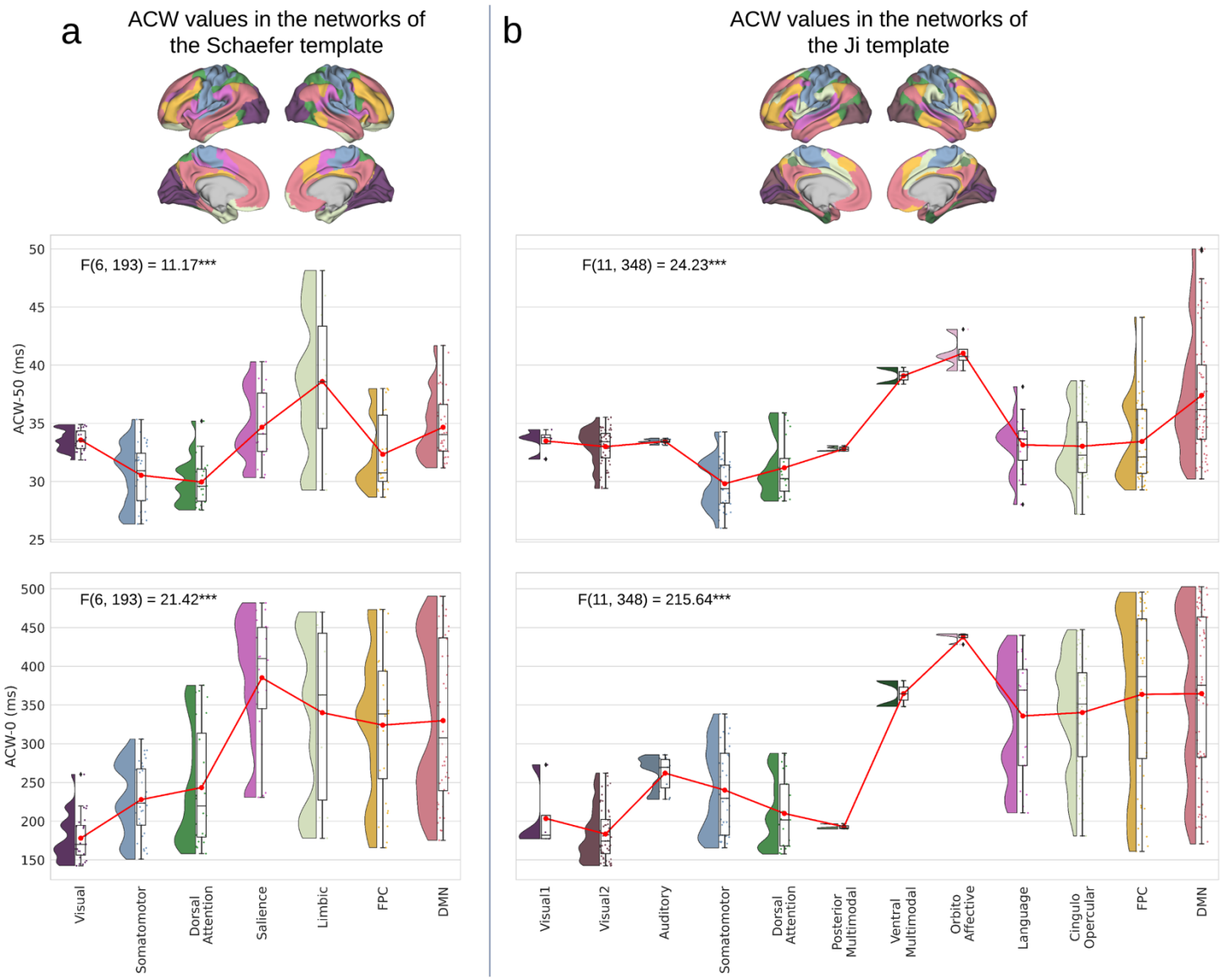

*Supplementary Figure 2.2: Autocorrelation window (ACW) during resting state for the networks. Values are presented in milliseconds. Brain plots show network definitions in different templates. Raincloud represent regions of different networks defined in (a) Schaefer and (b) Ji templates. Stars represent the significance level (*** ≡ $\alpha = 0.001$).*

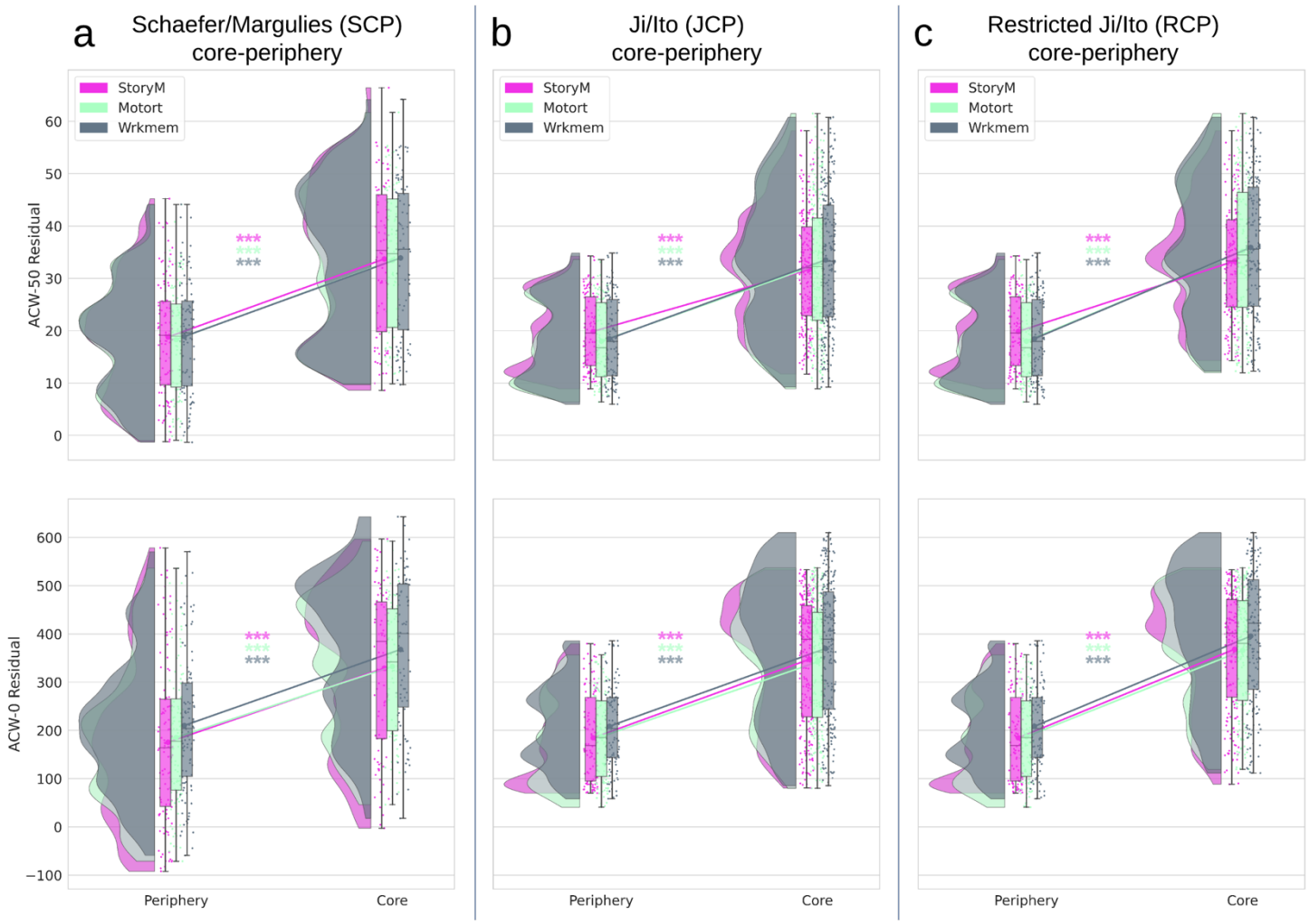

Supplementary Figure 2.3: Residual autocorrelation window (ACW) during different task states for the three core-periphery (CP) divisions after regressing out the anterior-posterior gradient. Raincloud represent regions divided into core and periphery. The y-coordinates were regressed out from ACW values in a linear regression model and then the residual ACW was plot along the core-periphery division. The results replicate our original results for all tasks. (a) Raincloud for the ACW values of core and periphery using the Schaefer parcellation template (SCP). The effect of core-periphery factor in the two-way ANOVA was significant for ACW-50 ($F(1,594) = 152.67, \eta^2 = 0.20$) and ACW-0 ($F(1,594) = 144.40, \eta^2 = 0.19$) (b) The extended core definition of the Ji parcellation template (JCP): ACW-50, $F(1,1074) = 514.64, \eta^2 = 0.32$; ACW-0, $F(1,1074) = 518.48, \eta^2 = 0.32$ (C) The restricted definition of core (RCP): ACW-50, $F(1,1074) = 565.43, \eta^2 = 0.38$; ACW-0, $F(1,1074) = 607.97, \eta^2 = 0.40$. Stars represent the significance level ($*** \equiv \alpha = 0.001$).

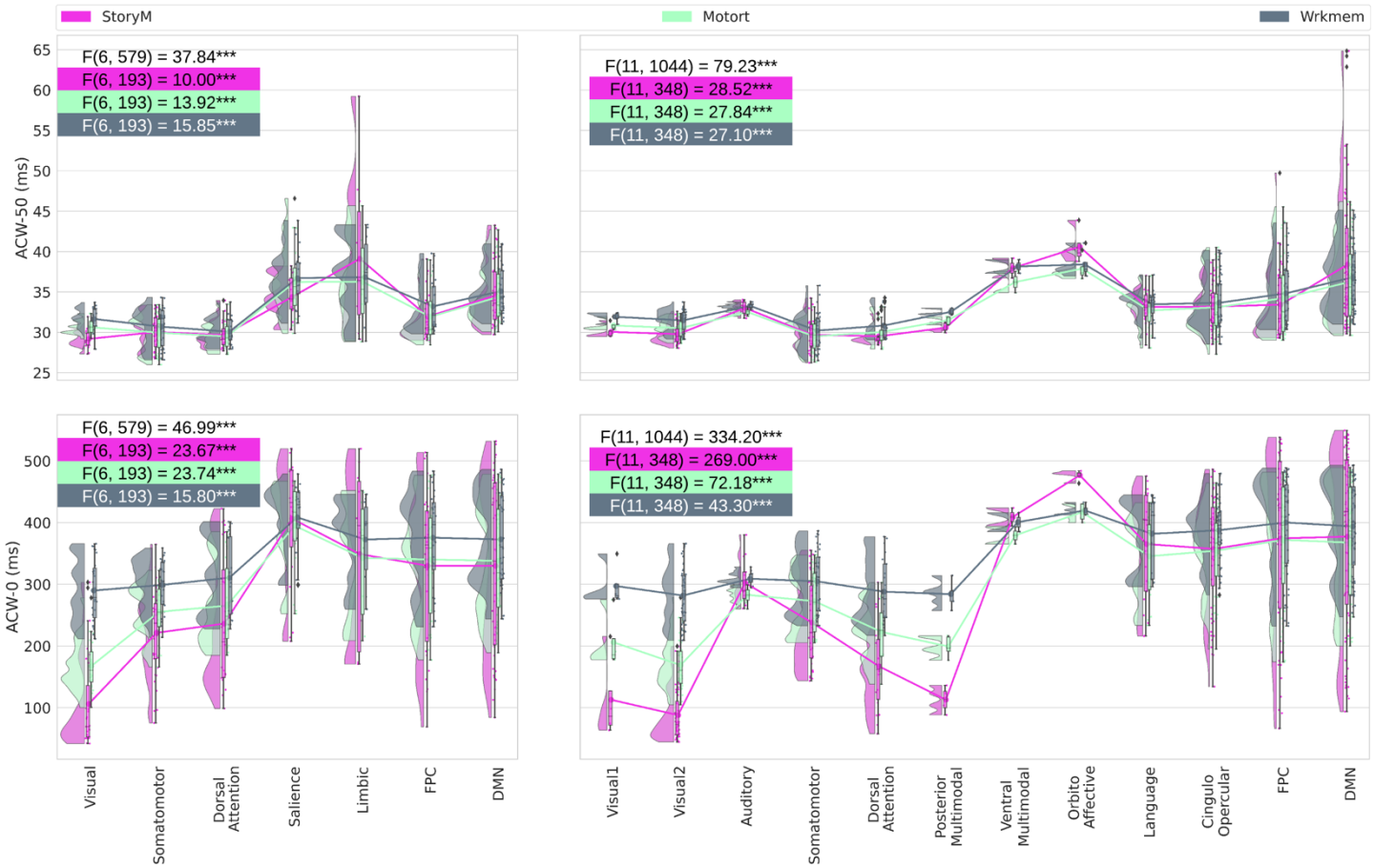

*Supplementary Figure 2.4: Autocorrelation window (ACW) during different task states for the networks. Values are presented in milliseconds. Raincloud represent regions of different networks defined in Schaefer (left) and Ji (right) templates. Stars represent the significance level (*** ≡ $\alpha = 0.001$). For each combination of template and scale (e.g. Schaefer and ACW-50, top left), first, a two-way ANOVA was calculated using task and network as factors to determine if network has any significant effect over the whole data. Then, a one-way ANOVA was calculated for each task using only the network as the factor to investigate the effect of network on each task. Values are presented in Supplementary Table 2.2.*

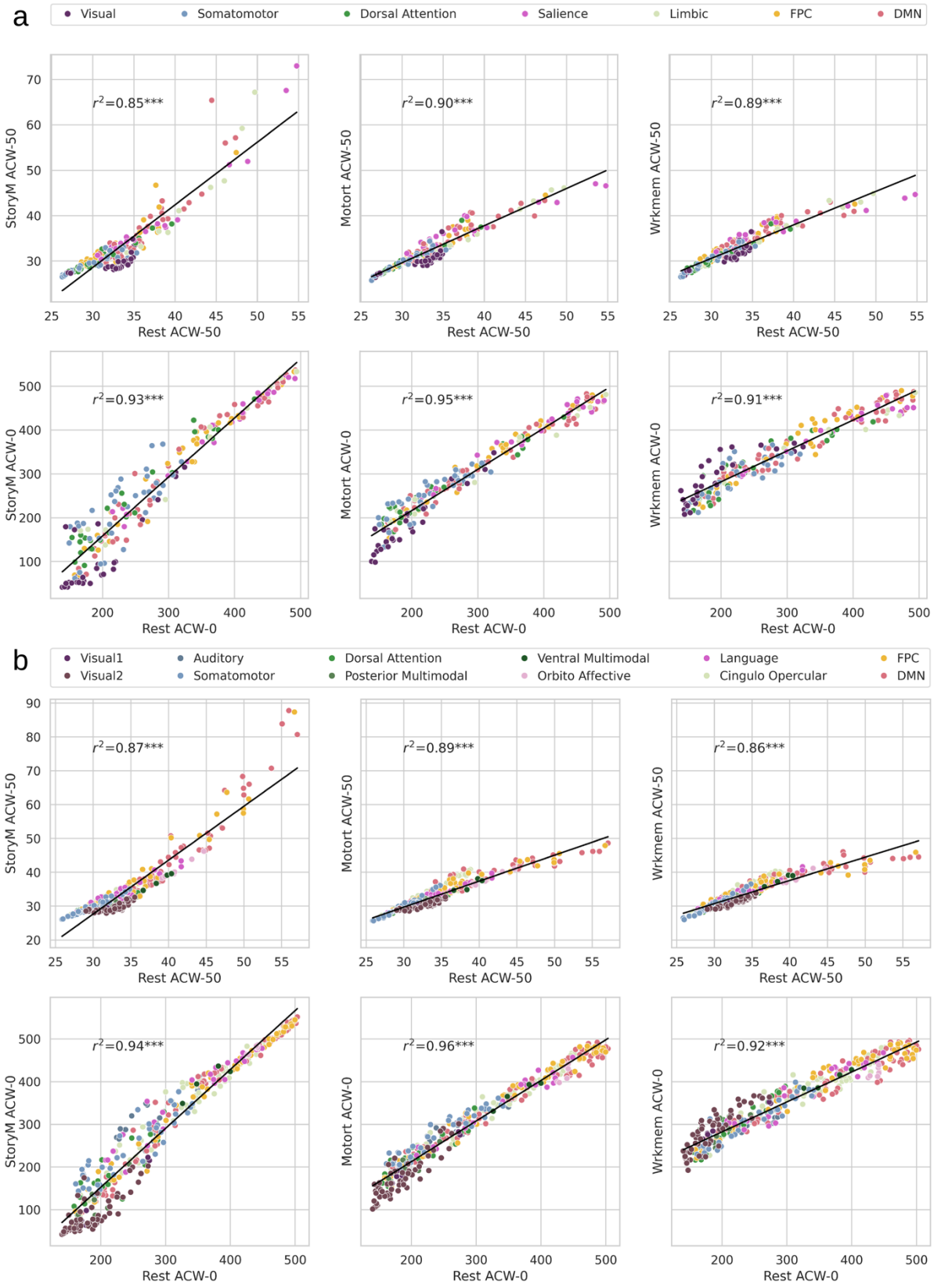

Supplementary Figure 2.5: Linear regression of ACW during different task states as a function of resting state for the Schaefer (a) and Ji (b) parcellation templates. Each scatter plot represents a task as a function of the resting state. Each dot represents a region's ACW value averaged over subjects. The linear relationship in all conditions is significant at $\alpha = 0.001$ and they indicate that at least 85% variance of the task is explained by resting state.

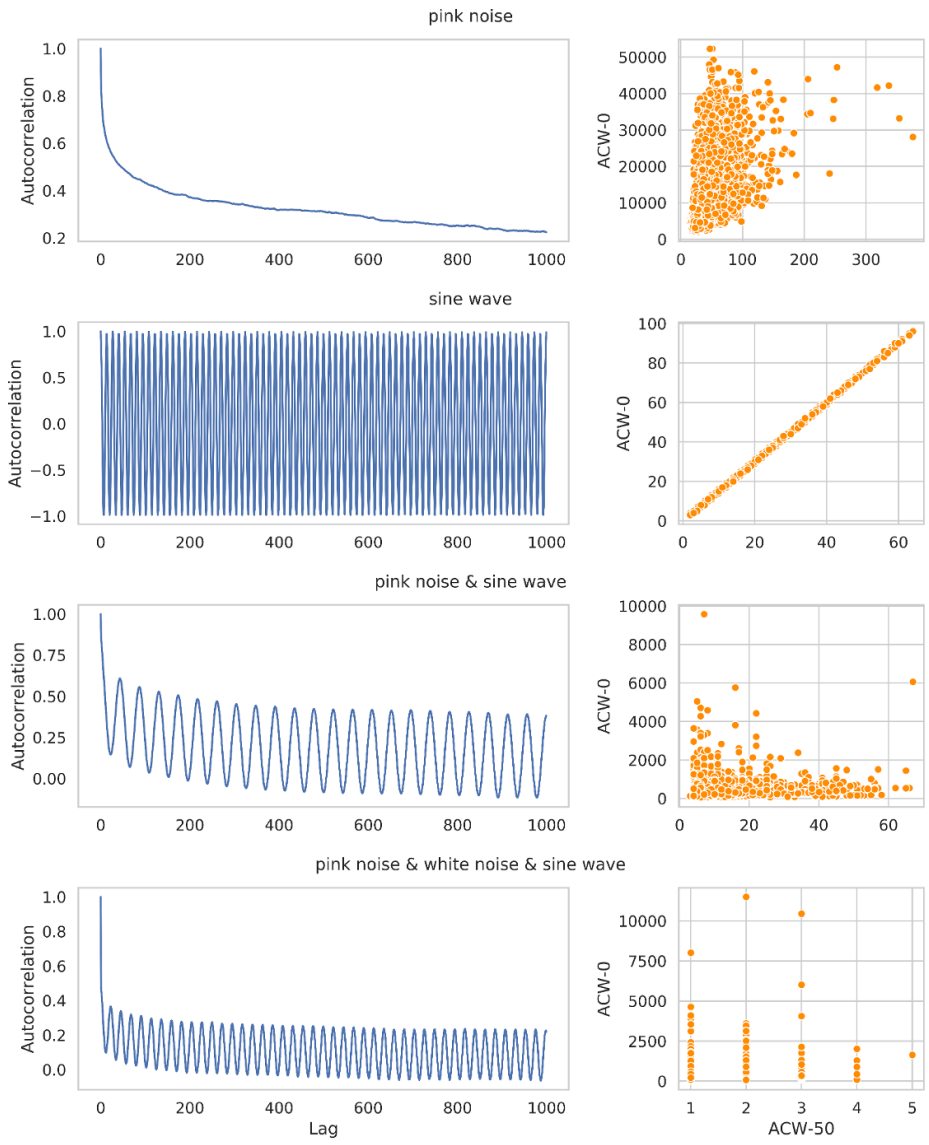

Supplementary Figure 2.6: ACW scales on simulated signals. Left shows the autocorrelation function (first 1000 lags) of a sample for each category of the simulated signals. Right shows the scatter plots for ACW-50 and ACW-0 of all signals in each category.

2.7.2 Supplementary Tables

Supplementary Table 2.1: Two-way ANOVA analysis for different core-periphery organizations during task state. Task condition (3 levels) and core-periphery (CP, 2 levels) where used as independent factors.

SCP	ACW-50	Task	$F(2,594) = 1.93, \eta^2 = 0.005, p = 0.15$
		CP	$F(1,594) = 57.69, \eta^2 = 0.087, p < 0.001$
		Interaction	$F(2,594) = 0.76, \eta^2 = 0.002, \mathrm{p} = 0.46$
	ACW-0	Task	$F(2,594) = 26.13, \eta^2 = 0.072, p < 0.001$
		CP	$F(1,594) = 70.47, \eta^2 = 0.097, p < 0.001$
		Interaction	$F(2,594) = 2.21, \eta^2 = 0.006, \mathrm{p} = 0.10$
JCP	ACW-50	Task	$F(2,1074) = 7.51, \eta^2 = 0.010, p < 0.001$
		CP	$F(1,1074) = 318.44, \eta^2 = 0.223, p < 0.001$
		Interaction	$F(2,1074) = 7.62, \eta^2 = 0.010, p < 0.001$
	ACW-0	Task	$F(2,1074) = 77.24, \eta^2 = 0.089, p < 0.001$
		CP	$F(1,1074) = 464.40, \eta^2 = 0.267, p < 0.001$
		Interaction	$F(2,1074) = 20.59, \eta^2 = 0.023, p < 0.001$
RCP	ACW-50	Task	$F(2,885) = 7.26, \eta^2 = 0.011, p < 0.001$
		CP	$F(1,885) = 311.75, \eta^2 = 0.254, p < 0.001$
		Interaction	$F(2,885) = 7.39, \eta^2 = 0.012, p < 0.001$
	ACW-0	Task	$F(2,885) = 69.47, \eta^2 = 0.085, p < 0.001$
		CP	$F(1,885) = 549.90, \eta^2 = 0.339, p < 0.001$
		Interaction	$F(2,885) = 23.14, \eta^2 = 0.028, p < 0.001$

Supplementary Table 2.2: Two-way ANOVA analysis for different core-periphery organizations during task state for residual ACW. Task condition (3 levels) and core-periphery (CP, 2 levels) where used as independent factors.

SCP	ACW-50	Task	$F(2,594) = 0.24, \eta^2 = 0.006, p < 0.001$
		CP	$F(1,594) = 152.67, \eta^2 = 0.204, p < 0.001$
		Interaction	$F(2,594) = 0.12, \eta^2 = 0.003, p < 0.001$
	ACW-0	Task	$F(2,594) = 2.98, \eta^2 = 0.008, p < 0.001$
		CP	$F(1,594) = 144.40, \eta^2 = 0.193, p < 0.001$
		Interaction	$F(2,594) = 0.03, \eta^2 = 0.0009, p < 0.001$
JCP	ACW-50	Task	$F(2,1074) = 3.31, \eta^2 = 0.004, p < 0.001$
		CP	$F(1,1074) = 514.64, \eta^2 = 0.322, p < 0.001$
		Interaction	$F(2,1074) = 0.19, \eta^2 = 0.0002, p < 0.001$
	ACW-0	Task	$F(2,1074) = 5.11, \eta^2 = 0.006, p < 0.001$
		CP	$F(1,1074) = 518.46, \eta^2 = 0.323, p < 0.001$

		Interaction	$F(2,1074) = 0.10, \eta^2 = 0.0001, p < 0.001$
RCP	ACW-50	Task	$F(2,885) = 2.99, \eta^2 = 0.004, p < 0.001$
		CP	$F(1,885) = 565.43, \eta^2 = 0.388, p < 0.001$
		Interaction	$F(2,885) = 0.26, \eta^2 = 0.0003, p < 0.001$
	ACW-0	Task	$F(2,885) = 5.05, \eta^2 = 0.006, p < 0.001$
		CP	$F(1,885) = 607.97, \eta^2 = 0.404, p < 0.001$
		Interaction	$F(2,885) = 0.10, \eta^2 = 0.0001, p < 0.001$

Supplementary Table 2.3: Post-hoc results for periphery vs. core in different task conditions for residual ACW. Tukey HSD method was used to determine the between factor significance of ANOVA on both residual ACW-50 and residual ACW-0 along different CP divisions.

		StoryM			Motort			Wrkmem		
		t	d	p	t	d	p	t	d	p
SCP	ACW-50	-7.72	-1.10	***	-6.99	-0.99	***	-7.21	-1.02	***
	ACW-0	-6.88	-0.98	***	-6.74	-0.96	***	-7.10	-1.01	***
JCP	ACW-50	-11.04	-1.25	***	-10.31	-1.16	***	-10.59	-1.20	***
	ACW-0	-11.67	-1.32	***	-11.17	-1.26	***	-11.63	-1.31	***
RCP	ACW-50	-12.82	-1.53	***	-11.88	-1.41	***	-12.16	-1.45	***
	ACW-0	-12.97	-1.54	***	-12.68	-1.51	***	-13.27	-1.58	***
d stands for Cohen's d effect size. The values are represented as periphery vs. core. Stars represent the significance level ($*** \equiv \alpha = 0.001$,$** \equiv \alpha = 0.01$).										

Supplementary Table 2.4: Two-way and one-way ANOVA analysis for networks in different ACW task states. First, a two-way ANOVA (task and network as the independent factors) was calculated to determine the overall effect of network on ACW scales, and then for each task, a one-way ANOVA was calculated using network as the independent factor.

Schaefer template	ACW-50	Overall	$F(6,579) = 37.48, \eta^2 = 0.27$
		StoryM	$F(6,193) = 10.00, \eta^2 = 0.23$
		Motort	$F(6,193) = 13.92, \eta^2 = 0.30$
		Wrkmem	$F(6,193) = 15.85, \eta^2 = 0.33$
	ACW-0	Overall	$F(6,579) = 46.99, \eta^2 = 0.29$
		StoryM	$F(6,193) = 23.67, \eta^2 = 0.42$
		Motort	$F(6,193) = 23.74, \eta^2 = 0.42$
		Wrkmem	$F(6,193) = 18.80, \eta^2 = 0.32$
Ji template	ACW-50	Overall	$F(11,1044) = 79.23, \eta^2 = 0.43$
		StoryM	$F(11,348) = 28.52, \eta^2 = 0.47$
		Motort	$F(11,348) = 27.84, \eta^2 = 0.46$
		Wrkmem	$F(11,348) = 27.10, \eta^2 = 0.46$
	ACW-0	Overall	$F(11,1044) = 334.20, \eta^2 = 0.67$
		StoryM	$F(11,348) = 269.00, \eta^2 = 0.89$
		Motort	$F(11,348) = 72.18, \eta^2 = 0.69$
		Wrkmem	$F(11,348) = 43.30, \eta^2 = 0.57$

Supplementary Table 2.5: Two-way ANOVA analysis for different core-periphery organizations in the change from resting to task state. Task condition (3 levels) and core-periphery (CP, 2 levels) where used as independent factors.

SCP	ACW-50	Task	$F(2,594) = 23.11, \eta^2 = 0.069, p < 0.001$
		CP	$F(1,594) = 10.63, \eta^2 = 0.016, p < 0.001$
		Interaction	$F(2,594) = 4.77, \eta^2 = 0.014, p < 0.001$
	ACW-0	Task	$F(2,594) = 71.38, \eta^2 = 0.183, p < 0.001$
		CP	$F(1,594) = 12.17, \eta^2 = 0.015, p < 0.001$
		Interaction	$F(2,594) = 14.80, \eta^2 = 0.038, p < 0.001$
JCP	ACW-50	Task	$F(2,1074) = 45.48, \eta^2 = 0.069, p < 0.001$
		CP	$F(1,1074) = 99.61, \eta^2 = 0.075, p < 0.001$
		Interaction	$F(2,1074) = 25.42, \eta^2 = 0.038, p < 0.001$
	ACW-0	Task	$F(2,1074) = 161.51, \eta^2 = 0.208, p < 0.001$
		CP	$F(1,1074) = 26.74, \eta^2 = 0.017, p < 0.001$
		Interaction	$F(2,1074) = 63.58, \eta^2 = 0.081, p < 0.001$
RCP	ACW-50	Task	$F(2,885) = 36.77\ \eta^2 = 0.066, p < 0.001$
		CP	$F(1,885) = 97.35, \eta^2 = 0.088, p < 0.001$
		Interaction	$F(2,885) = 25.09, \eta^2 = 0.045, p < 0.001$
	ACW-0	Task	$F(2,885) = 123.30, \eta^2 = 0.187, p < 0.001$
		CP	$F(1,885) = 34.92, \eta^2 = 0.026, p < 0.001$
		Interaction	$F(2,885) = 75.56, \eta^2 = 0.114, p < 0.001$

Chapter 3 The interplay between information flux and temporal dynamics in infraslow frequencies

3.1 Abstract

Unlike the brain's faster frequencies, the exact role of its more powerful infraslow frequencies (ISF, 0.01 – 0.1Hz) in information processing remains poorly understood. Do and how ISF process information? We investigate information processing and related temporal dynamics of ISF in resting and task state fMRI. To quantify information, we apply the Lempel-Ziv complexity (LZC), a measure of signal compression indexing information. The LZC is combined with direct measurement of the dynamics of ISF themselves, namely their power spectral density by median frequency (MF). We demonstrate the following: (I) topographical differences in resting state between higher- and lower-order networks, showing statistically lower LZC in the former; (II) task-related changes in LZC; (III) modulation of LZC associated with MF changes, with low and high MF resting-state values correlated with different degrees of LZC change. In sum, we provide evidence that ISF carry and process information as mediated through their temporal dynamics.

3.2 Introduction

The brain exhibits fluctuations in its neural activity which includes different frequency ranges. We know very well that the brain's faster frequencies in the range of 1 to 240Hz process information and thereby shape behavior and cognition as measured in EEG/MEG[105]–[109]. Unlike its faster frequencies, the function of the brain's very slow waves, its infraslow frequencies (ISF, 0.01 - 0.1Hz) is less understood [105], [110]. ISF are often conceived as noise stemming from vascular sources[111], [112] rather than carrying information. However, recent evidence hints upon a neurophysiological basis of ISF [47], [90], [99], [113]–[121], which suggests their potential involvement in processing information. Do ISF, like the brain's faster frequencies, process information during resting and task states? If so, how do ISF process information, i.e., through which pattern? The goal of our paper is to address these two questions. For that purpose, we probe "whether" ISF carry information by investigating them in fMRI with a well-established measure from the Information Theory field, i.e., Lempel-Ziv Complexity (LZC) (see below). To test "how" ISF process information, we combine LZC with a measurement of the dynamics of ISF, namely their power spectral density by median frequency (MF) (see below).

ISF are predominantly measured with functional magnetic resonance imaging (fMRI) that is based on the blood oxygen level-dependent (BOLD) signal [122], [123]. Some conceive the BOLD signal to reflect vascular low-pass filtering of higher frequency neural activity [111], [112] – in that case, the observed ISF would be at best vascular noise without a distinct neurophysiological basis. That is contradicted by recent results which demonstrate a specific neurophysiological basis of ISF [47], [90], [99], [113]–[121]. The neurophysiological basis of ISF is further supported by their occurrence in particular cortical layers [110], [114] as well as by various electrophysiological features like phase-specific distributions and coherence [47], [90], [113], [114], local field potentials (LFP) [115]–[122], and power spectrum [113]. Moreover, task-related changes in ISF have been reported for instance during attention [124], [125] and conscious

perception [126]. Together, such distinct neurophysiological basis of ISF suggests that they are not mere noise but carry and process information. However, "whether" the ISF do, in fact, carry information remains yet to be demonstrated.

Various fMRI studies demonstrated topographical organization of ISF with lower-order networks, i.e., sensory networks, and higher-order networks, i.e., default-mode network, executive network, and others, standing at opposite ends of the spatial hierarchy [52], [54], [127], [128]. Interestingly, such a spatial hierarchy converges with a corresponding temporal hierarchy along the continuum of fast-slow timescales [52], [54], [72], [74], [81], [82], [113], [127], [129]. These findings are mostly based on functional connectivity (FC) [52], [128] and intrinsic neural timescales as measured by autocorrelation window (ACW) in fMRI resting state [74]. They thus describe the spatial and temporal topographical organization of the brain's ISF.

This leaves open whether the ISF themselves including their spatial and temporal organization carry and process information. For that, one needs to operationalize information which, for instance, is provided by Lempel-Ziv Complexity (LZC) [130]–[132]: the LZC measures the number of distinct patterns in a binary sequence, namely the degree to which a signal can be compressed [133], [134]. It reflects the amount of information (number of bits) required to reconstruct a signal [133] (see the validity of LZC in fMRI [135]–[138] as well as in other imaging modalities including MEG, EEG, and spike train analysis [139]–[147]). Accordingly, applying the LZC allows probing "whether" the ISF carry information other than simply noise. Ideally, one wants to combine the LZC with a measure of the ISF themselves like their power spectral density, indexed by its median frequency (MF). In more general terms, MF measures the speed (or velocity) of the signal in a specific frequency range (e.g. the ISF) [148]–[152] by characterizing the distribution of its power spectrum. This allows probing "how" the ISF process information.

Specific aims and hypotheses.

The first specific aim is to investigate the LZC and MF of ISF in the resting state. This addresses our first key question namely "whether" ISF carry information. Our first hypothesis is based on the brain's topography namely, its spatial and temporal hierarchies: if the ISF carry information, we expect the LZC to exhibit different values in the resting state of the lower- and higher-order regions/networks. As most likely related to their continuous exposure to high loads of fast external information input [27], [28], [52], [54], [67], lower-order regions like sensory networks and multimodal sensory regions may show higher LZC and faster MF. While higher-order regions/networks, i.e., default-mode network (DMN), frontoparietal network (FPN), language network, and dorsal attention network do not receive such direct information input, but a "filtered" version of it [27], [28], [52]. For that reason, we expect lower LZC and lower MF in the high-order networks.

The second specific aim is to investigate changes in LZC and MF of ISF during different task states including a movie and a retinotopy task (as provided by 7T HCP). This serves the purpose to substantiate the first key question, namely that ISF carry information. Since the information load changes from resting to task state, we expect rest-task differences in

LZC along the lines of lower- and higher-order networks as both are known to process different loads and kinds of information during task states [135], [137], [141], [142], [153].

The third specific aim consists of linking LZC to the measurement of the ISF themselves, that is, their power spectral density as indexed by MF. This addresses our second key question, namely "how" the ISF process information. Given that we assume LZC to follow the spatial hierarchy of lower- and higher-order networks and MF to index a corresponding temporal hierarchy, we hypothesize close relation of rest and rest-task modulation of LZC to MF during rest and task states. To establish the LZC-MF relationship, we calculate different correlation and regression models. Furthermore, we conduct various simulation models applying different kinds (pink, white, etc.) and levels of noise to demonstrate that the LZC-MF relationship is specifically related to the brain's topography rather than noise. This serves the purpose to connect LZC, which measures "whether" ISF carries information, to MF that allows probing "how" the ISF process information: through power spectral density indexing their 'velocity' or 'speed'.

3.3 Materials and Methods

3.3.1 Experimental Design

Data were selected from Human Connectome Project's 7T dataset (rather than HCP 3T) to achieve a high signal-to-noise ratio (SNR) (and to have more fine-grained resolution) which is especially relevant for properly capturing spatiotemporal dynamics. Other reasons for choosing the 7T data were the longer and more continuous scanning during task states. We used HCP 3T resting-state data for validation purposes; in contrast, we did not use the task data of the 3T dataset because of their short block design which makes proper measurement of the dynamics with our measures impossible.

From the data of 1200 subjects released in HCP-1200 [92], 146 of them had completed the full 7T imaging protocol of the human connectome project (HCP) without any imaging quality issues. A total of 14 fMRI runs (TR=1s) including four resting-state (REST), four movie-watching (MOVIE), and six retinotopy (RET) of these participants were used in this study. Full details on data acquisition and preprocessing are provided in separate articles [154], [155]. In each MOVIE run, subjects had to watch a movie of approximately 15 minutes consisting of several clips separated by 20-seconds rest periods. Different clips were used in different runs (details are available at HCP S1200 Release Reference). For RET, stimuli were constructed by creating slowly moving apertures and placing a dynamic colorful texture within the apertures [Check ref. [156] for details].

Preprocessed data was downloaded from the HCP database at https://db.humanconnectome.org. The preprocessing pipeline includes registration to MNI space, alignment for motion, fieldmap correction, FIX denoising, and MSMAll group registration. Full details of all the steps are available in ref. [154], [157].

3.3.2 Data Processing & Statistical Analysis

All steps of the data processing were performed with in-house scripts written in Python programming language using numpy, scipy, cifti, joblib, matplotlib, and seaborn libraries. The source code is freely available at www.georgnorthoff.com/code/. For brain map visualization purposes, wb_view (part of Connectome Workbench software) was used.

All statistical analyses were performed in the statsmodel library [97] in Python and R v.3.6 and all p-values were corrected for multiple comparisons using the False Discovery Rate (FDR) method. The student's t-test was used to measure the statistical differences between lower- and higher-order networks. Moreover, Analysis of Variance (ANOVA) ANOVA was used to investigate the difference between the networks during each condition. All the statistical tests were accompanied by their non-parametric counterparts in the supplementary result section.

Template and network definition. The preprocessed data were high-pass filtered at 0.01 to both maintain the full frequency spectrum of the data [158] and remove noise. After that, signals were averaged over brain voxels defined in the template provided by ref. [96] to get one fMRI signal per region per subject per run. The template contains 717 regions categorized into 12 networks of visual1, visual2, auditory, somatomotor, posterior multimodal, ventral multimodal, orbito affective, dorsal attention, language, cingulo opercular, frontoparietal, and default-mode. To investigate our lower-order vs. higher-order hypothesis, we also divided the regions into lower-order and higher-order (HON) networks. Lower-order networks included the regions in the visual1, visual2, auditory, somatomotor, posterior multimodal, ventral multimodal and orbito affective networks. Regions inside dorsal attention, language, cingulo opercular, frontoparietal, and default-mode networks were put under the higher-order networks category.

Calculation of Lempel-Ziv complexity. To calculate the Lempel-Ziv complexity (LZC, Figure 3.1 white box), each signal was converted into a binary sequence. Previous studies [134], [159] suggest that the median of the signal's amplitude is a good candidate to use as a binarization threshold. After binarizing each region's signal and converting it to a string sequence, the Lempel-Ziv algorithm [133] was used to compute LZC. As earlier studies have pointed out, LZC is dependent on the length of the sequence, thus a normalization factor (more info in [134]) was used to remove that effect. LZC processing is illustrated in Figure 3.1A.

Calculation of Median Frequency. Median frequency (MF) was measured by first calculating the power spectral density (PSD) of each region's signal. PSD was calculated using the Welch algorithm [160] with a Hanning window implemented in the Scipy package of Python programming language. The median frequency (MF) was calculated from the PSD as the frequency which divides the area under the curve of PSD into two halves (Figure 3.4A).

Resting and task state topographical calculations. The values of both measurements (i.e. LZC and MF) were first calculated for each of the 14 fMRI runs and then averaged over the runs in all three conditions (REST, MOVIE and

RET). After that, based on the requirements of each analysis the values were either averaged over the lower- and higher-order division or the 12 aforementioned networks. The lower-order category was compared to the higher-order using student's t-test over regions.

Rest-task similarity. The similarity between resting and task states was addressed using spatial and regional correlations. The spatial correlation was calculated as a single Pearson correlation coefficient between resting and a task condition (e.g. REST vs. MOVIE) over brain regions after averaging over subjects (thus creating a single brain per condition). The regional correlation was used to measure the regional similarity between resting and task states. This correlation was calculated for each region across subjects between a pair of conditions (e.g. LZC during REST and MF during REST).

Percentage of change from resting state. The difference between resting and task states was calculated as a percentage of change per region per subject. Each region's REST and task (e.g. MOVIE) values were put in the $(\mathrm{REST} - \mathrm{TASK}) \times 100/\mathrm{REST}.$ formula to both measure the change from resting to task state and normalize against rest at the same time. Then, for each subject, the percentage of change values were either averaged over the 12 networks or along the lower- and higher order division. The difference between lower- and higher-order networks and the difference among the networks were statistically tested using the student's t-test and ANOVA methods.

T_1w/T_2w ***map.*** The ratio of T1- to T2-weighted images is suggested to provide a non-invasive neuroimaging proxy of anatomical hierarchy in the primate cortex [161]. So, we used it to investigate whether the relationship between LZC and MF is anatomically based. A cortical map containing the T_1w/T_2w was provided with the HCP dataset. The map was MSMAll registered and bias field-corrected. We parcellated the map into the regions/networks of our template by averaging the T_1w/T_2w values of voxels into different regions.

LZC-MF simulation. The relationship between LZC and MF was explored using simulated signals. 35000 pseudo-aleatory signals within seven different categories (5000 each, see Supplementary Figure 3.5 for a sample signal in each category) were simulated to investigate whether the LZC-MF relationship is non-linear or not and whether the relationship is specific to the brain. The seven categories were (I) pink noise, (II) white noise, (III) sine wave, and linear combinations of (IV) pink and white noises (V) pink noise and sine wave (VI) white noise and sine wave and (VII) pink noise, white noise and sine wave.

The weights of the signals linear combinations were chosen randomly. All random values were chosen from a uniform distribution and were controlled to produce signals in the same frequency range of our original data (0.01-0.5 Hz). Pink noise was chosen to model the scale-free behavior [99], white noise for pure randomness and sine wave for oscillation. The MF and LZC were calculated for each signal and used to further investigate the relationship between the two measurements, and validate LZC calculations in fMRI data.

Change in LZC from REST and MF-REST mediation model. To investigate the relationship between MF during resting state (MF-REST) and the change in LZC task from resting state, a mediation analysis was performed using the mediation library in R. Two separate models were created for the two task conditions. Each model consisted of MF-REST as the mediator, LZC during REST as the independent variable (IV) and LZC during a task condition as the dependent variable (DV). After running the model and observing the indirect effects of IV on DV, the significance of that effect was tested using bootstrapping procedures [162], [163]. Unstandardized indirect effects were computed for each of 1000 bootstrapped samples, and the 95% confidence interval was computed by determining the indirect effects at the 2.5th and 97.5th percentiles.

Change in LZC from REST and MF-REST moderation model. To further investigate the relationship between the change in LZC from REST and MF-REST, regions were divided into two categories based on their MF-REST values. The median of MF-REST was used as the threshold and the regions with lower (higher) MF-REST than the median were put into the low (high) MF-REST category. The median was used to balance the two categories. A new binary variable (Z) was created for each region's MF-REST category (0 = low MF-REST and 1 = high MF-REST). Z was injected in a linear regression model as a moderator: $Y = \beta_1 X + \beta_1 Z + \beta_1 XZ + \beta_4$. In the linear regression equation, Y is LZC during a task condition, X is LZC during resting state, and Z is the binary value of MF during resting state.

3.4 Results

The main aim of this article is to address our two key questions namely to investigate "whether" and "how" infra-slow frequencies (ISF) carry and process information during resting and different task states (see Figure 3.1 for an overview of our guiding questions and their results). We addressed these two key questions by splitting them into a sequence of four different questions as explicated in our overview in Figure 3.1. Using the 7T of HCP, fMRI signals of 146 subjects during resting and two different task states were parcellated into 717 brain regions defined in the template provided by Pappas and colleagues [96]. These regions were divided into 12 networks of Visual1, Visual2, Auditory, Somatomotor, Posterior Multimodal, Ventral Multimodal, Orbito Affective, Dorsal Attention, Language, Cingulo Opercular, Frontoparietal and Default. They were also divided into two categories of lower- and higher-order regions. Regions in Visual1, Visual2, Auditory, Somatomotor, Posterior Multimodal, Ventral Multimodal and Orbito Affective networks were put into the lower-order and the rest into the higher-order categories.

To operationalize and measure information, we used the Lempel-Ziv complexity (LZC) which is algorithmically defined as the number of different patterns in a binary sequence indexing the complexity of the BOLD signal (the white box of Figure 3.1 shows how LZC is calculated). LZC is formally defined as an index of how much a signal can be compressed, and in other words, it measures how "diverse" are the patterns that are present in a signal, i.e. higher LZC is associated with lower compressibility and more information [134], [164]. The amplitude of regional signals was individually binarized using its median as a robust threshold [134], [159] and then fed into the LZC algorithm yielding a single LZC

value per region of a subject during a specific condition (resting or task state). All the subsequent statistical tests were also validated with their non-parametric counterparts.

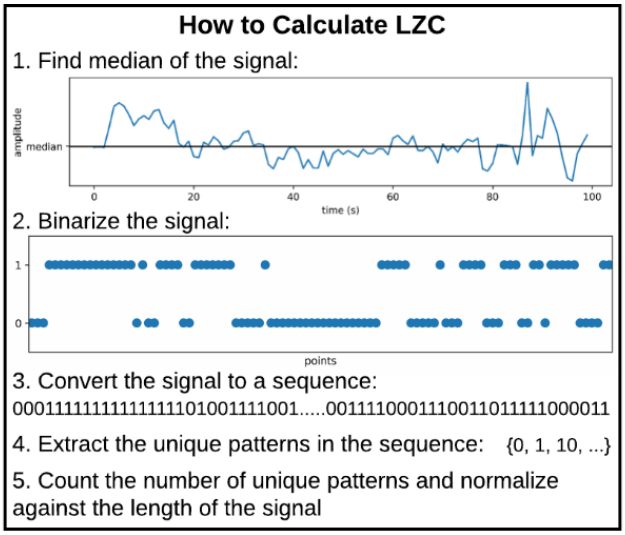

Figure 3.1: Overall view of how Lempel-Ziv Complexity (LZC) is calculated.

Preprocessed 7T fMRI data (TR=1) were downloaded from the Human Connectome Project (HCP) WU-Minn HCP 1200 subjects data release, and then high-pass filtered at 0.01 Hz (more detail about the data release is provided in the method section). The data includes resting state (REST, 16 minutes), and two task states of movie-watching (MOVIE, 15 minutes) and retinotopy (RET, 5 minutes).

3.4.1 The topography of LZC during the resting state

Our first question is to investigate the spatial distribution of LZC in the resting state (see below for simulation on the validity of LZC measurement in fMRI). After averaging over subjects, the regional distribution of LZC values (Figure 3.2A) suggested a specific spatial pattern of LZC. To investigate that, we used the 12 predefined networks (Figure 3.2B) and divided the LZC values into them (Figure 3.2C). This revealed different LZC patterns among the networks. Performing a one-way analysis of variance (ANOVA) over the 12 networks across regions showed significant ($p < 0.001$) differences among them ($F(11, 705) = 52.31, \eta^2 = 0.44$).

Significant differences in LZC values among networks paved the way to further investigate the topography of LZC along the lines of lower- and higher-order categories (Figure 3.2D). Again, the resting state LZC was averaged over subjects and then compared between lower- and higher-order regions (Figure 3.2E). Student's t-test (with the Cohen's d for the effect size) showed a significant $p < 0.001$ difference between the two types of networks ($t = 6.80, d = 0.51$) with the lower-order having higher LZC compared to the higher-order category. Together, these results show clear topographical differences in the spatial distribution of LZC (These results were also replicated in our 3T replication dataset in Supplementary Figure 3.1). Given that lower- and higher-order networks are known to process different kinds and degrees of information [165], our result of LZC following these topographical differences supports the assumption that ISF carry information. This provides a positive answer to our first key question "whether" ISF carry information.

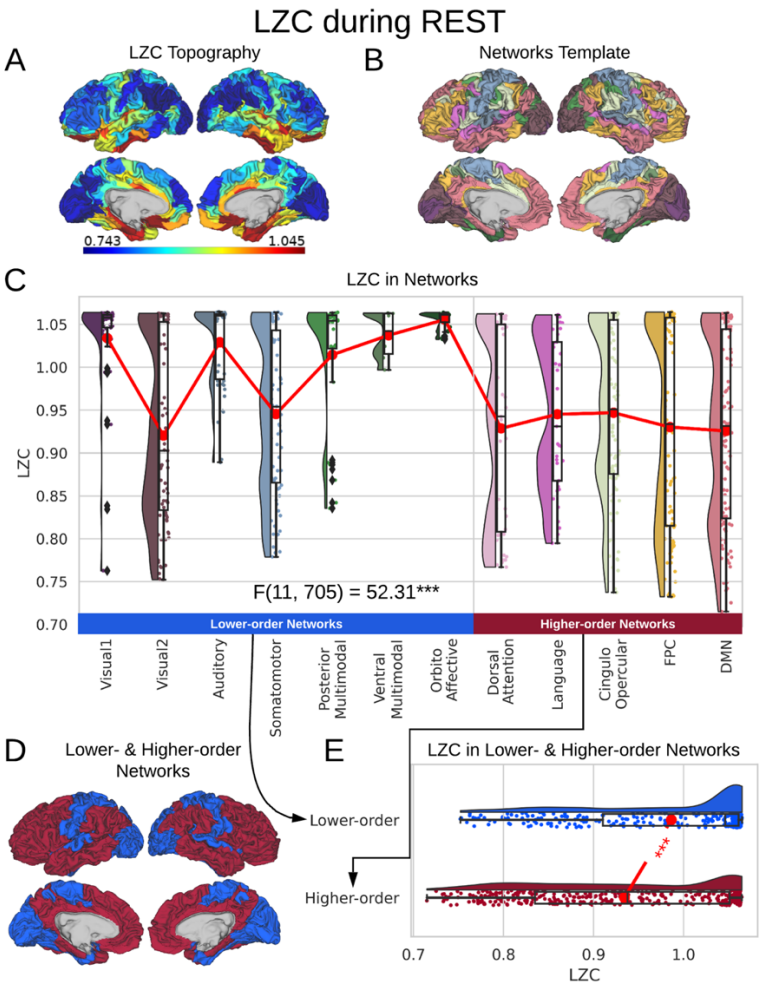

Figure 3.2: LZC during the resting state. Raincloud represent regions. (A) Spatial distribution of LZC during REST condition. LZC is calculated for a region after binarizing its BOLD signal's amplitude using the median as a threshold. (B) Brain map of the 12 networks defined in ref. [96]. Colors represent different networks. (C) Distribution of LZC values in different networks. Colors are the same as in B. Higher-order networks show lower LZC compared to lower-order ones. One-way analysis of variance (ANOVA) showed a significant ($p < 0.001$) difference among all networks ($F(11, 705) = 52.31, \eta^2 = 0.44$). (D) Brain map representing lower- and higher-order categories. (E) LZC during resting state along the lower- and higher-order categories. The student's t-test shows lower-order regions have significantly higher LZC compared to higher-order ones ($t = 6.80, d = 0.51, p < 0.001$). Stars represent the significance level ($*** \equiv \alpha = 0.001$)

3.4.2 The topography of LZC during task states

Spatial distribution of LZC was investigated during the two tasks of movie-watching (MOVIE) and retinotopy (RET) in three different ways: analysis of absolute values, spatial correlations, and analysis of percentage changes, i.e., rest-task difference. The two tasks have different complexity and temporal structure; one containing rich stimuli of movie clips viewed in long intervals and one containing very simple retinotopic stimuli viewed in short intervals. The different input structure of the two tasks suggests that they should impact the information processing in lower- and higher-order networks in different ways; showing that would further substantiate the assumption that ISF carry information.

Similar to our resting state analysis, LZC values were calculated for lower- and higher-order networks (Figure 3.3A) and their difference was statistically tested across regions. First, a two-way ANOVA with network order (2 levels: lower vs. higher) and task condition (2 levels: MOVIE vs. RET) as factors was conducted on the LZC values over the regions. The

model showed a significant ($p < 0.001$) effect of network order on LZC ($F(1, 1430) = 27.75, \eta^2 = 0.02$). Further analysis using student's t-test for each task condition, confirmed that lower-order networks have significantly higher LZC compared to higher-order ones in both MOVIE ($t = 4.36, d = 0.32, p < 0.01$) and RET ($t = 3.22, d = 0.24, p < 0.01$).

Moreover, dividing the LZC values into the 12 networks (Figure 3.3B) and conducting similar two-way ANOVA (factors: networks with 12 levels and task with 2 levels) on them also showed significant ($p < 0.001$) effect of the network on LZC values ($F(11, 2115) = 152.53, \eta^2 = 0.32$). Next, two separate one-way ANOVAs were designed to further test the effect of the network on LZC in each task. Both models showed significant $p < 0.001$ differences among the networks in LZC values (MOVIE: $F(11, 705) = 57.38, \eta^2 = 0.47$; RET: $F(11, 705) = 50.34, \eta^2 = 0.43$).

The differences in LZC between lower- and higher-order categories and also among the networks in the tasks were analogous to the previous resting state results, suggesting that the topography of LZC during task states was similar to the resting state. To test this hypothesis, we, in a second analysis, calculated the spatial correlation between the resting state (REST) and each task condition (MOVIE and RET, Figure 3.3C). For each pair of conditions, LZC values were first averaged across subjects yielding a pair of LZC maps, then the two maps were correlated over regions, using Pearson correlation, yielding a single correlation value. The result showed significantly high correlation coefficients for both MOVIE ($\alpha = 0.96, p < 0.001$) and RET ($\alpha = 0.93, p < 0.001$). These data, further support the assumption that the resting state LZC topography is preserved during the two tasks.

Even though resting state LZC topography was similar in resting and task states, we, nevertheless, observed increases and decreases in LZC during the two task states. Therefore, in a third step, we calculated the percent of LZC change from the resting state for each region. For each task, the regional LZC values were subtracted from and then divided by their corresponding resting state values ($(\text{resting state} - \text{task state})/\text{resting state}$); thus, normalizing the task state against the resting state, i.e., rest-task difference. We used the statistical models we applied during the task states, also to rest-task differences, i.e., to their percentage change values. Two-way ANOVA with network order (lower vs. higher) and task condition (MOVIE vs. RET) showed significant ($p < 0.001$) effect of network order on the percentage of change ($F(1, 1430) = 173.06, \eta^2 = 0.04$), and further student's t-test showed a higher percentage of change in higher-order networks compared to lower-order ones in both MOVIE ($t = 7.28, d = 0.54, p < 0.01$) and RET ($t = 12.04, d = 0.90, p < 0.01$). On the network level, similar to task analysis, significant ($F(11, 1410) = 34.39, \eta^2 = 0.07, p < 0.001$) effect of the network in a two-way ANOVA model (network and condition) was followed by significant differences among the networks in two separate one-way ANOVAs for MOVIE ($F(11, 705) = 26.55, \eta^2 = 0.29, p < 0.001$) and RET ($F(11, 705) = 20.54, \eta^2 = 0.24, p < 001$).

Although percentage of LZC change was statistically different between lower- and higher-order categories (Figure 3.3D), and over the 12 networks (Figure 3.3E), it presented distinctive results for the two tasks. In the MOVIE, positive values

(decrease in LZC from REST to MOVIE) were observed in visual, auditory, and language networks. In contrast, LZC values were prominently increased from REST to our second task, i.e., RET (negative percentage of change) in all networks. Taken together, LZC topography during rest along the lines of lower- and higher-order networks is largely preserved during and thus carried over to the different task states. Additionally, one can nevertheless observe task-related changes in LZC once one subtracts task from rest; these concerned LZC differences between lower- and higher-order networks during the tasks. Hence, task-related LZC changes seem to loosely reflect the different input structures of our two tasks, which further supports the assumption that ISF do indeed carry information.

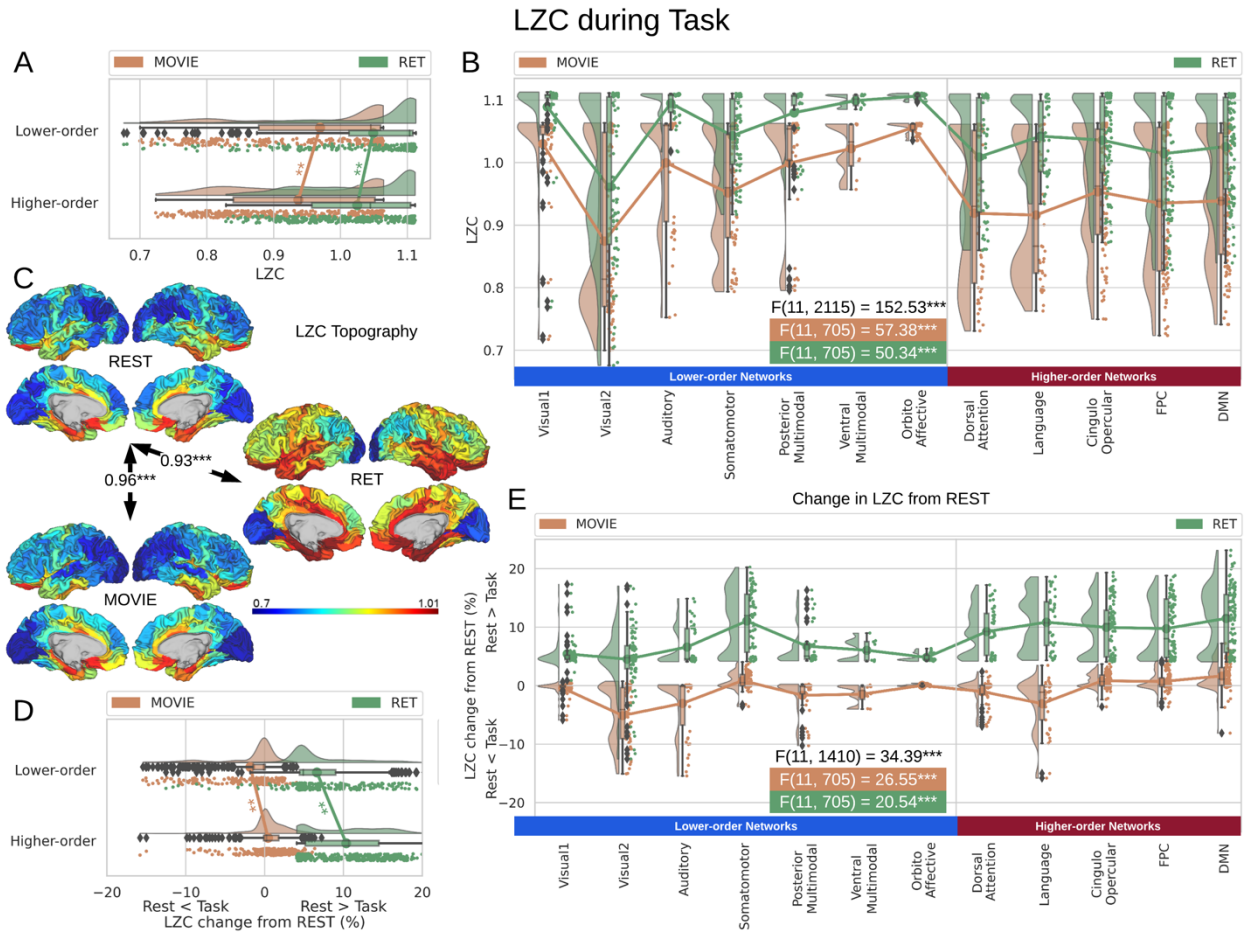

Figure 3.3: LZC during the task states. Points in the rain plots represent regions. (A) LZC during MOVIE and RET for lower- and higher-order networks. The paired student's t-test between lower- and higher-order networks is significant with $t = 4.36, d = 0.32$ *for MOVIE and* $t = 3.22, d = 0.24$ *for RET. (B) LZC during the two task conditions for the 12 networks. Three separate ANOVA models (One over the whole data, one for only the MOVIE, and one for only the RET data) showed significant differences among the networks. (C) Spatial distribution of LZC during REST, MOVIE and RET conditions alongside their corrected spatial correlation coefficients. The correlation is calculated over the regions to show the spatial similarity between resting and task states. (D) Change in LZC from REST to both task conditions for lower- and higher-order networks. Similar to task state results, the change was also significantly different between the two categories. (E) Change in LZC from REST to MOVIE and RET is also significantly different among the 12 networks. Stars represent the significance level (*** ≡* $\alpha = 0.001$, ** ≡ $\alpha = 0.01$*).*

3.4.3 Temporal dynamics - Median Frequency in rest and task states

To link the LZC in resting and task states to the ISF themselves, we characterized the distribution of their power spectral density (PSD) using the Median frequency (MF). MF is defined as the frequency which divides the area under the power spectral density into two halves. It was chosen to provide a summary measure of the distribution of low versus high frequencies in the PSD of ISF (Figure 3.4A, see also Methods for the details).

Calculating MF over different brain networks revealed a topographical distribution analogous to the one of LZC (Figure 3.4B and Figure 3.4C). Student's t-test showed significantly ($p < 0.001$) higher MF in lower-order networks compared to higher-order ones in both resting ($t = 6.96, d = 0.52$) and task states (MOVIE: $t = 5.77, d = 0.43$; RET: $t = 6.07, d = 0.45$). Furthermore, tested with one-way ANOVA, the topographical distribution was also significantly ($p < 0.001$) different among the 12 networks (REST: $F(11, 705) = 28.37, \eta^2 = 0.30$; MOVIE: $F(11, 705) = 28.26, \eta^2 = 0.30$; RET: $F(11, 705) = 33.00, \eta^2 = 0.33$). These results are also replicated in the 3T dataset (Supplementary Figure 3.2). Together, these results show that the topographical differentiation of lower- and higher-order networks also holds on temporal grounds, namely based on the power spectral density of the ISF as measured by MF.

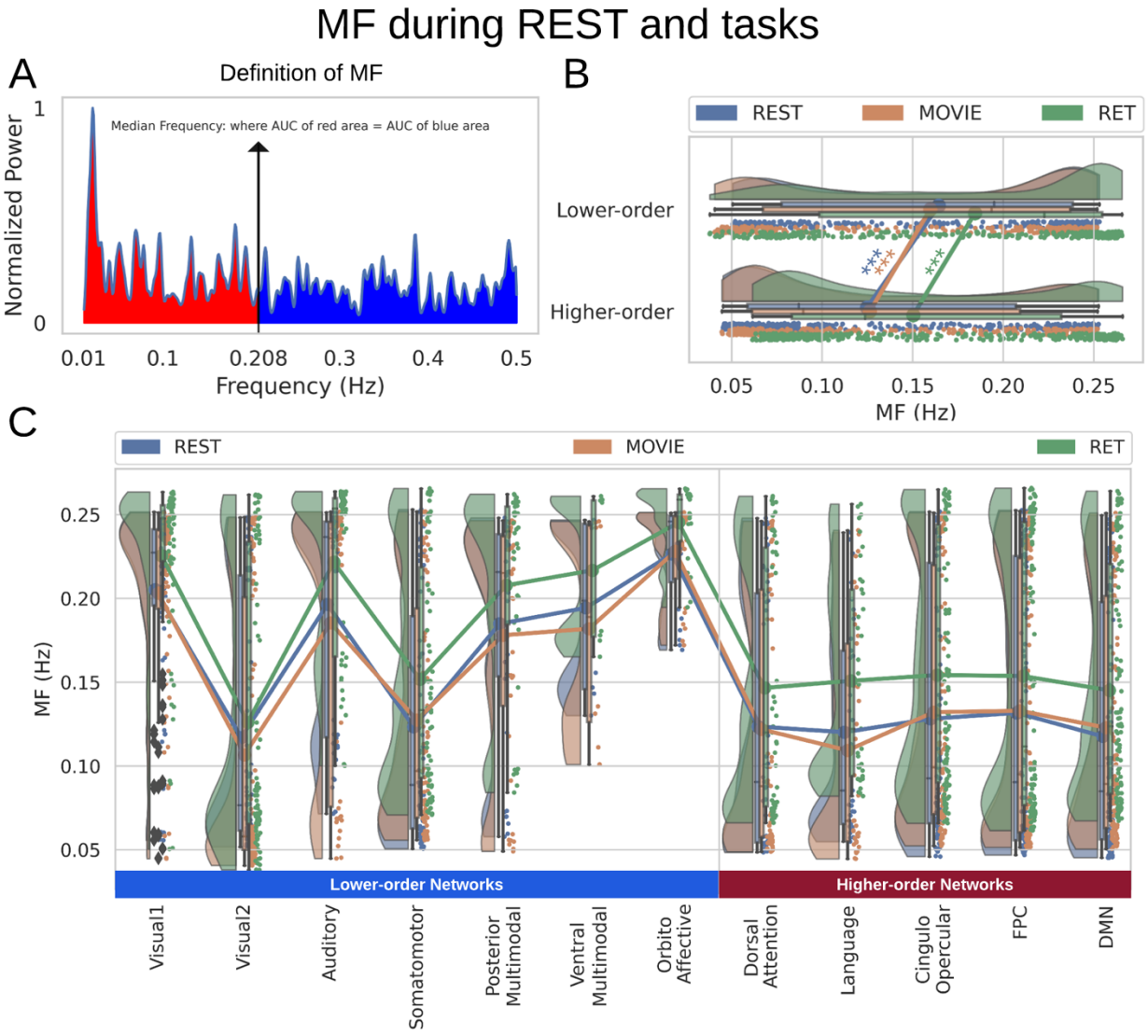

*Figure 3.4: MF during both resting and task states. Points in the rain clouds represent regions. Stars represent the significance level (*** ≡ $\alpha = 0.001$). (A) A power spectrum of a sample signal. Median frequency is calculated as the frequency at which the area under the curve (AUC) of power up to that frequency (red area) is equal to AUC beyond that point (blue area). (B) Similar to LZC, MF is significantly higher in lower-order networks compared to higher-order ones. (C) MF is also significantly different among the 12 networks during both resting and task states.*

3.4.4 The relationship between LZC and MF

The similarity in the topographical distribution of LZC and MF raises the question of their relationship. Specifically, it allows us to address our second key questions, namely "how" ISF process information. This was addressed in four steps. First, for each condition (REST, MOVIE, or RET) we calculated the regional correlation between LZC and MF. Regional correlation is calculated per region across subjects as the Pearson correlation between LZC and MF values (Figure 3.5A). The p-values were corrected for multiple comparisons using the False Discovery Rate (FDR) method at $\alpha = 0.05$ while non-significant coefficients were ignored. This revealed a variety of correlation values for the LZC-MF relationship across the wide range of 0.43 to 0.88 across the different regions. Given such a wide range of correlation values, we assumed that topographical differences strongly shape the LZC-MF relationship; this was addressed in subsequent analyses.

In the second step, the LZC-MF relationship was explored in more detail by looking at their values in different brain regions. First, both LZC and MF values were averaged over subjects and then each region's LZC value was plotted against its corresponding MF value (Figure 3.5B). This suggested a non-linear regime between LZC and MF over brain regions across all three conditions. Specifically, we observed that regions with lower MF in rest exhibit largely different LZC values in both rest and task whereas regions with higher MF in rest no longer showed marked LZC differences in both rest and task. Together, this amounts to a non-linear relationship in the topography of LZC and MF with high and low MF exerting different impacts on LZC (also replicated in 3T dataset in Supplementary Figure 3.3).

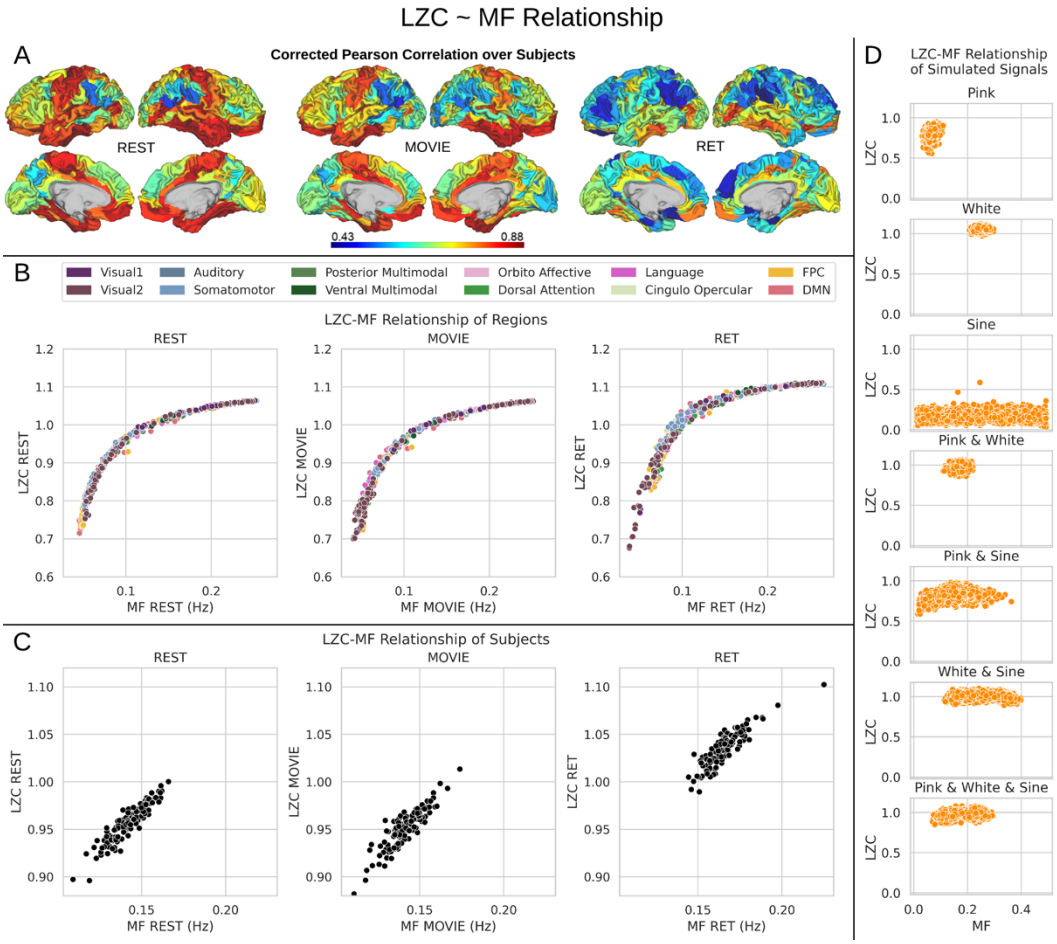

Figure 3.5: The relationship between LZC and MF. (A) Regional Pearson correlation between LZC and MF for the three conditions of REST, MOVIE and RET. The p-values are corrected using the FDR method at $\alpha = 0.05$. The wide range of correlation values (0.43 - 0.88) suggests topographical differences affect the LZC-MF relationship. (B) Regional scatter plots of LZC-MF relationship for the three conditions. Each point is a region averaged over subjects, and the colors show the regions belonging to specific networks. All plots show LZC as a nonlinear function of MF. (C) Scatter plots of LZC-MF relationship for different subjects in the three conditions. Each point is a subject averaged over regions. The nonlinear relationship can no longer be observed. (D) Simulation of the LZC-MF relationship with seven different types of signal. Each plot shows the distribution of LZC as a function of MF for 5000 simulated signals. The non-linear relationship cannot be observed in the simulated signals suggesting that it is unique to the brain signal.

We tested whether this non-linear relationship is specifically related to the topographical distribution of LZC and MF (topographical relationship) rather than inter-individual differences between subjects (Step 3). To do so, LZC and MF values were averaged over all regions leaving a pair of MF and LZC values per subject (subject-based relationship). This (Figure 3.5C) revealed a relationship different from the topographical one, suggesting a linear trend for the subject-based relationship of LZC and MF: the higher the MF in a specific individual (across all its regions), the higher its LZC (across all its regions, Figure 3.5C). One caveat is that the range of value for the calculation of inter-individual LZC-MF relationship is lower than the one in our regional topographic LZC-MF; for that reason, we cannot fully exclude potential non-linear regime in inter-individual LZC-MF relationship.

As the fourth step, the LZC-MF relationship was further explored by using the brain's T_1w/T_2w values (see Methods) to test whether it is structurally based. T_1w/T_2w is suggested to provide a non-invasive proxy of anatomical hierarchy in primate cortex [161]. For both LZC and MF, each region's values were averaged over subjects and then the regional

distribution was plotted as functions of T_1w/T_2w values (Supplementary Figure 3.4A for LZC and B for MF). This also failed to show the specific topographical relationship between LZC and MF observed previously. That suggests the non-linear relationship of LZC and MF to hold independent of their underlying anatomical relationship; we thus assume that the non-linear topographical LZC-MF relationship is primarily driven by the dynamics of ISF, rather than being based on structural anatomical grounds (also replicated in 3T dataset in Supplementary Figure 3.3).

3.4.5 Simulation of the relationship between LZC and MF

As a final confirmatory analysis to show the truly topographical nature of the non-linear LZC-MF relationship, we decided to analyze simulated data. Seven different categories of pseudo-aleatory signals (without any topographical distribution) were simulated in the same frequency range (0.01-0.5) as our data with the same sampling rate. The categories were pink noise, white noise, sine wave, and their linear combinations (e.g. white and pink noises or white noise and sine wave). Each category contained 5000 signals (total of 35000, see Supplementary Figure 3.5 for a sample signal in each category) with different combinations of power set randomly in the same ranges as the real signals.

Pink noise was utilized to simulate scale-freeness [99], sine wave for oscillation and white noise for pure randomness. The parameters for each signal and the weights for their linear combinations used random values chosen from uniform distributions to bound the signals in the predefined frequency range of our real data. Calculating LZC and MF on these signals and plotting them against each other (Figure 3.5D) showed no specific relationship between the two measurements. These results, thus, suggest that the non-linear relationship between MF and LZC is related to the topographical distribution of low and high MF values in different brain regions rather than remaining independent of such topographical distribution. These results also provide evidence for the dissociation between LZC and MF, as the correlation between them is different depending on the signals assessed. Moreover, our simulation shows that LZC is not measuring noise in the BOLD signal of fMRI.

3.4.6 The relationship between LZC change from resting state and MF during resting state: the dynamic range of LZC

Is the change of LZC from rest to task in specific regions dependent upon the power spectral density, i.e., MF, of that particular region? Answering this question will allow us to address our second key question, namely "how" ISF process information. If rest MF mediates LZC rest-task differences, one would strongly assume that the power spectral density (MF) of ISF processes changes in information load during the transition from resting to task state as measured by LZC. We, therefore, investigated how the degree of change in LZC from resting to task state is related to the power spectrum during rest (MF-REST). The "change" values of all regions were plotted against their corresponding MF values during rest (MF-REST) for both task conditions (Figure 3.6A). Careful consideration of these plots alongside a mediation analysis of LZC with MF as a mediator (see supplementary results for details) suggested that there is a relationship between the range of change in LZC values and MF-REST.

Following that, we decided to conduct a median-split of the MF-REST values across brain regions. That served the purpose of calculating the "change" values in dependence on low MF-REST and high MF-REST. Plotting both categories with box plots (Figure 3.6B), revealed a large difference in the range of change in LZC values (i.e. the range of change in LZC from resting to task states) between low and high MF-REST categories. To test whether this difference is significant or not, the "change" values of each subject were divided into two categories of low and high MF-REST. Then, the significant ($p < 0.001$) difference between the two was confirmed by Student's t-test over subjects (MOVIE: $t = 33.73, d = 3.47$; RET: $t = 46.00, d = 5.52$).

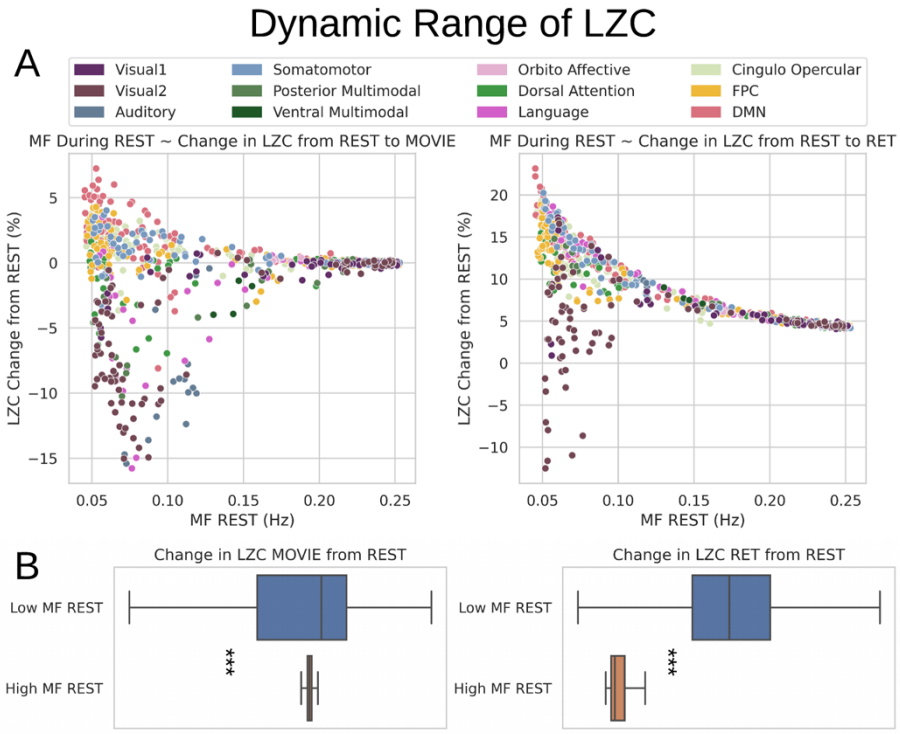

*Figure 3.6: The relationship between the change in LZC from REST and MF during REST. (A) The scatter plot of MF-REST (x-axis) vs. the change in LZC (y-axis) from REST to MOVIE (left) and RET (right). The plots indicate a decrease in the range of the "change" as a function of MF-REST. (B) Box plots showing the range of the "change" values for low-MF and high-MF during REST. MF-REST was median-split into low and high categories. Statistics were conducted using student's t-test over subjects. For each subject, a range of LZC change was calculated in low and high MF categories. For both conditions (MOVIE and RET) the range of LZC change in low-MF is significantly wider than high-MF. Stars represent the significance level (*** ≡ $\alpha = 0.001$).*

These data suggest that the range of LZC change values in low MF-REST regions is significantly higher than in high MF-REST regions. Together, these results suggest that the range in which the region's LZC can change is associated with the level of MF-REST (low or high). Therefore, we speak of a dynamic range of LZC which we hypothesize to be related to PSD of the region as indexed by MF: low rest MF yields a large dynamic range of LZC, i.e., a wide range of rest-task differences among its regions, while high rest MF is related to small a dynamic range of LZC, i.e., narrow range of rest-task differences among its regions.

To further test the dynamic range of LZC, we incorporated a moderation model to see if MF-REST being low or high can moderate the relation between LZC during rest and task states. A binary moderator variable (Z) for MF-REST being

low (Z = 0) or high (Z = 1) was defined. Then, the effect of LZC-REST and Z was explored on LZC during the two task conditions using linear regression (see Methods for details). The model showed significant moderation of the LZC rest-task relationship with MF-REST being low or high. For MOVIE the effect of the moderator was 0.08 ($t = 9.63, p < 0.001$). Likewise, for RET the effect of the moderator was 0.42 ($t = 44.52, p < 0.001$). In other words, our moderation analysis suggests that the effect of LZC during REST on LZC during MOVIE (or RET) is moderated by MF during REST.

Taken together, these results show strong evidence for the relationship of MF and LZC in a non-linear topographical way. The level of MF in a region's resting state drives its propensity for change in its information processing during the transition from resting to task state as measured by LZC. Regions with low rest MF indicating strong power in the very slow ranges of ISF can yield a larger spectrum of LZC changes during the task (relative to rest) than regions with high MF. Hence, the very slow frequency ranges of resting state MF seem to foster larger dynamic ranges in the regions' information processing as manifest in rest-task differences. This addresses our second key question, namely "how" ISF process information: they process information through their power spectral density as indexing their "velocity" or "speed".

3.4.7 Replication with 3T data

Topographical resting state LZC/MF of 3T data. 3T resting state data was analyzed using the same procedure as our 7T data (Supplementary Figure 3.1 for LZC and Supplementary Figure 3.2 for MF). The difference between lower- and higher-order networks was statistically tested with student's t-test between the two across regions which showed that both LZC and MF is significantly ($p < 0.001$) higher (LZC: $t = 3.60, d = 0.27$; MF: $t = 5.30, d = 0.40$) in lower-order networks compared to higher-order ones. Furthermore, LZC and MF were also significantly ($p < 0.001$) different among the 12 networks tested with one-way ANOVA (LZC: $F(11, 705) = 44.15, \eta^2 = 0.40$; MF: $F(11, 705) = 52.22, \eta^2 = 0.44$). These results validate our original topographical findings.

The relation between LZC and MF in 3T data. As another confirmatory analysis, the relationship between LZC and MF was investigated in resting state 3T data. Like before, first the two measurements were correlated with each other using Pearson methods (Supplementary Figure 3.3A). Moreover, LZC was plotted as a function of MF both for each region (Supplementary Figure 3.3B left) and for each subject (Supplementary Figure 3.3B right). The non-linear relationship over the brain regions was again observed in the 3T data. Both regional (averaged over subjects) LZC and MF were separately plotted as functions of T_1w/T_2w values which didn't show any specific non-linear relationship (Supplementary Figure 3.3C). Taken together, these results replicate our findings on LZC and MF relationship.

3.5 Discussion

We here investigate the role of ISF in information processing by addressing "whether" and "how" ISF carry and process information in resting and task state fMRI. Our main findings in both main (7T HCP) and replication (3T HCP) data sets are: (I) significantly different resting state LZC and MF in lower- and higher-order networks with the latter showing

lower LZC and MF values; (II) task-related LZC changes during different tasks in lower- and higher-order networks; (III) non-linear topographical relationship of LZC and MF with regions showing lower rest-MF values being related to lower resting state LZC and larger capacity for task-rest changes in LZC. Together, these findings provide evidence that ISF carry and process information (LZC) through their power spectral density, i.e., 'velocity' or 'speed' (MF).

3.5.1 Do ISF carry information? Topographical differences in complexity and dynamics of lower- and higher-order networks

The first key question is "whether" ISF carry information. Our findings strongly suggest that this is indeed the case. We show different degrees of LZC in different networks during the resting state. Higher-order networks like the DMN, FPN, language, and dorsal attention exhibit lower values of LZC in the resting state. In contrast, lower-order networks like sensory networks, orbito affective, and multimodal show high LZC values. Hence, taken together, the ISF signal is more regular and more compressible, i.e., lower LZC, in higher-order networks than in lower-order networks. More generally, this means that lower-order networks carry more information in their signal, i.e., it cannot be as much compressed as measured by LZC, than higher-order networks with their lower LZC.

Our findings complement previous results that show analogous differences between lower- and higher-order networks. Spatially, lower-order networks are more locally connected while higher-order networks are more globally connected throughout the whole brain. This led, recently, to the so-called core-periphery organization [52], [54]: Lower-order unimodal networks like sensory networks are at the periphery while higher-order transmodal networks like DMN and FPN constitute the core as they are connected throughout the whole brain. Recent data suggest such core-periphery organization to be mirrored also in the brain's temporal organization as its intrinsic neural timescales are shorter in the lower-order networks, i.e., the periphery, and longer in the higher-order networks, i.e., the core [27], [28], [67], [68], [79], [166]. Our data extend these findings by showing that lower- and higher-order networks carry different degrees of information (LZC) which converges with corresponding differences in their temporal dynamics (MF). This, suggests that intrinsic information processing (LZC) and brain dynamics (MF) converge in the topographical differentiation of lower- and higher-order networks.

The differential role of lower- and higher-order regions in information processing is further supported by our results in task states. We observed network- and task-specific changes during the two tasks relative to the resting state. Together, extending previous findings [137], the observed task-rest differences in LZC further support the assumption of task- and network-specific changes in LZC and, more generally, the involvement of ISF in carrying information in both resting and task states.

3.5.2 How do ISF process information? ISF process information (LZC) through their temporal dynamics (MF)

So far, we have addressed the question of "whether" ISF carry information. That was addressed by demonstrating that the ISF show topographical differences in LZC during rest and task which follows the well-established information

hierarchy of lower- and higher-order networks. This leaves open "how" the ISF process information, that is, through what underlying mechanism? To address this question, we included median frequency (MF) as a measure of brain dynamics operating by the characterization of the PSD distribution. We saw a similar topographical pattern in MF as in LZC. This suggests a close relationship of LZC and MF meaning that the power spectral density of ISF may mediate and thus process their information. Probing this assumption, we tested various correlation and simulation models.

Spatial correlation confirmed such a close relationship; however, regional MF-LZC correlation revealed quite a variety of different degrees in their correlation within the different regions. Such a wide variety of LZC-MF correlations across different regions suggests a differential relationship of regions with low and high MF to LZC. This was confirmed by subsequent analyses. We obtained a non-linear topographical pattern in the LZC-MF relationship in both rest and task states. Regions with low MF at rest showed lower rest LZC and more differentiation in their respective LZC rest-task changes than those regions exhibiting high rest MF. We could further demonstrate that such non-linear relationship is related specifically to the topographical distribution of low and high MF values rather than being associated with inter-individual differences, anatomical differences in T_1w/T_2w of the different regions, or some other kinds of LZC-MF relationship independent of their topographical distribution (as tested for in simulation).

Further, we observe that the MF is related to the range of possible LZC rest-task changes. Regions with low MF values during rest show much larger changes in their rest-task LZC values than those with high MF (see supplementary results). Hence, MF in rest seems to modulate the capacity for change in LZC during the transition from rest to task: regions with low MF and thus more power in the slower ISF ranges have a higher likelihood of exhibiting larger changes in their information processing, i.e., increases or decreases, during the transition from rest to task states. Hence, it is the brain dynamics of the different regions' resting state rather than the regions themselves (independent of their dynamics) that is related to the topographical distribution of LZC during rest and task.

How can brain dynamics (MF) during rest modulate and shape information processing (LZC) in ISF? Low values in MF reflect stronger power in the very infraslow frequency fluctuations which can be characterized by extremely long cycle durations. These long cycle durations are assumed to be ideal for summing and pooling different stimuli occurring at different points in time such that their respective information is processed and thus lumped together [55], [91], [105], [108], [110]. Such summing and pooling may thus enable higher degrees of integration of temporally distinct stimuli. That, in turn, leads to less complex signal dynamics with lower LZC values. One would consequently expect that regions showing lower values in MF should also exhibit lower LZC values which is exactly what we observed in our data.

This supposed modulation of the LZC-MF relationship by the pooling and summing of stimuli through cycle duration may also account for the observed differences in the rest-task changes of the LZC in regions with low and high rest MF. Given the inverse relationship between power and frequency, i.e. the scale-freeness of the brain oscillations [99], if a region shows low MF, the power of its long cycle duration is stronger than the one of a region with higher MF. That may

allow the low rest MF region to pool, sum, and ultimately integrate more external stimuli during task states [91] than a region with high rest MF. This, in turn, changes the degree of that region's complexity and thus its LZC to a large degree. This stands in contrast to a high rest MF region that, due to its lower power in the long cycle duration, cannot pool and sum as many external stimuli and consequently cannot as much change its LZC from rest to task. That remains to be tested in future modelling studies though.

3.5.3 Limitations

There are a few considerations that should be considered in this study. First, task-unspecificity should also be replicated using different tasks in different modalities and domains; however, concerning our metrics, we included two tasks with completely different complexity and temporal structure. The movie presents a continuous task while the retinotopy is an event-related trial-based discontinuous task. The inclusion of tasks with two different structures accounts for the recent suggestion [167] of considering and including tasks with different structures, i.e., continuous vs. trial-based. Second, this study contains no behavioral measurement, but on the other hand, the tasks measured pure perception and stimulus processing with no interference of cognitive demands, thus no-report paradigms as distinguished from report paradigms [168]. The reliance on no-report paradigms allowed to isolate stimulus-related effects, i.e., movie and visual stimuli during retinotopy, as they are supposed to be related to, specifically, primary sensory networks like visual and auditory networks. Hence, the no-report paradigms are ideal to test the response of primary networks independent of any task-related confounds as in report paradigms. Third, the frequency of the retinotopic stimuli might impact the median frequency. Investigating this idea is beyond the scope of this work and is an interesting topic for further research.

3.6 Conclusion

The infraslow frequency fluctuations (ISF) are more powerful than faster frequencies but less well understood. Here we investigate "whether" they carry information (LZC) and, if so, "how" they mediate information processing, namely through which of their features. In addressing the first question, our findings strongly support that ISF carry information as the LZC shows differences in lower- and higher-order networks in rest and task states as well as task-specific and -unspecific changes. Moreover, responding to the second question, we demonstrate that the degree of LZC rest-task changes is driven by rest MF levels in a non-linear topographical way. This suggests that ISF carry and process information (LZC) through their temporal dynamics, i.e., power spectral density as an index of their 'velocity' or 'speed'. In conclusion, our findings demonstrate that ISF carry and process information through their temporal dynamics supporting the recently introduced concept of "Spatiotemporal Neuroscience" [32], [33].

3.7 Supplementary Material

3.7.1 Validation of LZC statistical tests through non-parametric testing

To further validate our previous main results, nonparametric testing was also performed for our resting and task state results. The difference in resting state LZC values among the networks was tested using Kruskal-Wallis non-parametric test which showed significant ($p < 0.001$) differences among the 12 networks ($H = 141.45, \eta^2 = 0.19$). Mann-Whiney

test also showed significant ($p < 0.001$) differences between resting state LZC values of lower- ($n = 331, median = 1.05$) and higher-order ($n = 386, median = 0.94$) categories ($U = 83476.50, \eta^2 = 0.07$).

Our task state results were also validated using non-parametric testing. First, lower- and higher-order task data were divided into four combinations of task (MOVIE vs. RET) and category (lower- vs. higher-order) factors. Kruskal-Wallis test showed significant ($p < 0.001$) differences among these four categories ($H = 321.99, \eta^2 = 0.22$). In order to further validate the difference between lower- and higher-order categories, two separate Mann-Whiney tests (one for each task) were performed validating our previous results in both MOVIE ($U = 77071, \eta^2 = 0.03, n_1 = 331, median_1 = 1.05, n_2 = 386, median_2 = 0.94$) and RET ($U = 80296, \eta^2 = 0.05, n_1 = 331, median_1 = 1.10, n_2 = 386, median_2 = 1.04$) with adjusted $p < 0.001$.

The difference among the 12 networks in the two tasks was also validated first by dividing the LZC values into 24 categories (12 networks x 2 tasks) and then performing Kruskal-Wallis test. The non-parametric test revealed significant differences ($p < 0.001$) differences among the categories ($H = 504.59, \eta^2 = 0.34$). In the next step the effect of network alone was investigated with two separate Kruskal-Wallis tests: each one the LZC values of a specific task over all the 12 networks. These two tests also validated our previous results indicating significant ($p < 0.001$) differences of LZC values among the networks in MOVIE ($H = 133.87, \eta^2 = 0.17$) and RET ($H = 144.78, \eta^2 = 0.19$).

3.7.2 Rest to task mediation analysis

To explore whether MF during rest has any effect on the change in LZC from rest to task state, we performed a mediation analysis on the LZC and MF-REST values (Supplementary Figure 3.6). In the model, the effect of LZC-REST on LZC-MOVIE (LZC-RET) was investigated considering MF-REST as the mediator. This allowed us to explore whether the relationship between LZC during REST and MOVIE (RET) is mediated by MF during REST. The indirect effect was 0.84 * 0.23 = 0.17 (-1.01 * 0.34 = -0.34). We tested the significance of this indirect effect using bootstrapping procedures [163] in the mediation library [162] of R. Unstandardized indirect effects were computed for each of 1000 bootstrapped samples, and the 95% confidence interval was computed by determining the indirect effects at the 2.5th and 97.5th percentiles.

The bootstrapped unstandardized indirect effect was 0.16 (-0.24), and the 95% confidence interval ranged from 0.10 to 0.22 (-0.29 to -0.19). Thus, the indirect effect was statistically significant ($p < 0.001$) showing that MF-REST can indeed be considered as a partial mediator for the change in LZC from rest to task states. It is worth to mention that the mediation analysis was performed with (the above results) and without averaging over subjects to control for the inter-individual effect in bootstrapping. In the with-averaging analysis, first, the data was averaged over subjects then fed into the model, but in the latter one, the subject-level data was used.

In the without-averaging model, the subject-level data was fed into our mediation model. Like before, LZC-REST was used as the independent variable, LZC-MOVIE (LZC-RET) as the dependent one and MF-REST as the mediator. The indirect effect was 0.64 * 0.33 = 0.21 (-0.64 * 0.14 = -0.08). The bootstrapped unstandardized indirect effect was 0.21 (-0.09), and the 95% confidence interval ranged from 0.21 to 0.22 (-0.099 to -0.09). Thus, the indirect effect was statistically significant (p<0.001), confirming our original with-averaging results.

3.7.3 Supplementary Figures

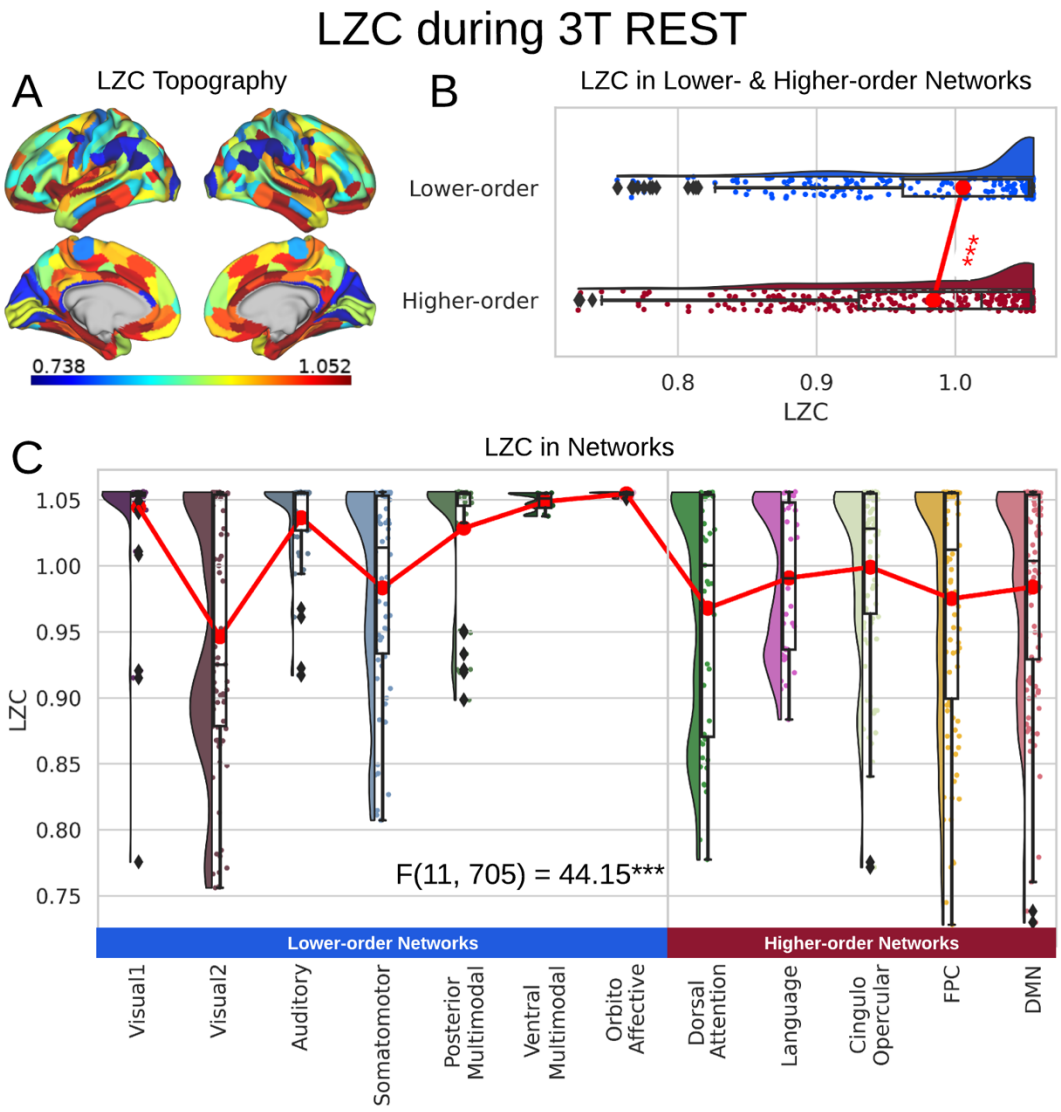

Supplementary Figure 3.1: LZC during the 3T resting state. Raincloud represent regions. (A) Spatial distribution of LZC during 3T REST condition. (B) LZC during rest for lower- and higher-order networks. Student's t-test showed significant ($p < 0.001$) differences between lower- and higher-order networks ($t = 3.60, d = 0.27$). This was also validated using Mann-Whiney non-parametric test ($U = 77278, \eta^2 = 0.03$) (C) LZC during REST for the 12 networks. One-way ANOVA showed a significant ($p < 0.001$) difference among the networks ($F(11,705) = 44.15, \eta^2 = 0.40$) which was also validated using Kruskal-Wallis non-parametric test $H = 129.46, \eta^2 = 0.17$). Stars represent the significance level ($*** \equiv \alpha = 0.001$).

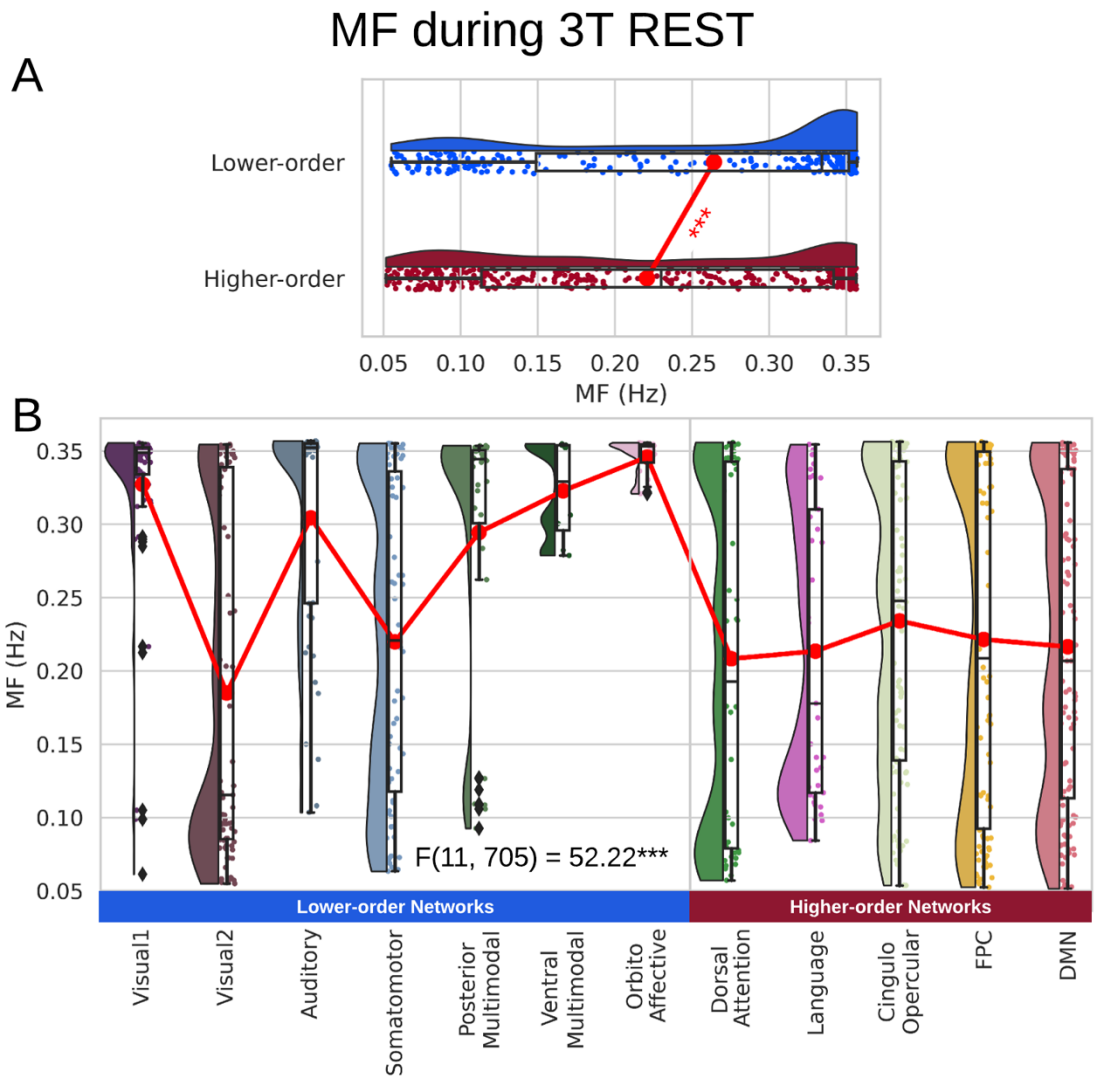

Supplementary Figure 3.2: MF during the 3T resting state. (A) MF during rest for lower- and higher-order networks showing higher MF in lower-order networks. (B) LZC during rest for the 12 networks. One-way ANOVA showed a significant difference among the networks.

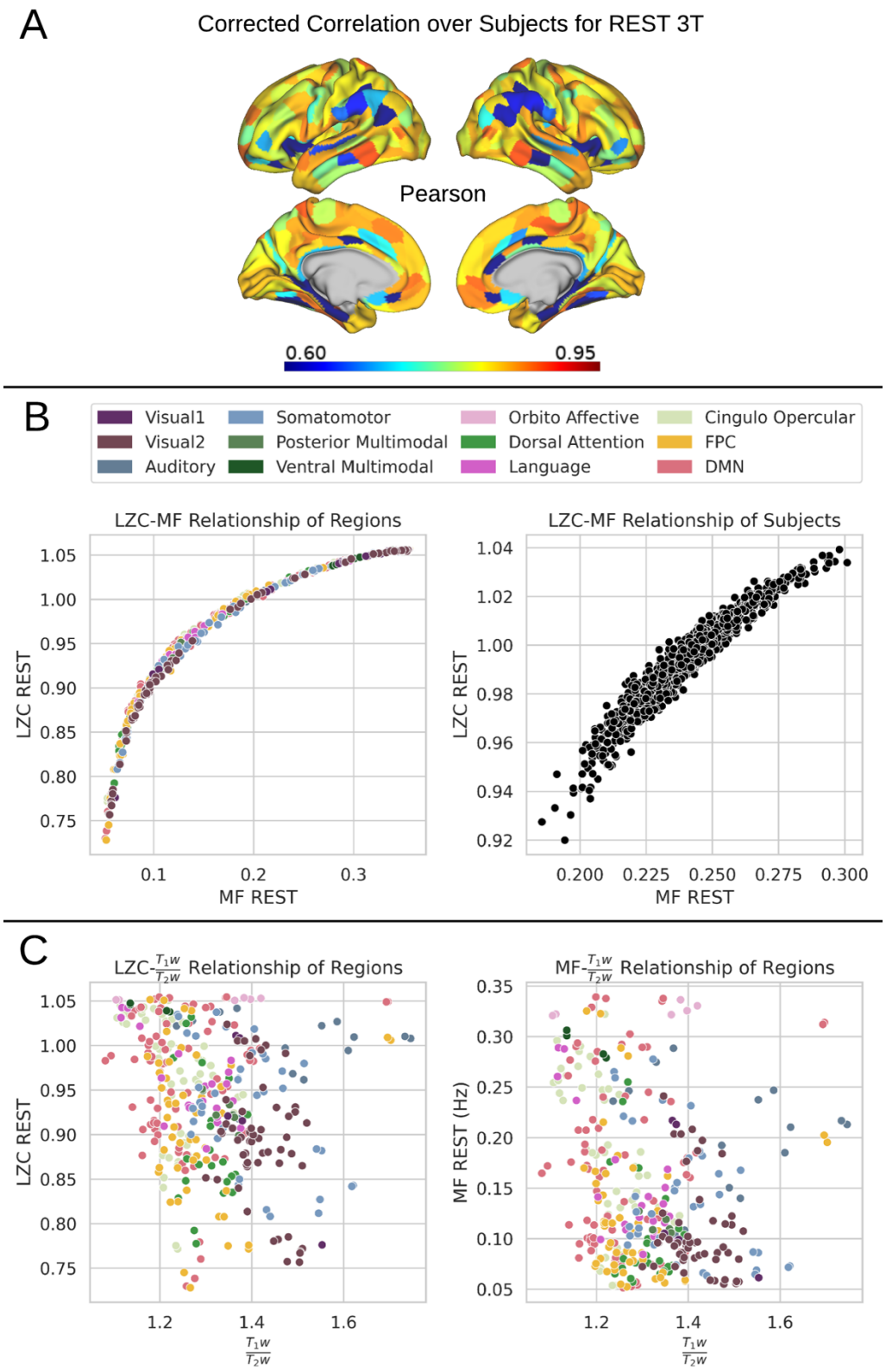

Supplementary Figure 3.3: The relationship between LZC and MF during 3T resting state. (A) Regional correlation between LZC and MF was computed by the Pearson method and corrected for multiple comparisons by the FDR method. (B) Regional scatter plots of LZC-MF relationship during 3T REST. LZC is plotted as a function of MF. Left shows scatter plot of regions averaged over subjects. Right shows subjects averaged over regions. (C) Scatter plots of LZC (left) and MF (right) as functions of structural T_1w/T_2w T_1w/T_2w values. Each point is a region averaged over subjects.

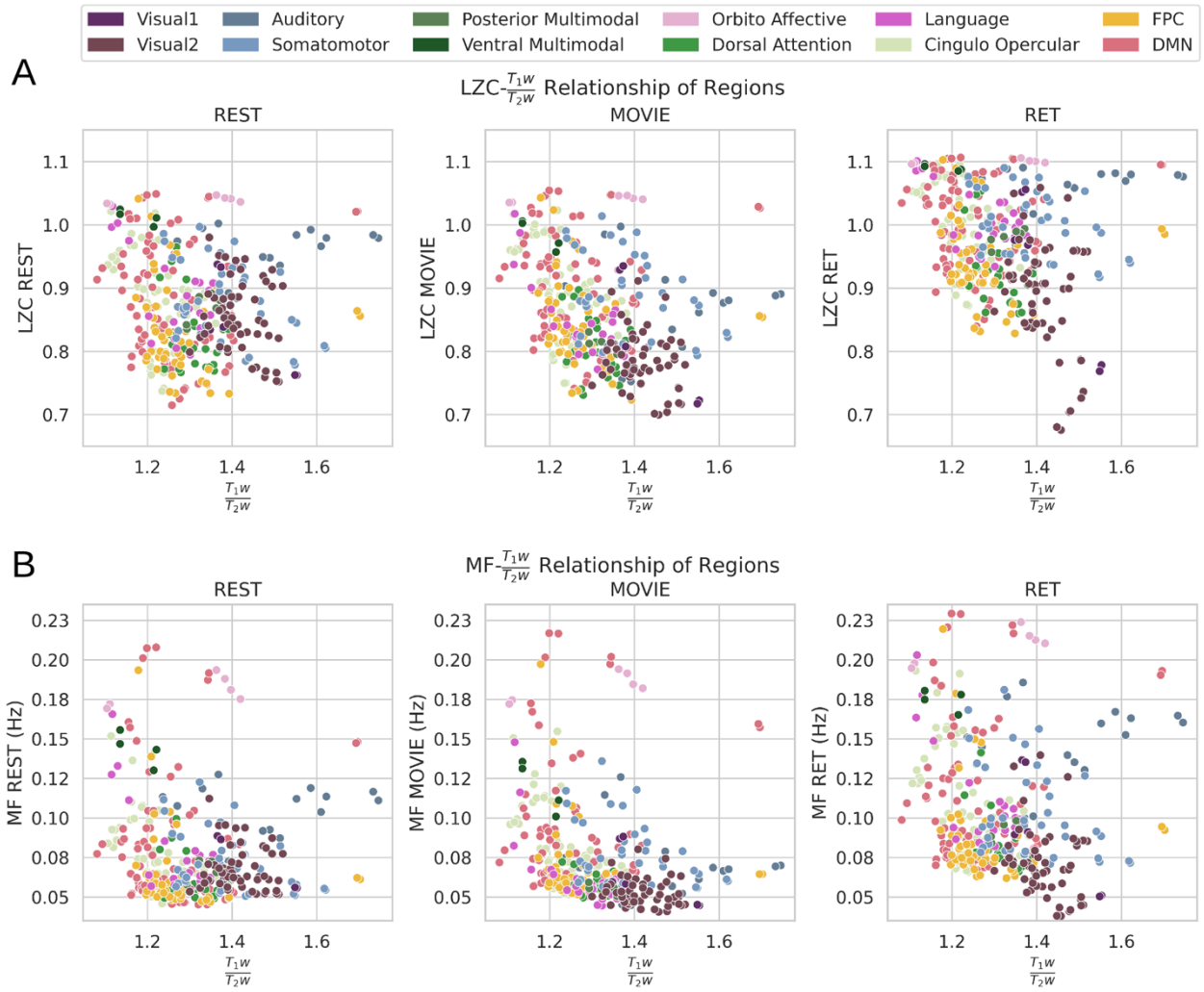

Supplementary Figure 3.4: LZC/MF relationship with T_1w/T_2w. The relationship between structural T_1w/T_2w values and LZC/MF. The distribution of LZC (A) and MF (B) values were calculated for each region and plotted as functions of their corresponding T_1w/T_2w values in all three conditions of REST (left), MOVIE (middle) and RET (right). No non-linear relationship can be observed.

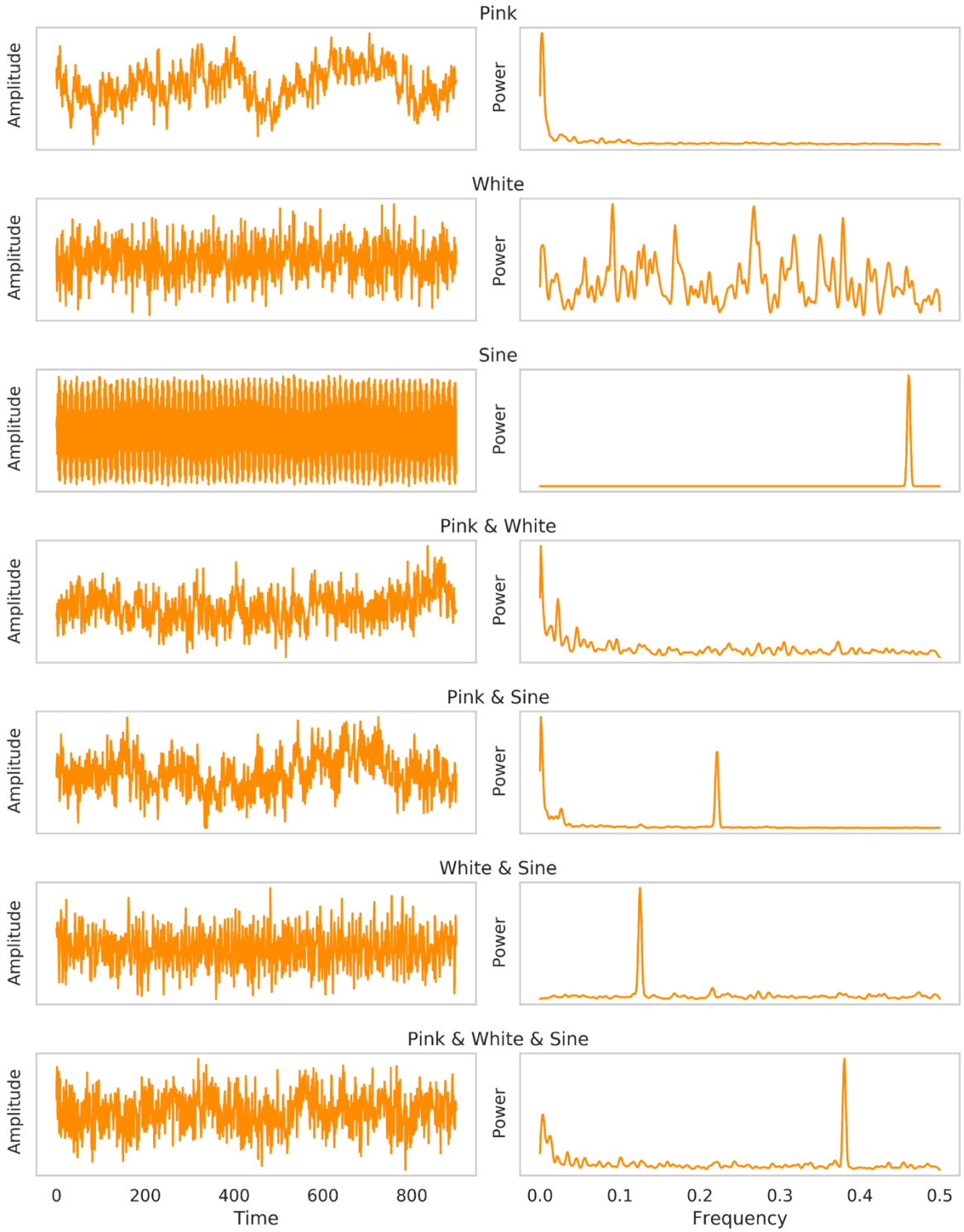

Supplementary Figure 3.5:Sample simulated signals in each category. Left plots are the sample signals in the time domain and the right ones are the same signals in the frequency domain (their power spectral distribution). For each category 5000 similar signals with different parameters were calculated and used in our LZC-MF relationship analysis.

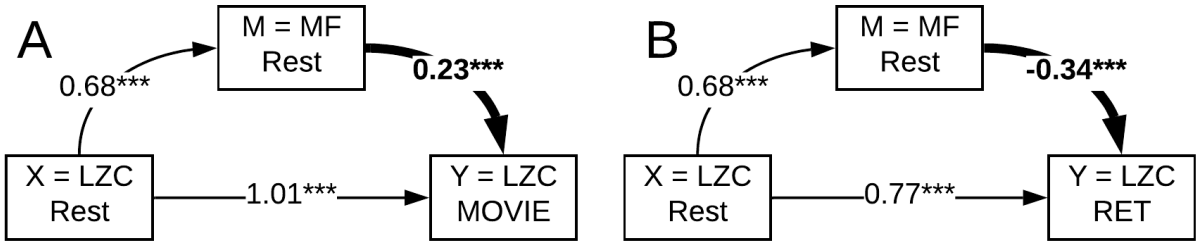

Supplementary Figure 3.6: Mediation model to investigate the role of MF-REST in the change in LZC from resting to task state. LZC-REST is used as the independent variable and the model investigates whether the effect of LZC-REST on LZC-MOVIE (A) or LZC-RET (B) as the dependent variable is mediated by MF-REST. The bootstrapped model showed significant partial mediation through MF-REST.

Chapter 4 Intrinsic neural timescales are key for input processing

4.1 Abstract

We can process and integrate multiple timescales into one meaningful whole; like when perceiving simultaneous melodies standing against the accompaniment in the background. Recent evidence suggests that the brain itself displays a complex multiscale temporal organization. Different regions exhibit different timescales in the resting state as described by the concept of "intrinsic neural timescales"; however, their exact role or function in the brain and its neural processing remains yet unclear. We review recent human fMRI and EEG/MEG data as well as non-human data on intrinsic neural timescales during both resting and task states. Following the findings and known mechanisms in physics and related mathematical principles, and similar to how the quartz crystal keeps the time in a watch, we propose that intrinsic neural timescales are key in input processing including: (I) input sharing across different species; (II) encoding of the input stochastics through intrinsic neural timescales; (III) input structuring with temporal integration and segregation; and (IV) input sampling with shifting of the input towards slower modes. In conclusion, intrinsic neural timescales take on a key role in specifically the brain's input processing and do thereby deeply ground the human brain within its environmental and non-human evolutionary context. This carries major implications for other brain theories like predictive coding, psychiatric disorders, and artificial intelligence.

4.2 Graphical Abstract

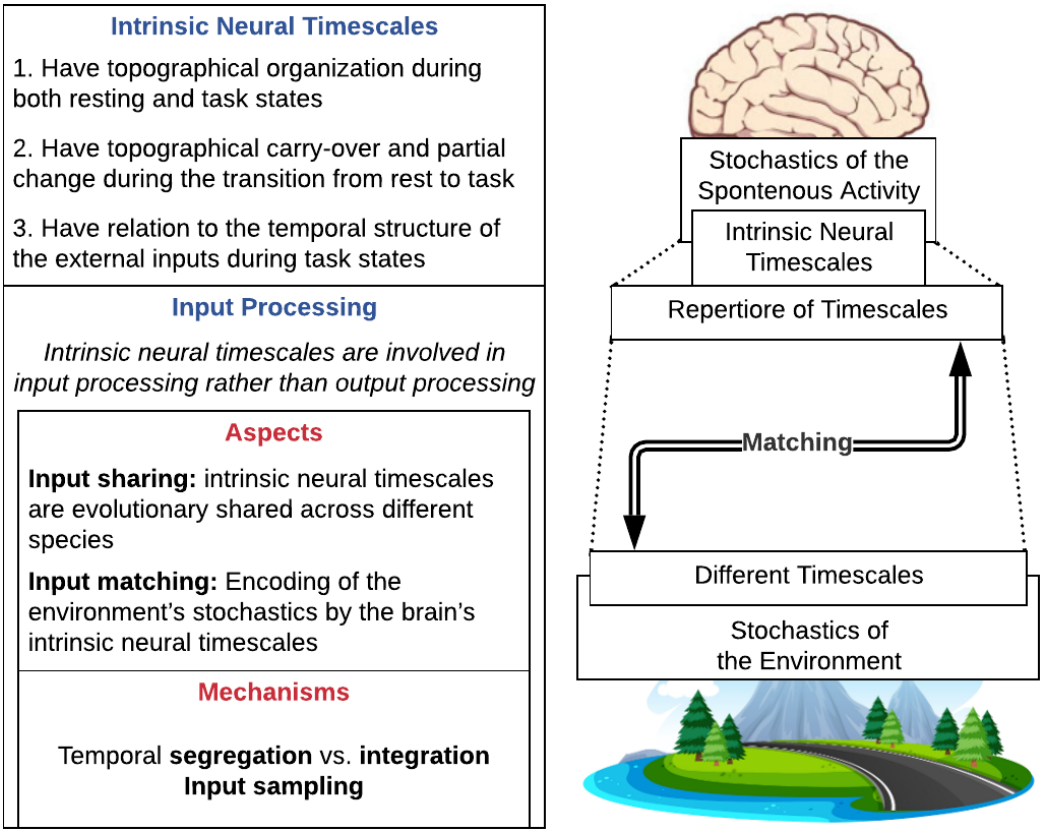

4.3 Introduction

Our environment bombards the brain with a variety of regular and irregular inputs on different timescales. Consider one of the temporally most complex inputs, music. We are able to simultaneously perceive the music's different timescales and, even better, are able to integrate them into one meaningful whole like a melody which, moreover, can be distinguished from the ongoing accompaniment in the background. How can our brain process and integrate such multi-scale inputs? Similar to the role of the quartz crystal in keeping the time in a watch, recent evidence suggests that the brain itself exhibits 'intrinsic neural timescales' [27], [28], [63], [67], [75], [169]–[173]. As measured by the autocorrelation window (ACW) in resting state, lower-order unimodal sensory regions show short timescales compared to higher-order transmodal regions like the default-mode network [26], [27], [64], [67], [72]–[75], [79], [80], [161], [169]–[178]. However, the specific function or role of the intrinsic neural timescales in the brain and its neural processing remains unclear, so far.

Reviewing various findings on intrinsic neural timescales in both human and non-human species, we propose that they are key in processing and structuring inputs on different timescales. Specifically, the brain utilizes its own intrinsic neural timescales to actively sample and expand the extrinsic timescales of the multiscale inputs it receives from both environment and body. This allows the brain to encode the stochastic structure of its environmental inputs according to its own stochastic structure determined by its intrinsic neural timescales. That, as we will detail, is mediated by specific computational mechanisms like temporal integration/segregation and input sampling with shifting towards slow frequencies.

We first review empirical evidence on intrinsic neural timescales during both resting and task states. That is followed by a second part where we link intrinsic neural timescales to distinct facets of input processing, like encoding of stochastics and their sharing by different species. In the third part, borrowing from Physics and Mathematics, we explore the computational mechanisms driving input processing by the intrinsic neural timescales; this includes temporal integration and segregation of the input as well as a sampling mechanism that shifts subsequent stages of input processing towards slower frequency modes. We conclude that the role or function of intrinsic neural timescales consists in processing and structuring the multi-scale inputs from the environment which, to some degree, is evolutionarily shared across human and non-human species. Given their key role in the brain's input processing, intrinsic neural timescales carry major implications for free energy/active inference (section 4.8.1), psychiatric disorders (section 4.8.2), and artificial intelligence (section 4.8.3).

4.4 Part I: Intrinsic neural timescales in rest and task states

4.4.1 Resting State I: Temporal hierarchy of unimodal and transmodal regions

Murray and colleagues [75] investigated single-cell recording data in monkeys and calculated their autocorrelation function (ACF) in pre-stimulus intervals. From that, they measured the duration of the temporal window at a correlation

decay of 50%, i.e., autocorrelation window (ACW). They observed shorter ACW in lower-order unimodal sensory regions while higher-order transmodal regions like prefrontal cortex exhibited longer ACW [75]. Subsequent computational modelling studies employed large-scale monkey-, human-based structural connectivity networks [67], [94], or a standard model of synchronization, i.e., Kuramoto model [28] (0.01 to 0.1Hz): they also demonstrated longer intrinsic neural timescales (as measured by ACW) in prefrontal regions while they remained shorter in sensory and motor cortex (see also ref. [79], see also other models of neural dynamics in refs. [179], [180]).

The computational findings are supported by observations of a corresponding hierarchy of timescales in real human data using fMRI [72], [74]. Operating in the infraslow frequency range (0.01 to 0.1Hz), resting state fMRI studies applied the autocorrelation function to the BOLD signal and, following Murray and colleagues[75], determined the ACW at 50% of correlation decay [72]–[74]. Employing small [73], [80] or large-scale [72], [73], [94] fMRI data sets, all studies observed shorter ACW in unimodal regions including sensory and motor regions/networks on the cortical level. In contrast, transmodal regions including higher-order networks like central-executive networks (CEN), dorsal attention networks (DAN), and default-mode network (DMN) generally showed longer ACW.

In addition to a temporal hierarchy on the cortical level, Raut and colleagues [74] also tested for ACW in subcortical regions like thalamus, cerebellum, striatum, and hippocampus. Interestingly, they again observed that gradients of ACW within each of these subcortical regions, especially in thalamus and striatum, seem to mirror the temporal hierarchy on the cortical level. Together, these data strongly suggest that both cortical and subcortical regions display an intrinsic hierarchical organisation with unimodal sensory and motor regions showing shorter timescales while transmodal higher-order association regions exhibit longer timescales.

These findings were all obtained in human fMRI that measures BOLD activity in the infraslow frequency range (0.01 - 0.1Hz). That raises the question whether the distinction of shorter unimodal and longer transmodal intrinsic neural timescales is also present in faster frequency ranges between 1 and 70Hz as they can be typically measured with EEG/MEG. Indeed, two recent human resting state MEG studies [94], [175] demonstrate longer ACW in higher-order transmodal regions/networks like CEN and DMN, whereas it was significantly shorter in unimodal sensory regions. Hence, these findings suggest that intrinsic neural timescales follow the same topographical distribution in faster frequencies (1 - 70Hz) as those in slower frequency ranges (0.01 - 0.1Hz). Such ubiquitous occurrence suggests a most basic or fundamental, though yet unclear, role or function of intrinsic neural timescales for the brain.

4.4.2 Resting State II: Intrinsic neural timescales and functional connectivity

How are the intra-regional intrinsic neural timescales related to inter-regional connections? The intrinsic neural timescales are constituted by both intra-regional cellular features [67], [174], [181], [182] and inter-regional connectivity [67], [74], [75], [176]. Intra-regional cellular features concern the excitation-inhibition balance (EIB) with its local recurrent wiring [183] as in supragranular feedforward and infra-granular feedback connections [26], [67], [74], [182] (see also ref. [176] for demonstrating the relevance of population codes).

In addition to the intra-regional cellular features, intrinsic neural timescales are also strongly shaped by inter-regional connectivity. Chaudhuri and colleagues [174] demonstrated that purely local connectivity itself is insufficient to yield the diversity of timescales across cortex. Moreover, in their monkey-based computational model [67], they remove all long-range projections which significantly restricts the range of different timescales and abolishes the intrinsic temporal hierarchy. The relationship of intra-regional intrinsic neural timescales and inter-regional functional connectivity holds again across different species as it can be observed in both monkeys [172] and humans [72], [74], [94], [184]–[187].

How exactly is inter-regional functional connectivity related to the intrinsic neural timescales? Two recent studies in human fMRI show that the duration of intrinsic neural timescales in the different regions, as measured by resting state ACW, is positively correlated with the degree of the same region's change in functional connectivity during task: the longer the region's resting state ACW, the stronger its task-related change in its functional connectivity to other regions [72], [188]. That is further supported by Raut and colleagues [74] who demonstrated that the individual variability in ACW across different regions is directly related to the individual variation of the functional connectivity pattern of the same regions (see also [184], [189]–[193]).

Together, these findings suggest a close relationship of intrinsic neural timescales to the brain's inter-regional connectivity pattern – intra-regional temporal features are, in part, constituted by long-range inter-regional connections. Such intimate link between intra-regional timescales and inter-regional connectivity means that the different timescales can interact and integrate with each other which may enlarge the number of available timescales, i.e., the repertoire of timescales, as we will illustrate later.

4.4.3 Rest-task Overlap: From intrinsic neural timescales to temporal receptive windows

Are the resting state's intrinsic neural timescales related to task states? A positive answer to this question would support their involvement in input processing. The relevance of intrinsic neural timescales for input processing is strongly suggested by the excellent studies by Hasson and colleagues [77], [78], [80], [194]–[196] (ref. [63] for review). They demonstrate that shorter temporal segments of external stimuli (like single words of stories or short episodes in movies) are processed preferentially in lower-order unimodal sensory regions while the longer intervals (like whole paragraphs in stories or longer episodes in movies) are related to activity changes in higher-order transmodal regions. Given that external inputs are processed and structured in temporal terms, i.e., according to different durations, Hasson and colleagues [63] speak of "temporal receptive windows" (TRW) which more or less correspond to what are described as "temporal receptive fields" on the cellular level [76].

Does the spatial or topographical pattern of the intrinsic neural timescales overlap between rest to task states, i.e., rest-task overlap? While such rest-task overlap has well been demonstrated for functional connectivity [72], [128], [197], [198], it remains an open issue in the case of the intrinsic neural timescales. The various task studies on the brain's TRW show a spatial pattern that is well in accordance with the hierarchical organization of the intrinsic neural timescales in

the resting state. In the same way, the ACW is the longest in the DMN during the resting, task states also show that the DMN processes the longest sequence of inputs and information [77], [78]; while the shorter resting state ACW in unimodal sensory regions seems to find its equivalent in the short sequences of inputs processed in these regions [63]. Hence, comparison of rest ACW and task TRW shows analogous hierarchical topographical organisation suggesting close relationship of rest and task, i.e., rest-task modulation or interaction [90], [101], [199]–[201].

If there is such rest-task overlap, one would assume that the hierarchical organisation of resting state ACW is carried over to and thus present in the TRW during task states. Evidence for such rest-task overlap comes from both computational modelling and brain imaging. Gollo and colleagues [28] conducted a modelling study based on a synchronization model (Kuramoto model) with simulations of transcranial magnetic stimulation (TMS): they show that regions with longer ACW, as located in the core, display lower and more sluggish activity changes in response to external stimuli than sensory regions with their shorter ACW at the periphery that exhibit higher amplitude and faster response to external stimuli (see also refs. [26], [79]). Analogous results were observed in the modelling study by Chaudhuri and colleagues [67] who applied electrical stimulation to V1 in visual cortex to his monkey-based network model (see also ref. [94]).

These computational data on rest-task overlap of intrinsic neural timescales are supported by human brain imaging data. A recent human fMRI study by Ito and colleagues [72] investigated ACW in resting state and the amplitude during different task states. They demonstrated negative correlation of resting state ACW duration (in different regions) with the magnitude of task-related activity, i.e., amplitude, in the same regions: the longer the region's resting state ACW, i.e., transmodal regions, the lower its task-related amplitude, while regions with shorter ACW, i.e., unimodal regions, exhibit higher amplitude during different tasks. These results support the assumption that the resting state's intrinsic neural timescales may strongly shape input processing during task states as manifested in rest-task overlap in their topographical organization [28], [200], [202].

4.4.4 Rest-task Modulation: Intrinsic neural timescales shape task states and behavior/cognition

The rest-task overlap strongly suggests that the resting state's intrinsic neural timescales may also shape or modulate the temporal features of task states including associated cognition – this amounts to what we describe as rest-task interaction or modulation (see also refs. [101], [199], [203]). This has recently been addressed by Golesorkhi and colleagues [175] (see also ref. [80] for initial steps). Applying MEG, they investigated the ACW-50 and ACW-0 (see above) not only during rest but also during three different task states (motor, story-math, working memory). They showed that the resting state's ACW and its hierarchical core-periphery organisation strongly predict their task states: the resting state's core-periphery organisation of ACW was essentially preserved during all three task states as topographical rest-task correlation yielded high values (0.8 – 0.9) [175]. These results suggest that the resting state's hierarchical organisation of its intrinsic neural timescales is essentially carried over and preserved during task states in a task-unspecific way.

Golesorkhi and colleagues [175] also observed some task-specific changes (Figure 4.1) when calculating rest-task difference (which subtracts and cancels out the shared, i.e., correlating temporal hierarchical organisation). Specifically, higher-order network regions showed strong ACW shortening during especially the story-math task (which was presented in 30s intervals) but only minimal changes in motor and working memory tasks. A reverse pattern was observed in lower-order network regions where ACW was shortened considerably during working memory but minimally in story-math and motor tasks. These data suggest that, once one subtracts the hierarchical temporal organization present in both rest and task, task-specific changes can be observed. One can then also see that the ACW itself and, more generally, the intrinsic neural timescales can be modulated during task states – they are dynamic and adaptive rather than static and non-adaptive. Albeit more studies are needed, task-related modulation seems to mainly concern the shortening of the ACW relative to rest.

In addition to task states, intrinsic neural timescales also shape behavior and cognition. Studies in monkeys demonstrated that longer duration of the resting state's intrinsic neural timescales (as obtained during baseline intervals sandwiched between task) is associated with better behavioral performance in a variety of different tasks; these include longer duration of the delays in delay discounting task [75], stronger spatial response coding in the delay period during a non-match-to-goal task [204], and modulating working memory performance during later periods, i.e., delay [172]. On the human side, recent fMRI and/or EEG studies demonstrate that the resting state's ACW is directly related to higher-order cognition like the level of consciousness [49], [205], the sleep stage [178], the sense of self [48], [104], [110], [206], and psychiatric disorders (see section 4.8.2 for details). Albeit tentatively, these data show that intrinsic neural timescales strongly shape behavior including perception and higher-order cognition like consciousness and self. Since task states, as well as perception and cognition, are dependent upon various kinds of inputs, together, these data are well compatible with the assumption that intrinsic neural timescales are key in input processing and structuring.

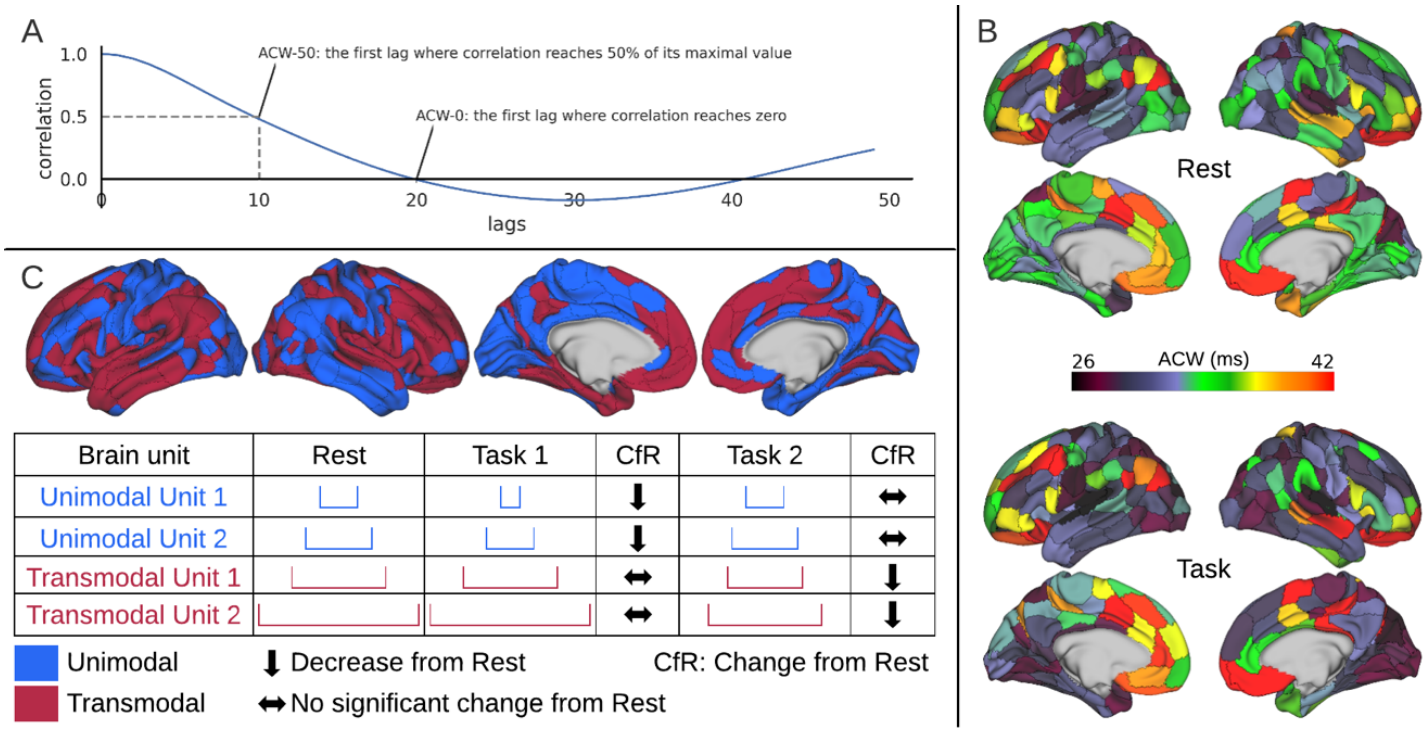

Figure 4.1: Autocorrelation window (ACW) in resting and task states. A) ACW is defined as the first lag in which the correlation of the signal with itself drop below 50% of the maximum correlation. It is measured from the autocorrelation function (ACF). B) The ACW shows topographical differences between regions during resting and task states. The colormap is in milliseconds and represents the length of ACW. C) The brain map represents the uni-transmodal organization of the brain regions. The table schematically shows how ACW changes from resting to task states and also from unimodal to transmodal units in two arbitrary tasks and four sample units. The table is only for illustration purposes.

4.5 Part II: Input processing through intrinsic neural timescales

Key findings of the intrinsic neural timescales are (I) their topographical organisation during both resting and task states along uni- and transmodal regions/networks, (II) their topographical carry-over and partial change during the transition from rest to task [175], and (III) their relation to the temporal structure of the external inputs during task states [63], [77], [194], [195], [207], [208]. Together, this suggests their involvement in specifically the brain's input processing. Considering intrinsic neural timescales, in the following, we first address the importance of input processing as distinguished from output processing and then discuss two important facets: (I) cross-species input sharing (II) and stochastic matching of the input between the environment and the brain.

4.5.1 Input vs. Output: Capacity or predisposition for input processing

Are intrinsic neural timescales engaged in either input or output processing? This was recently addressed by Zilio and colleagues [178], who investigated the ACW in resting state EEG in subjects with physiologic, pharmacologic, and pathological alterations of consciousness. Under such conditions, input processing is known to be altered in distinct ways, i.e.; progressive decrease (NREM sleep stages N1, N2, N3), isolation from external inputs but preserved capacity for processing of internal inputs (from the own body and brain) (REM sleep and ketamine), and extreme deficiency or complete absence of both external and internal inputs (unresponsive wakefulness syndrome, sevoflurane). Additionally, they included subjects with complete loss of motor function, e.g., output processing, whereas input processing and consciousness are preserved (locked-in syndrome (LIS) and amyotrophic lateral sclerosis (ALS)).

The results (Figure 4.2) show abnormally long ACW in the unresponsive wakefulness syndrome, through abnormal strengthening of slow frequency power (and concurrent weakening of fast frequency power). Also, both the physiologic and pharmacologic alterations of consciousness showed abnormal prolongation of the ACW in line with the progressive decrement of the capacity of input processing in the different behavioral states. The motor conditions, in contrast, exhibited 'normal' ACW with a preserved balance of slow and fast frequencies in the power spectrum. Together, these findings support the involvement of intrinsic neural timescales in specifically input processing rather than output processing; if the ACW was involved in both input and output processing, it should have changed in both types of conditions, altered states of consciousness and motor conditions.

However, one needs to be careful. As Zilio and colleagues [178] investigated only resting state, they cannot directly relate the ACW to actual input processing as investigation of task states with actual inputs are needed to make that claim. Given that the disorders and the alterations of consciousness are known to exhibit deficient input processing [209]–[213], their findings suggest that the resting state's intrinsic neural timescales exert the capacity for input processing, i.e., a neural predisposition [55], [87], [214], [215]. Even when not being exposed to actual multiscale inputs from the extrinsic environment, the resting state still exhibits its own intrinsic neural timescales as indexing its capacity for processing the former. This is, for instance, the case in sleep where, despite not actually processing environmental inputs, we can still be awoken at any time by strong enough external inputs - the brain's capacity or predisposition of input processing preserved [209]. In contrast, that remains impossible in total anesthesia and coma where even the strongest external inputs will not wake one up – the brain's capacity or predisposition of input processing is lost.

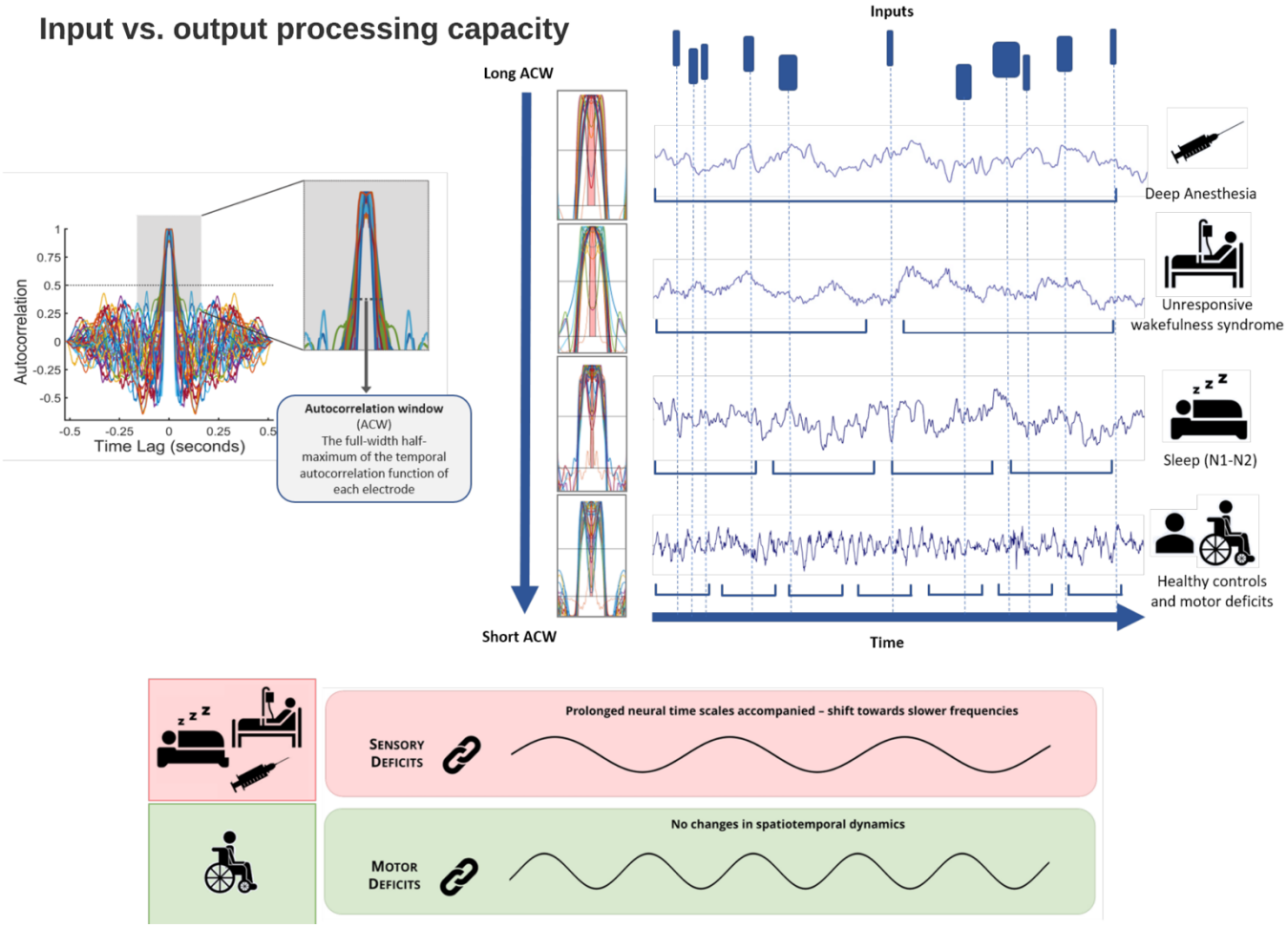

Figure 4.2: Input vs. output processing. On a whole-brain level, healthy awake subjects and subjects with motor deficits but preserved input processing (ALS, LIS) present short ACW, i.e., normal neural timescales accompanied by a balance of slow and fast frequencies, which is associated with a normal capacity of encoding inputs, while other physiological, pharmacological, and pathological conditions, e.g., sleep (N1-N2), unresponsive wakefulness syndrome and deep anesthesia (e.g., sevoflurane) show a progressive stretching of the ACW, i.e., prolonged neural timescales accompanied by a shift towards slower frequencies, that consequently lead to the abnormal prolongation of the input processing temporal window (the EEG signals and the ACW representations are taken from the datasets investigated in Zilio et al. [178]).

4.5.2 Input sharing: Cross-species evolutionary preservation of intrinsic neural timescales

We so far demonstrated the significance of intrinsic neural timescales in input processing. If the intrinsic neural timescales are involved in processing inputs from the external environment, one would assume that different species that somewhat share one and the same environment should, to some degree, overlap or share, at least in part, their intrinsic neural timescales. There is indeed evidence for such input sharing across species as it is manifested in the cross-species evolutionary preservation of intrinsic neural timescales.

The data in part I already demonstrated that the regional differentiation of the intrinsic timescales along the transmodal-unimodal gradient holds in both monkeys [67], [75], [176] and humans [72]–[74], [175]. This can even be extended to other species as it is supported by cross-species studies on both cellular [216], [217] and more regional-systemic [218] levels. Shinomoto and colleagues [216], [217] show, in a first step, regional differentiation in the cellular firing pattern of different regions in monkey brain: spiking pattern are regular in motor areas, random in visual areas, and bursty in

prefrontal cortex. In a second step, they demonstrate that such temporal fingerprinting in the regions' temporal structure of their firing pattern holds even across different species including monkey, cats, rats, and mice; the differences in firing patterns between different regions within one species are larger than the firing pattern differences within one and the same region across different species [216], [219]. Together, these data demonstrate that neural firing patterns on the cellular level of specific regions are preserved across different species.

Analogous observations of cross-species evolutionary preservation have been made on the more regional-systemic level of oscillations. Buzsáki and colleagues [218] demonstrate that various oscillatory rhythms like alpha, spindle, and ripples are present in more or less the same frequency range in different species including humans, monkey, dogs, bat, gerbil, guinea pig, rabbit, mouse, and hamster (see also ref. [219]).

Importantly, Buzsáki and colleagues [218] observe that such preservation of the same frequencies across different species holds independent of brain size: even if the brain size changes and becomes larger throughout evolution, the frequency range of the rhythmic pattern remains the same in different mammals. They conclude that temporal organisation of the brain is a key priority in evolution: "In summary, the preservation of temporal constants that govern brain operations across several orders of magnitude of timescales suggests that the brain's architectural aspects such as scaling of the ratios of neuron types, modular growth, system size, inter-system connectivity, synaptic path lengths, and axon caliber, are subordinated to a temporal organizational priority." (ref. [218] p.755).

Are the human brain's intrinsic neural timescales an evolutionary preserved manifestation of our ancestors' timescales including their key role in processing external inputs from the environment? The findings by both Shinomoto and colleagues [216], [217] and Buzsáki and colleagues [218] suggest exactly that. One would consequently expect that human behavior, if based upon its evolutionarily preserved intrinsic neural timescales, should resemble the behavior of non-human species. For instance, Zhang and Ghazanfar [220] propose that the timescales of human infant vocal production can be seen in line with the multiple intrinsic neural timescales of vocal production in marmoset monkeys, songbirds, and other vertebrates. Together, these findings suggest that intrinsic neural timescales are, in part, preserved evolutionarily across different species which may be manifested in somewhat similar forms of behavior. (Figure 4.3A).

4.5.3 Input matching: Encoding of the environment's stochastics by the brain's intrinsic neural timescales

How is it possible that different species share their intrinsic neural timescales? The reason for such cross-species similarity cannot be found in the brain itself as cross-species temporal similarities occur across different brain sizes [218]. Picking up the suggestion by Shinomoto and colleagues [216], [217], cross-species similarity may rather be related to similarity in function and, as we specify, in the nature of the inputs. Different species share more or less the same environmental, i.e., ecological context and consequently are exposed to the same input that share similar timescales. Specifically, even if the inputs themselves are elaborated in somewhat distinct ways by the species-specific sensory

organs, the input stochastics, e.g., the relation between inputs may nevertheless be processed in more or less similar ways across the different species.

Are the brain's intrinsic neural timescales related to the input stochastics in the environment? Stephens and colleagues [80] demonstrate that regional differences in the brain's intrinsic neural timescales, as indexed by their power spectrum in their study, are related to the temporal structure of the processed information with the former aligning to the latter: (I) regions with shorter intrinsic neural timescales and faster dynamics, i.e., early auditory cortex, are activated during shorter stimulus segments (e.g., single phonemes or words) (see also refs. [221]–[223] for more support in terms of entrainment); (II) regions with intermediate timescales and balanced slow-fast dynamics, i.e., superior temporal gyrus and inferior frontal gyrus, are recruited by intermediate durations in the stimuli' temporal structure (e.g., the structure of sentences); and (III) regions with longer intrinsic timescales and slower dynamics, i.e., precuneus and medial prefrontal cortex, are activated by slowly varying stimulus dynamics (e.g., stimulus narrative, see also refs. [63], [77], [78], [80], [224]).

These findings raise yet another question, though. How can the limited number of intrinsic neural timescales of the brain's 364 regions process and sample a seemingly unlimited and constantly changing number of extrinsic neural timescales of the environment? Given that there is positive relation of intra-regional intrinsic neural timescales and inter-regional functional connectivity [72], [74], [224], we propose direct interaction between the different regions' intrinsic neural timescales – such interaction may enlarge the number of possible timescales, i.e., the "repertoire of timescales", as we say (Figure 4.3B). We can take the structure of DNA as an analogy. This complex structure is created from only four bases of adenine, thymine, guanine and cytosine. If a species has a high number of regions with different intrinsic neural timescales, their degree of possible interaction through inter-regional functional connectivity is much higher than in a species with only low number of regions exhibiting distinct intrinsic neural timescales and/or low inter-regional functional connectivity.

A large repertoire of timescales may extend the organism's ability to encode and sample the input stochastics in a more fine-grained and temporally differentiated way, that is, according to distinct timescales in the environment. That, in turn, may reduce the error in the brain's encoding of the input stochastics relative to the latter's stochastic occurrence in the natural world. Accordingly, we tentatively suppose that species with a higher number and large repertoire of intrinsic neural timescales are prone to lower degrees of error in their input processing – they can better align to their environmental context in a more fine-grained way than species with a low number of intrinsic timescales and/or a small repertoire (Figure 4.3C).

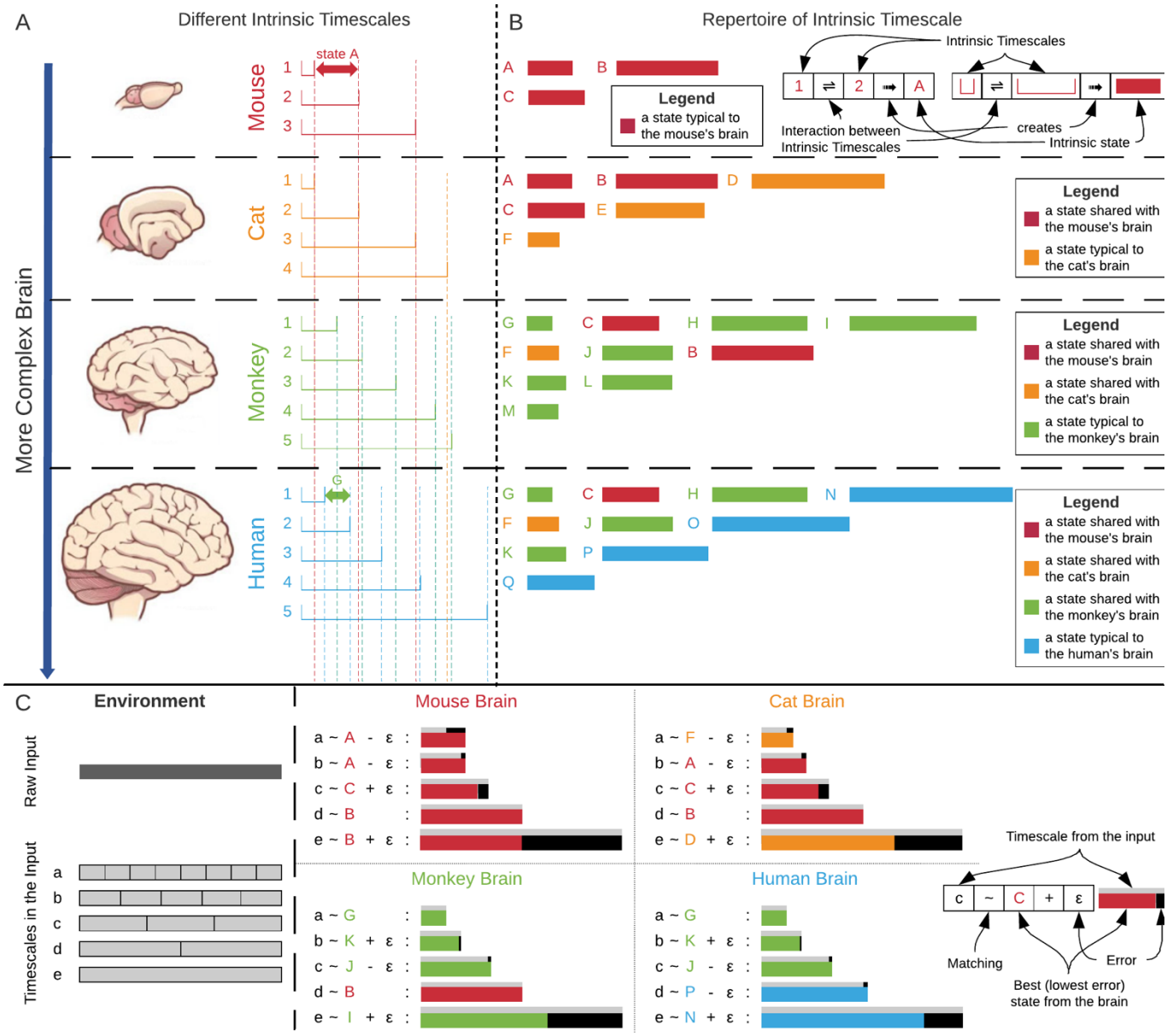

Figure 4.3: Evolutionary cross-species stochastic matching of the input. All parts are for illustration purpose only and the sequence of brains is not intended to represent any evolutionary hierarchy. A) Intrinsic timescales in the brains' of four sample species. On a general scale, a more complex brain has higher number of intrinsic timescales (e.g., human vs. mouse). Also, different brains may have timescales with similar or different lengths. B) The interaction between different intrinsic timescales may create species' repertoire of timescales. Each state in the repertoire is the result of the interaction between a pair of timescales. For example, state A is the result of the interaction between timescales 1 and 2. Here, for the sake of simplicity the interaction is defined as the difference between the lengths of two timescales. Although, the timescales themselves are unique to each species' brain, the interactions (states) can be shared between different species, e.g., state C is shared between all four sample species. So, the repertoire of states in each species' consists of some states that are typical to that species and some states that are shared with other species. C) The interaction between the environment and the brain happens through the matching of timescales. On the left, we have the environment and a sample input which contains several timescales with different lengths (a, b, c, d, e). On the right, the matching between the input and each species' brain is illustrated. Each timescale in the input is matched to the best state from the repertoire of timescales. The best state is the state that yields the least error.

4.6 Part III: Mechanisms for associating intrinsic timescales and input processing

4.6.1 Temporal segregation and temporal integration

What are the mechanisms by which the intrinsic neural timescales shape input processing? The various task state studies conducted by the group around Hasson with the formulation of the temporal receptive window suggest that the intrinsic

neural timescales may structure the input into segments of different durations, e.g., short and long segments like single words, sentence, and paragraph [63], [77], [78], [80], [225]. Such temporal structuring may mean that certain inputs are processed together with high degrees of their temporal integration, amounting to some form of 'temporal smoothing' [91], [225]. While other inputs may be processed in a more segregated and, therefore, temporally precise way entailing higher degrees of temporal segregation (see refs. [91], [178]). Together, this amounts to a balance of temporal integration vs. segregation in input processing.

How can intrinsic neural timescales structure inputs by modulating their balance of temporal integration vs. segregation? The ACW measures the degree of correlation of neural activity patterns across different time points. If only a low number of distinct time points correlate with each other, the correlation is low indexing short ACW. This means that inputs at especially more distant time points are sampled independent of each other – they will be processed with high degrees of temporal segregation but low temporal integration [91]. Moreover, the processing of single inputs may then be more or less restricted to their actual durations as, due to low correlation with low ACW, they are not expanded (in a virtual way) beyond their actual physical durations, i.e., temporal expansion [35]. Accordingly, short intrinsic neural timescales predispose that inputs are processed with high temporal precision in both their time points and durations with low degrees of 'temporal smoothing'. Such pattern of input processing is strongly supported by the short duration of the intrinsic timescales in unimodal regions like the sensory cortex that show short ACW in rest and short TWR during task states [27], [28], [63], [64], [67], [80] (Figure 4.4).

The reverse pattern of input processing seems to hold in transmodal regions as their rest ACW and task TRW are much longer than those in unimodal regions [27], [28], [63], [64], [67], [80]. Longer ACW indicates higher correlation of neural activity across more distant time points. Inputs at different time points are here not sampled independently of each other but somewhat linked together across time resulting in 'temporal summing and pooling' and ultimately high degrees of temporal integration [91]. Moreover, the duration of the single inputs' neural processing may virtually, i.e., neuronally expand beyond their actual physical duration: even if the stimulus is already physically absent, distant time points' neural activities may still correlate highly with the one at the actual stimulus' time points - this amounts to high temporal smoothing and low temporal precision [35] (also ref. [91] who speaks of "temporal pooling and summing"). For instance, higher-order transmodal regions like prefrontal cortex support temporal integration and expansion of sensory [65], [80], [196], [226], [227], motor, and cognitive information [63], [75], [88], [170]. This is well compatible with the idea that these regions like the prefrontal cortex are involved in higher-order cognition like memory, imagination, abstraction, self, and consciousness.

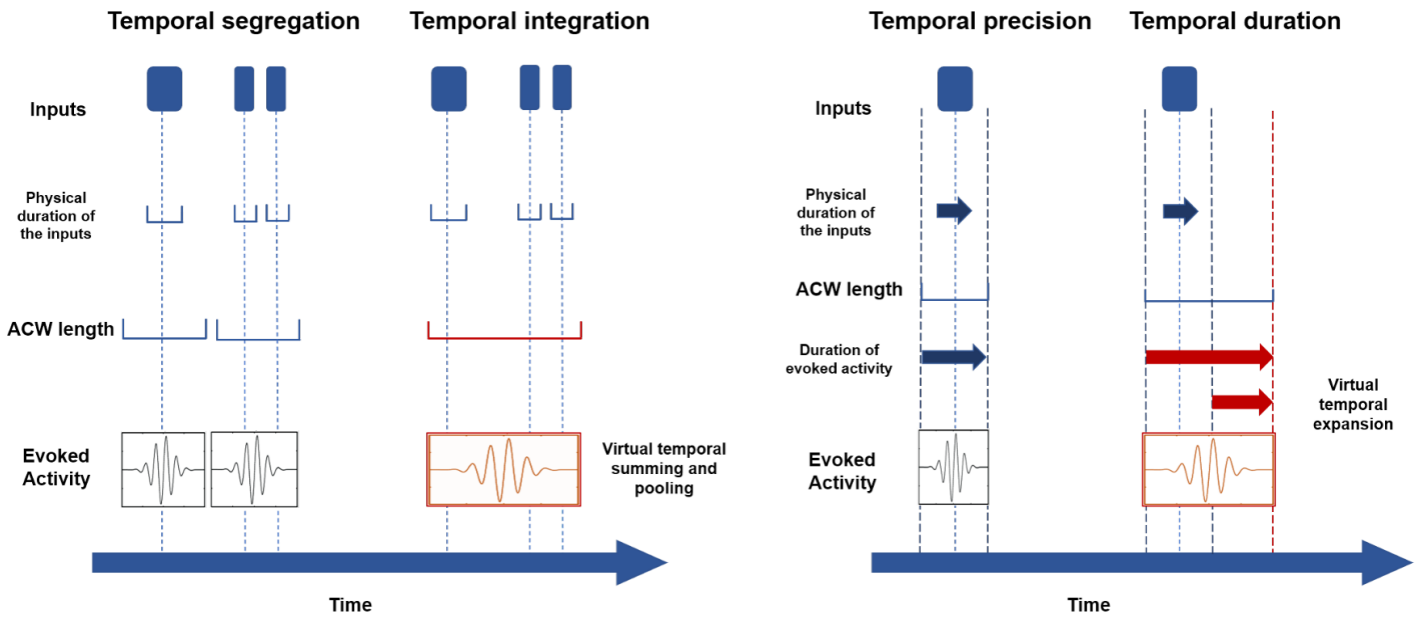

Figure 4.4:Temporal integration vs. segregation in task-evoked activity. Shorter ACW (especially in unimodal regions) permits to distinguish fast stimuli (high degree of segregation) with a precise temporal encoding consistent with the physical duration of the stimuli (high temporal precision), while longer ACW (especially in transmodal regions) permits higher correlation of neural activity across time (high degree of integration), leading to the virtual expansion of the actual stimulus (high temporal duration).

4.6.2 Intrinsic neural timescales operate as an input sampler

So far, we have demonstrated how the intrinsic neural timescales process the input in particular timescales by modulating them through temporal integration and segregation. However, the brain is confronted with a variety of different inputs in various or multiples scales with the number of timescales in the environment far exceeding the available timescales of the brain [218], [228], [229]. How can the brain bridge the gap between its own restricted timescales and the more expanded ones of its environmental context? Ideally, the brain encodes all inputs from the larger-scale environment within its own smaller-scale neural activity without losing any information, i.e., minimal error.

The empirical data show hierarchical organisation of the timescales within the brain according to a fast-slow gradient from uni- to transmodal regions. The inputs may be sampled in a more or less analogous way when transitioning from the faster uni- to the slower transmodal regions; this implies what in mathematics is described as “down-sampling” from a faster input stochastics to a slower one [230]. We suppose that the intrinsic neural timescales act as input samplers, that is, down-sampling.

Under this assumption, sensory networks would be the first to carry out this down-sampling process. Unimodal and sensory networks show shorter intrinsic timescales compared to transmodal ones [80], [175]. This implies that the first sampling would be done at a higher frequency and, progressively, said sampling would be on more widely spaced timescales, i.e., down-sampling (see Figure 4.5A for a general diagram of this process). This is well compatible with a recent study by Wengler and colleagues [231]. They investigate fMRI-based ACW in subsequent regions of three sensory-based input streams, sensorimotor, visual, and auditory. In their data, the ACW shows a short to long gradient

from primary over secondary sensory to higher-order sensory regions (like frontal eye field and dorsolateral prefrontal cortex). This holds for all three sensorimotor, visual, and auditory systems. Albeit indirectly, this supports our view of the fast-slow gradient mediating the continuous down-sampling of the input when transitioning from lower-order uni- to higher-order transmodal regions.

Mathematically speaking, the fast-slow gradient with continuous down-sampling entails a shift from faster to slower frequencies in the input stochastics, that is, a decrease in its maximum interpretable frequency. The more input processing advances towards the transmodal end of the fast-slow gradient, the more its fast frequency-based temporal precision decreases. This means that different inputs may no longer be distinguishable from each other anymore something which, in signal processing, is described as “aliasing” [230]. (Figure 4.5A right). Accordingly, the stronger the down-sampling going along with lower sampling rate of the input, the slower the maximum frequency that can be reconstructed from a discrete signal, i.e., a signal after a sampling process [230], [232].

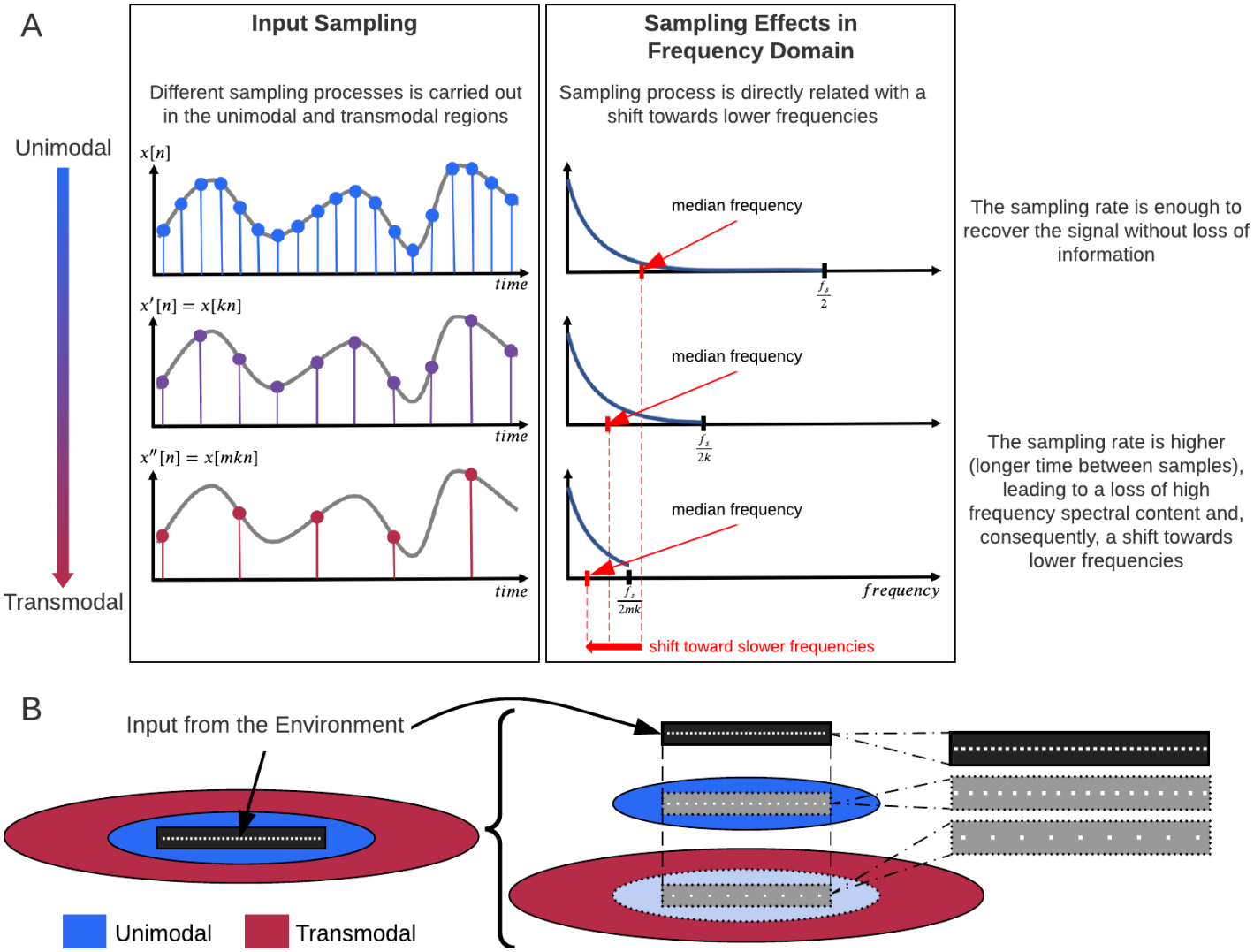

Figure 4.5: Input sampling in the uni- and transmodal units. A) The sub-sampling of a signal and shift in the frequency. The more the input signal is sampled, the more shift toward slower frequencies. The first row shows the original signal with sampling frequency fs in time (left) and frequency

(right) domains. The second row shows the same signal k-sampled in, that is, the sampling frequency is fs/k. The spectral component of this signal is shifted toward slower frequency compared to the previous one. Third row shows the same signal, but mk-sampled. B) The same concept as (A) in the brain's uni- and transmodal regions. The input is processed by both unimodal and transmodal regions, each time passing from a sampling machine, thus shifting toward slower frequencies (slow mode).

On the neuronal side, down-sampling along the fast-slow gradient of the input stochastics results in a shift of the spectral content towards lower frequencies, which can be easily indexed by the median frequency (MF). In fact, for signals where most of the spectral content is found in slow frequencies, as in brain's fMRI and EEG / MEG signals, this is exactly what one can observe. They have a $1/f$ distribution with stronger power in slow frequencies and less power in faster frequencies. Analogously, the down-sampling process carried out by the intrinsic neural timescales necessarily leads to a removal of the faster frequencies to achieve good resolution of the inputs' slow frequencies [230], [232]. One loses the inputs' information in the faster frequencies but preserves its, disproportionally strong, slow frequency information. A reduction in the sampling frequency causes the information to be maintained in slower frequencies with their higher spectral power at the cost of losing the detailed information provided by the faster frequencies. In other words, the original inputs may be shifted towards the slower frequencies. Down-sampling along a fast-slow gradient may thus be optimal for preserving the maximal amount of input information given the time-scale differences between environmental context (where the input is coming from) and the brain.

We propose that the uni-transmodal gradient of ACW and its spectral content are key in mediating the fast-slow gradient of down-sampling. Longer ACW in transmodal regions are related to stronger power in infraslow frequencies as compared with faster ones, whereas shorter ACW in unimodal regions are more dominated by their (relative) shift towards faster frequencies, meaning that their median frequency is lower [64], [70], [80], [189], [205], [233] (Figure 4.5B). This raises the question for the role or function of slower frequencies like delta (1-4Hz), slow cortical potentials in the 0.1 to 1Hz range, and the infraslow frequencies (0.001 - 0.1Hz) in input processing. Unlike faster frequencies like gamma (> 30Hz), beta (14-30Hz), alpha and theta [228], [229], the role or function of these slower frequencies is currently not clear yet (see also refs. [110], [233], [234]).

We know that intrinsic neural timescales are closely linked to slow frequencies and their long cycle durations (see also refs. [64], [178]). Longer cycle durations means that more inputs can be temporally integrated within one cycle and subsequently be processed together. The longer intrinsic neural timescales in especially the transmodal regions thus sample [64], [178] the inputs in favor of a slow mode – the originally faster inputs are filtered and processed in a slow frequency way, i.e., sub-sampling (see refs. [64], [74], [80], [91], [105], [234], [235]; see also ref. [110]). On a more cognitive level, this means that internally-oriented cognition like mind-wandering [236] or mental time travel [20], as mediated by transmodal regions, may be characterized by predominant slow modes (see also ref. [237]).

Support for a key role of intrinsic neural timescales in input sampling comes from a recent combined human EEG and modelling study. SanCristobal and colleagues (in revision) show that the neural processing of a looming sound (3s) is directly related to the resting state's ACW: the longer the resting state's ACW, the better the task-related power changes

in delta, alpha and beta could track the physical dynamics of the looming sound. This supports the assumption that the resting state's intrinsic neural time scales display the capacity for input sampling with the consequent bias towards the slow frequency mode. Next, they complement these data by a computational model probing for the slower mode (Ornstein-Uhlenbeck model): longer ACW exerts lower sampling frequency with a shift towards slower frequencies in input sampling which, in turn, makes it impossible to obtain information from faster frequencies. Together, these findings support the assumption that intrinsic neural timescales mediate input sampling by tilting or biasing it towards a slow frequency mode.

4.7 Conclusion

How can the brain process temporally complex inputs as music and language and, even better, integrate them into one meaningful whole as, for instance, a melody or a sentence? Analogous to the role of quartz crystal in keeping the time, we propose that the intrinsic neural timescales take on a key role or function for the brain's input processing. This is supported by the major role of intrinsic neural timescales in both resting and task states including their carry-over from rest to task. Following these findings, we propose that a key function of the intrinsic neural timescales consists in input processing including its different facets like cross-species input sharing and encoding of input stochastics. Moreover, we propose that input processing is achieved through various computational mechanisms including temporal integration, segregation, and sampling in the brain. Taken together, their key role in input processing through distinct mechanisms renders intrinsic neural timescales highly relevant for current views of the brain's function as in free energy/active inference (section 4.8.1) and psychiatric disorders (section 4.8.2), as well as for artificial intelligence (section 4.8.3).

4.8 Supplementary Material

4.8.1 Box 1: From free energy to intrinsic neural timescales

The free energy principle (FEP) conceives neuronal dynamics as a gradient flow on a quantity known as *variational free energy* (as presupposing Bayesian statistics [25]). Taken in that way, free energy provides a specific cost function for optimizing and reducing the organism's energetic cost. FEP crucially focuses on the variational free energy of the "pair" of agent- and environment- dynamics, with the minimization of free energy driving these to align. This leads us to a formal theory of active inference in the brain which has also been referred to as *self-evidencing* [238].

Self-evidencing describes that the brain refers to its own internal state and, as we would say, to its own intrinsic neural timescales, rather than exclusively to the external environmental inputs when making inferences about their underlying causes. This is essential to survival, but, in pathological instances, can lead to false inferences about the environmental causes of inputs. This is paradigmatically the case in psychiatric disorders where one can often observe aberrant beliefs with subjects inferring something to be there when it is not (e.g., hallucinations) or infer that something is not there when it is (e.g., an agnosia or dissociative disorder) [239], [240].

Where and how do the brain's intrinsic neural timescales come in? Recent studies characterize the self and its alterations (as in depression or schizophrenia) by intrinsic neural timescales [48], [70], [104], [241], [242]. At the same time, the self has been modelled in terms of variational free energy and active inference/predictive coding [243], [244]. Converging both means that what is described as "deep temporal models" or "temporal thickness" [245] in the context of active inference [79], [246] may be connected with and specified by the intrinsic neural timescales. The intrinsic neural timescales including their regional differentiation may provide the kind of "deep temporal model" active inference and predictive coding require to better predict mental features like self.

Future studies may want to converge and, even better, include a computational model of the intrinsic neural timescales in the formalisms of variational free energy and active inference. For instance, the free energy principle has already been used as a powerful computational formalism for modelling diverse mental features; these include consciousness and affect/emotion [247]–[251] as well as the self, including its different facets like the dynamic self, the bodily self and the subjective self ("I" vs "me") [243], [244], which all can be subsumed under the umbrella notion of 'spatiotemporal self' [102], [252].

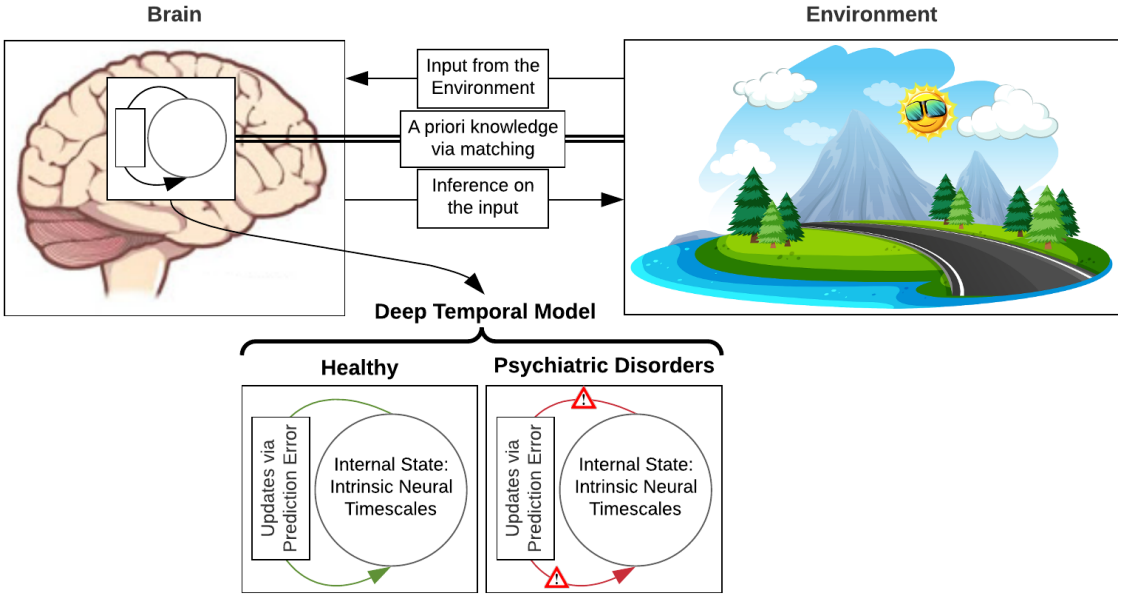

Supplementary Figure 4.1: Connecting the deep temporal model to the intrinsic neural timescales. The brain builds a priori model through matching with the environment. Intrinsic neural timescales can be a major building block of the internal state of the brain. Based on the deep temporal model, the internal state of the brain (intrinsic neural timescales) updates through the prediction error. In psychiatric disorders, it could be the case that this update procedure fails and the error does not decrease.

4.8.2 Box 2: From intrinsic neural timescales to psychiatric disorders

Are intrinsic neural timescales relevant for behavior and cognition? Evidence for that comes from their changes in psychiatric disorders. A recent resting state fMRI study [73] applied the ACW in subjects with autism. They observed significantly shorter ACW in primary sensory regions (visual, sensorimotor, auditory) in adult autism spectrum disorder (ASD) compared to healthy subjects; these changes correlated negatively with the severity of autism. In contrast, ACW in right caudate was significantly longer in ASD which also correlated with the degree of repetitive restrictive behavior in ASD subjects.

They then investigated fMRI resting state ACW an adolescent children ASD dataset where they obtained similar ACW changes in the same regions including analogous correlation results. This means that there is a developmental component to the intrinsic timescales. That was complemented by investigating the neuro-anatomical basis through calculating the local grey matter volume. Significant positive correlation of local grey matter volume with the duration of ACW in the same region was observed which also hold for the regions altered in ASD. Finally, they calculated mediation analysis showing the grey matter volume in the above-mentioned regions were mediated in their impact on autistic symptoms by the duration of the ACW [73].

The relevance of intrinsic timescales in autism is further supported by another fMRI resting state study in ASD [253]. They calculated the PLE (and spectral entropy) and observed that ASD showed increased PLE with stronger power in slow frequencies in specifically regions of the salience network (insula, supragenual anterior cingulate cortex, thalamus) (see also ref. [62] showing that the salience network exhibits the highest variability and flexibility among the different networks). Moreover, they demonstrated that such increased PLE in salience network was not observed in schizophrenia. Moreover, this was specific for PLE whereas other measures like regional homogeneity (REHO) and neural variability (SD) did not show any changes in these regions in ASD. These results hold the promise that intrinsic neural timescales may serve as marker for differential diagnosis of ASD, schizophrenia, and other psychiatric disorders [202], [254], [255].

One recent study in schizophrenia including mostly post-acute first-episode subjects showed abnormally long ACW (and high PLE) in several electrodes during a task state involving self-specificity (i.e., enfacement task) [242]. They also demonstrated that the degree of change in ACW from rest to task was significantly lower in schizophrenia subjects, that is, unlike in healthy subjects, they barely shortened their ACW during the task. Most remarkably, analogous ACW prolongation during task and its reduced rest-task difference was not observed during a non-self task, i.e., auditory oddball – this suggests close relationship of ACW with self-specificity as observed in healthy subjects.

Moreover, applying moderation model, they showed that the degree of ACW mediated the relationship between self-disturbance and negative symptoms in schizophrenia participants. As in the autism study by Watanabe and colleagues [73], these data support the assumption that changes in intrinsic timescales may be related to psychopathological symptoms and, more generally, be relevant for behavior and cognition. This is further supported in a recent study on psychosis in schizophrenia [231] in which they provide support for hierarchical models of psychosis via showing different intrinsic neural timescales alterations for hallucinations vs. delusions in auditory and somatosensory cortices.

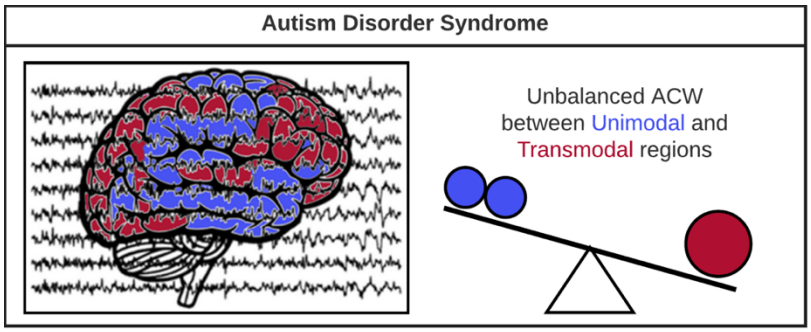

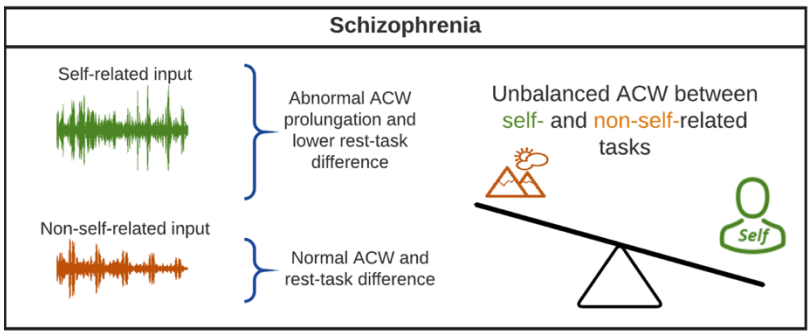

Psychiatric Disorder	Rest	Task
Autism Spectrum Disorder	↓ ACW - Primary sensory regions ↑ ACW - Right caudate ↑ PLE - Salience network	---
Schizophrenia	↔ PLE - Salience network	↓ Rest-task change: poor shortening of ACW during self-related task ↑ ACW/PLE - self-related task ↔ ACW - no change in non-self task

Supplementary Figure 4.2: Unbalanced ACW in unimodal vs. transmodal regions and self-related vs. non-self-related tasks. The different lengths of ACW observed in subjects with autism and schizophrenia compared to healthy subjects suggest that changes in the intrinsic neural timescales may be associates to the psychopathological symptoms of these disorders, in terms of cognitive and behavioral performances.

4.8.3 Box 3: From intrinsic neural timescales to artificial agents

We saw that the environmental hierarchies of different events may be recapitulated and thus modelled by the brain itself within its own intrinsic hierarchical organization, i.e., its temporo-spatial hierarchy. There is no need for the living to represent a model of the environment in their head: "An agent does not have a model of its world – it is a model. In other words, the form, structure, and states of our embodied brains do not contain a model of the sensorium – they are that model." [256]. The agent is a temporo-spatial model of its environment displaying a more or less analogous temporal structure albeit in a miniature scale-free way.

The brain can be conceived as a free energy-driven temporo-spatial model of the temporo-spatial hierarchies of its environmental context. That results in temporal and spatial nestedness of the brain within its respective environmental context. Despite different temporal (and spatial) scales across body, brain, and environments, they are nevertheless connected through self-similarity in their shape or form. Just like the smaller Russian doll is contained within the larger

one (same shape, different size), the brain and its temporo-spatial model nest in a self-similar way within the much larger environment [257]. Given such temporo-spatial self-similarity between brain and environment, we may better focus on "what our head's inside of" rather than searching for "what inside our heads" [258].

This carries major implications for modelling artificial agents as it entails the need to include an intrinsic temporal and spatial hierarchy in the agent. Future AI models may want to implement such intrinsic spatial and temporal organization in their artificial agents, including the different time scales and the core-periphery organization (see ref. [259] – for first steps in this direction in artificial agents using what they describe as 'multiple time scale recurrent neural network', refs. [260], [261] who emphasize the need for temporal hierarchies in artificial agents for their adaptation to the environment).

Spatiotemporal hierarchies would extend the current – often module-based – models of artificial agents [40] by combining top-down (providing the agent's inner input) and bottom-up (providing the agent's outer input) layers – that Tani uses in his compelling model of an artificial agent [260], [262], [263]. Most importantly, by conjoining it with the free energy principle (FEP), the artificial agent's intrinsic temporo-spatial hierarchy may be a small-scale but self-similar model of its own environmental context. To achieve that, the agent's temporo-spatial hierarchy needs to be highly dynamic and continuously changing, so as to adapt to the changing environmental dynamics. More specifically, this means that the causal (or temporo-spatial) architecture of the environment must be recapitulated or installed in the agent's temporo-spatial dynamics in such way as to allow the agent to minimize its variational free energy with its respective environmental context.

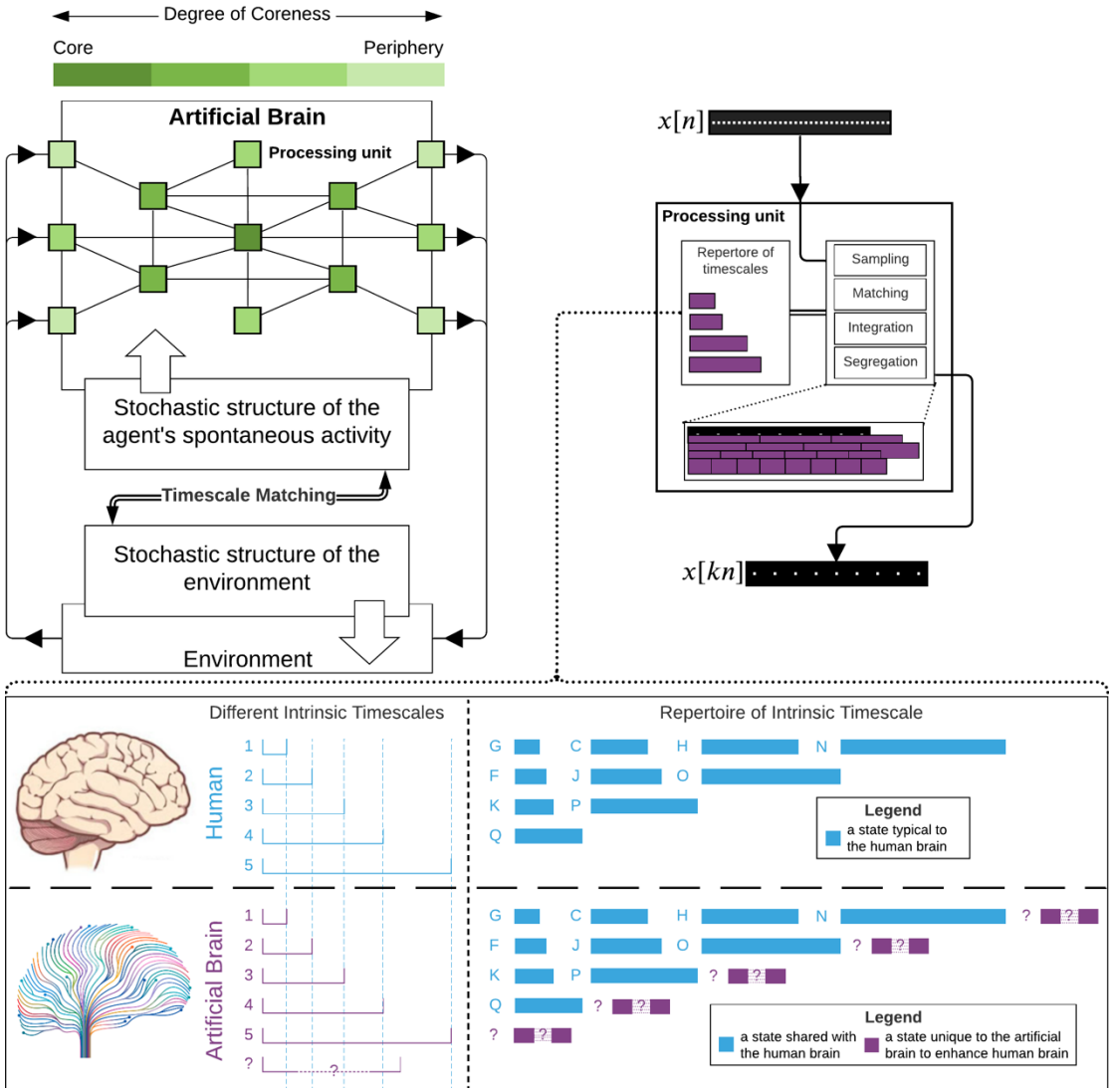

Supplementary Figure 4.3: A suggested schematic of agent-environment interaction. The agent and the environment are in a closed loop with the environment affecting the agent and vice-versa. The stochastic of the agent's spontaneous activity acts as its interface and interacts with the environment's interface, i.e. its stochastic structure, through timescale matching. The agent's processing units are organized in a core-periphery structure. In each processing unit, the input is sampled, matched, integrated or segregated based on the intrinsic properties of the unit

Chapter 5 Conclusion and Future Works

Exploring the brain from a dynamical system's point of view, one might ask what makes it special in its interaction with the environment, and can we build AI based on that knowledge? Investigating this question has been the main goal of this work. It can be argued that the intrinsic stochastic features of the brain are what makes it special. Considering that, a recent model characterizes the brain's intrinsic features in terms of spatiotemporal dynamical terms: the brain's spatiotemporal hierarchies shape what is called 'brain's intrinsicality' (Figure 5.1). The brain's intrinsicality may show potential applications in designing artificial intelligence (AI).

Byproducts	Mental Features: self, moral decision making, psychiatric disorders, consciousness					
Manifestations	Temporal Correlation	Global signal	Complexity	Autocorrelation window	Rest-task interaction	…
Mechanisms	Input sampling	Input segregation vs. integration	Input matching	Repertoire of timescales		
Design	Core-periphery architecture	Global/local feedback	Intrinsic neural timescales	Model building		
Principles	Free energy	Self-organized criticality	Scale freeness			

Figure 5.1: The proposed model of the brain's intrinsicality. The dynamical system of the brain works toward maintaining its principles, and for that it has some design rules. The principles and design rules are implemented using different intrinsic mechanisms and are manifested in different metrics which can be found in signals recorded from the brain. The red items are the ones which were empirically investigated in this work. The blue ones are proposed in this work. All mental features are byproducts of this complex dynamical system at work.

In this dissertation we investigated intrinsic neural timescales as the fundamental building blocks of the brain's intrinsicality. We explored their vital role in input processing in the brain and developed a cross-species testable model for them. Sampling, segregation and integration were also identified as three mechanisms for extracting information from input to the brain. Simulating input sampling in the human brain and validating its cross-species consistency in the non-human primates can be future continuation of this work. Furthermore, repertoire of timescales was introduced as the probable mechanism for the brain's alignment with the environment. This was introduced as a mechanism based on a combination of previous literature and physics of alignment; however, testing it is beyond the scope of this work and can be the topic of future investigations.

On the manifestation level, these ideas were put into empirical test using autocorrelation window (ACW) and Lempel-Ziv Complexity (LZC) as known manifestation of intrinsic neural timescales and information processing in the brain, respectively. Moreover, the core-periphery organization and its consistency from rest to task state (rest-task interaction) was investigated on both temporal and spatial grounds using a combination of human brain data (both magnetoencephalography and functional magnetic resonance imaging), machine learning, advanced statistics and simulation analysis.

In terms of artificial intelligence, the spatiotemporal dynamics of the brain's intrinsicality provides potential key insights for Artificial General Intelligence (AGI). In particular, the key to unlocking the general intelligence might be, as outlined in Supplementary Figure 4.3, robust alignment with the environment, brain-like input processing and brain-like architecture. In the future, this idea can be put into test by designing a deep learning model which follows the intrinsic architecture of the brain. Intuitively, this model should have a plastic architecture and be trained with naturalistic input.

As previously mentioned, one key feature of the brain's intrinsic organization is its distinction of regions in the core (middle of the brain) from those at the periphery (at the outer surface). Others and my own brain imaging investigations demonstrate that this so-called core-periphery organization (which can also be seen in other biological and even social systems) is characterized in the brain by intrinsic neural timescales. Importantly, such dynamic core-periphery organisation is key in the brain's complex behavior including its adaptive and behavioral capacity in response to environmental changes. Designing and implementing the dynamic core-periphery organization therefore provides one potential key in widening and enlarging the adaptive behavior of artificial agents based on the deep learning model.

Glossary

- Intrinsic neural timescales: the term refers to temporal windows of neural activity during which neural activity is strongly correlated with itself as measured by the autocorrelation function (ACF). These temporal windows are already present in the resting state, that is, independent of any external inputs, for which reason they are intrinsic to the brain. Moreover, the different regions of the brain like unimodal or transmodal exhibit different durations in their temporal windows; therefore, one can speak of multiple timescales in the brain's neural activity.
- Temporal receptive windows: these refer to the duration of a meaningful external input like a word (short), sentence (longer), and a whole paragraph (very long). The intrinsic neural timescales of the brain may provide temporal windows that allow receiving and processing inputs of different durations.
- Unimodal vs transmodal regions: Unimodal regions are lower-order sensory regions like primary and secondary visual cortex or auditory cortex; they are defined by processing exclusively inputs of one particular sensory modality, visual, auditory, etc. while not processing those of other modalities. Transmodal regions, in contrast, process inputs from different sensory modalities like visual, auditory, etc. including higher-order regions like the prefrontal cortex.
- Neural predispositions of consciousness (NPC). The NPC refer to necessary but insufficient neural conditions of consciousness; the neural correlates of consciousness (NCC) are sufficient for the actual manifestation of consciousness.
- Temporal segmentation: this refers to the parsing of the input according to its temporal structure including the duration of its distinct elements like words, sentences, and paragraphs in a text.
- Predictive coding/active inference: Following Bayesian statistics, predictive coding is an instance of active inference that refers to the capacity to predict the next potentially incoming input, the empirical prior, which is then compared with the actual input itself yielding a prediction error, that is, the discrepancy between predicted and actual input.
- Input processing: the concept of input can be understood in more narrow ways when referring to sensory or exteroceptive inputs from the external environment like visual, auditory or somatosensory inputs. While a wider meaning would include also the input from the own body, the interoceptive input. Finally, even strong spontaneous activity changes of the brain's resting state can serve as an internal input like in auditory hallucination.
- Temporal prediction: Temporal prediction refers to the capacity to anticipate or predict at a particular point in time the next input; longer intrinsic neural timescales may yield an earlier prediction of the next input than shorter intrinsic neural timescales. As shown in Box 1, the length of the intrinsic neural timescales yields an important influence over the prediction of the next input with longer timescales probably yielding an earlier prediction.
- Temporal self-evidencing: this refers to that the generation of the predicted input requires that the system itself, i.e., the brain, must refer to itself and its own neural activity in order to make possible a prediction. We here suppose that the brain must refer to its own intrinsic neural timescales in order to predict the input hence we speak of temporal self-evidencing.

References

[1] G. Northoff, A. Heinzel, M. de Greck, F. Bermpohl, H. Dobrowolny, and J. Panksepp, "Self-referential processing in our brain-A meta-analysis of imaging studies on the self," *NeuroImage*, vol. 31, no. 1, pp. 440–457, May 2006, doi: 10.1016/j.neuroimage.2005.12.002.

[2] K. Friston, "Am I Self-Conscious? (Or Does Self-Organization Entail Self-Consciousness?)," *Frontiers in Psychology*, vol. 9, no. APR, Apr. 2018, doi: 10.3389/fpsyg.2018.00579.

[3] G. Northoff, "Personal Identity and Cortical Midline Structure (CMS): Do Temporal Features of CMS Neural Activity Transform Into 'Self-Continuity'?," *Psychological Inquiry*, vol. 28, no. 2–3, pp. 122–131, Jul. 2017, doi: 10.1080/1047840X.2017.1337396.

[4] M. R. Arbabshirani, S. Plis, J. Sui, and V. D. Calhoun, "Single subject prediction of brain disorders in neuroimaging: Promises and pitfalls," *NeuroImage*, vol. 145, pp. 137–165, Jan. 2017, doi: 10.1016/j.neuroimage.2016.02.079.

[5] C. Hu *et al.*, "Distinct and common aspects of physical and psychological self-representation in the brain: A meta-analysis of self-bias in facial and self-referential judgements," *Neuroscience & Biobehavioral Reviews*, vol. 61, pp. 197–207, Feb. 2016, doi: 10.1016/j.neubiorev.2015.12.003.

[6] R. J. Murray, M. Schaer, and M. Debbané, "Degrees of separation: A quantitative neuroimaging meta-analysis investigating self-specificity and shared neural activation between self- and other-reflection," *Neuroscience & Biobehavioral Reviews*, vol. 36, no. 3, pp. 1043–1059, Mar. 2012, doi: 10.1016/j.neubiorev.2011.12.013.

[7] S. Dehaene, L. Charles, J.-R. King, and S. Marti, "Toward a computational theory of conscious processing," *Current Opinion in Neurobiology*, vol. 25, pp. 76–84, Apr. 2014, doi: 10.1016/j.conb.2013.12.005.

[8] S. Dehaene, H. Lau, and S. Kouider, "What is consciousness, and could machines have it?," *Science*, vol. 358, no. 6362, pp. 486–492, Oct. 2017, doi: 10.1126/science.aan8871.

[9] W. SINGER, "Consciousness and the Binding Problem," *Annals of the New York Academy of Sciences*, vol. 929, no. 1, pp. 123–146, Jan. 2006, doi: 10.1111/j.1749-6632.2001.tb05712.x.

[10] A. K. Engel, P. Fries, and W. Singer, "Dynamic predictions: Oscillations and synchrony in top–down processing," *Nature Reviews Neuroscience*, vol. 2, no. 10, pp. 704–716, Oct. 2001, doi: 10.1038/35094565.

[11] J. R. Searle, "Consciousness," *Annual Review of Neuroscience*, vol. 23, no. 1, pp. 557–578, Mar. 2000, doi: 10.1146/annurev.neuro.23.1.557.

[12] J. R. Searle, "How to study consciousness scientifically," *Philosophical Transactions of the Royal Society of London. Series B: Biological Sciences*, vol. 353, no. 1377, pp. 1935–1942, Nov. 1998, doi: 10.1098/rstb.1998.0346.

[13] L. Mudrik, N. Faivre, and C. Koch, "Information integration without awareness," *Trends in Cognitive Sciences*, vol. 18, no. 9, pp. 488–496, Sep. 2014, doi: 10.1016/j.tics.2014.04.009.

[14] L. Mudrik, "The primary (dis)function of consciousness: (Non)Integration," *Behavioral and Brain Sciences*, vol. 39, p. e189, Nov. 2016, doi: 10.1017/S0140525X15002198.

[15] G. Tononi, M. Boly, M. Massimini, and C. Koch, "Integrated information theory: From consciousness to its physical substrate," *Nature Reviews Neuroscience*, vol. 17, no. 7, pp. 450–461, Jul. 2016, doi: 10.1038/nrn.2016.44.

[16] C. Koch, M. Massimini, M. Boly, and G. Tononi, "Neural correlates of consciousness: progress and problems," *Nature Reviews Neuroscience*, vol. 17, no. 5, pp. 307–321, May 2016, doi: 10.1038/nrn.2016.22.

[17] C. Koch, "What Is Consciousness?," *Nature*, vol. 557, no. 7704, pp. S8–S12, May 2018, doi: 10.1038/d41586-018-05097-x.

[18] M. Boly, M. Massimini, N. Tsuchiya, B. R. Postle, C. Koch, and G. Tononi, "Are the Neural Correlates of Consciousness in the Front or in the Back of the Cerebral Cortex? Clinical and Neuroimaging Evidence," *The Journal of Neuroscience*, vol. 37, no. 40, pp. 9603–9613, Oct. 2017, doi: 10.1523/JNEUROSCI.3218-16.2017.

[19] K. Christoff, Z. C. Irving, K. C. R. R. Fox, R. N. Spreng, and J. R. Andrews-Hanna, "Mind-wandering as spontaneous thought: A dynamic framework," *Nature Reviews Neuroscience*, vol. 17, no. 11, pp. 718–731, Nov. 2016, doi: 10.1038/nrn.2016.113.

[20] D. L. Schacter, D. R. Addis, D. Hassabis, V. C. Martin, R. N. Spreng, and K. K. Szpunar, "The Future of Memory: Remembering, Imagining, and the Brain," *Neuron*, vol. 76, no. 4, pp. 677–694, Nov. 2012, doi: 10.1016/j.neuron.2012.11.001.

[21] Y. Fan, N. W. Duncan, M. de Greck, and G. Northoff, “Is there a core neural network in empathy? An fMRI based quantitative meta-analysis,” *Neuroscience & Biobehavioral Reviews*, vol. 35, no. 3, pp. 903–911, Jan. 2011, doi: 10.1016/j.neubiorev.2010.10.009.
[22] P. Haggard, “The Neurocognitive Bases of Human Volition,” *Annual Review of Psychology*, vol. 70, no. 1, pp. 9–28, Jan. 2019, doi: 10.1146/annurev-psych-010418-103348.
[23] J. LeDoux and N. D. Daw, “Surviving threats: neural circuit and computational implications of a new taxonomy of defensive behaviour,” *Nature Reviews Neuroscience*, vol. 19, no. 5, pp. 269–282, May 2018, doi: 10.1038/nrn.2018.22.
[24] H. Lau and D. Rosenthal, “Empirical support for higher-order theories of conscious awareness,” *Trends in Cognitive Sciences*, vol. 15, no. 8, pp. 365–373, Aug. 2011, doi: 10.1016/j.tics.2011.05.009.
[25] K. Friston, “The free-energy principle: A unified brain theory?,” *Nature Reviews Neuroscience*, vol. 11, no. 2, pp. 127–138, Feb. 2010, doi: 10.1038/nrn2787.
[26] L. Cocchi, L. L. Gollo, A. Zalesky, and M. Breakspear, “Criticality in the brain: A synthesis of neurobiology, models and cognition,” *Progress in Neurobiology*, vol. 158, pp. 132–152, Nov. 2017, doi: 10.1016/j.pneurobio.2017.07.002.
[27] L. L. Gollo *et al.*, “Dwelling quietly in the rich club: Brain network determinants of slow cortical fluctuations,” *Philosophical Transactions of the Royal Society B: Biological Sciences*, vol. 370, no. 1668, p. 20140165, May 2015, doi: 10.1098/rstb.2014.0165.
[28] L. L. Gollo, J. A. Roberts, and L. Cocchi, “Mapping how local perturbations influence systems-level brain dynamics,” *NeuroImage*, vol. 160, pp. 97–112, Oct. 2017, doi: 10.1016/j.neuroimage.2017.01.057.
[29] A. A. Fingelkurts, A. A. Fingelkurts, and C. F. H. Neves, “Natural world physical, brain operational, and mind phenomenal space–time,” *Physics of Life Reviews*, vol. 7, no. 2, pp. 195–249, Jun. 2010, doi: 10.1016/j.plrev.2010.04.001.
[30] A. A. Fingelkurts, A. A. Fingelkurts, and C. F. H. Neves, “Mind the physics: Physics of mind,” *Physics of Life Reviews*, vol. 25, pp. 75–77, Aug. 2018, doi: 10.1016/j.plrev.2018.01.012.
[31] S. Dehaene and J.-P. Changeux, “Experimental and Theoretical Approaches to Conscious Processing,” *Neuron*, vol. 70, no. 2, pp. 200–227, Apr. 2011, doi: 10.1016/j.neuron.2011.03.018.
[32] G. Northoff, S. Wainio-Theberge, and K. Evers, “Is temporo-spatial dynamics the ‘common currency’ of brain and mind? In Quest of ‘Spatiotemporal Neuroscience,’” *Physics of Life Reviews*, 2019, doi: https://doi.org/10.1016/j.plrev.2019.05.002.
[33] G. Northoff, S. Wainio-Theberge, and K. Evers, “Spatiotemporal neuroscience--what is it and why we need it,” *Physics of Life Reviews*, vol. 33, pp. 78–87, 2020.
[34] G. Northoff, *The Spontaneous Brain*. 2019. doi: 10.7551/mitpress/11046.001.0001.
[35] G. Northoff and Z. Huang, “How do the brain’s time and space mediate consciousness and its different dimensions? Temporo-spatial theory of consciousness (TTC),” *Neuroscience and Biobehavioral Reviews*, vol. 80, pp. 630–645, Sep. 2017, doi: 10.1016/j.neubiorev.2017.07.013.
[36] D. Ha and J. Schmidhuber, “World Models,” Mar. 2018, doi: 10.5281/zenodo.1207631.
[37] L. Han *et al.*, “Modeling maize above-ground biomass based on machine learning approaches using UAV remote-sensing data,” *Plant Methods*, 2019, doi: 10.1186/s13007-019-0394-z.
[38] M. Tegmark, *Life 3.0: Being human in the age of artificial intelligence*. Knopf, 2017.
[39] T. J. Prescott, D. Camilleri, U. Martinez-Hernandez, A. Damianou, and N. D. Lawrence, “Memory and mental time travel in humans and social robots,” *Philosophical Transactions of the Royal Society B: Biological Sciences*, 2019, doi: 10.1098/rstb.2018.0025.
[40] T. J. Prescott and D. Camilleri, “The synthetic psychology of the self,” in *Cognitive Architectures*, Springer, 2019, pp. 85–104.
[41] J. Tani, “An interpretation of the ‘self’ from the dynamical systems perspective: A constructivist approach,” *Journal of Consciousness Studies*. 1998.
[42] E. C. Brown and M. Brüne, “The role of prediction in social neuroscience,” *Frontiers in Human Neuroscience*. 2012. doi: 10.3389/fnhum.2012.00147.
[43] C. M. Heyes and C. D. Frith, “The cultural evolution of mind reading,” *Science*. 2014. doi: 10.1126/science.1243091.
[44] S. P. L. Veissière, A. Constant, M. J. D. Ramstead, K. J. Friston, and L. J. Kirmayer, “Thinking Through Other Minds: A Variational Approach to Cognition and Culture,” *Behavioral and Brain Sciences*, 2019, doi: 10.1017/S0140525X19001213.

[45] T. Metzinger, “Why is mind-wandering interesting for philosophers?,” in *The Oxford Handbook of Spontaneous Thought: Mind-Wandering, Creativity, and Dreaming*, 2018. doi: 10.1093/oxfordhb/9780190464745.013.32.
[46] K. Friston, J. Kilner, and L. Harrison, “A free energy principle for the brain,” *Journal of Physiology-Paris*, vol. 100, no. 1–3, pp. 70–87, Jul. 2006, doi: 10.1016/j.jphysparis.2006.10.001.
[47] J. Zhang *et al.*, “Breakdown in the temporal and spatial organization of spontaneous brain activity during general anesthesia,” *Human Brain Mapping*, vol. 39, no. 5, pp. 2035–2046, May 2018, doi: 10.1002/hbm.23984.
[48] A. Wolff *et al.*, “The temporal signature of self: Temporal measures of resting-state EEG predict self-consciousness,” *Human Brain Mapping*, vol. 40, no. 3, pp. 789–803, Oct. 2019, doi: 10.1002/hbm.24412.
[49] Z. Huang *et al.*, “Disrupted neural variability during propofol-induced sedation and unconsciousness,” *Human Brain Mapping*, vol. 39, no. 11, pp. 4533–4544, Nov. 2018, doi: 10.1002/hbm.24304.
[50] E. Tagliazucchi *et al.*, “Increased Global Functional Connectivity Correlates with LSD-Induced Ego Dissolution,” *Current Biology*, vol. 26, no. 8, pp. 1043–1050, Apr. 2016, doi: 10.1016/j.cub.2016.02.010.
[51] N. T. Markov, M. Ercsey-Ravasz, D. C. Van Essen, K. Knoblauch, Z. Toroczkai, and H. Kennedy, “Cortical high-density counterstream architectures,” *Science*. 2013. doi: 10.1126/science.1238406.
[52] D. S. Margulies *et al.*, “Situating the default-mode network along a principal gradient of macroscale cortical organization,” *Proceedings of the National Academy of Sciences of the United States of America*, vol. 113, no. 44, pp. 12574–12579, Nov. 2016, doi: 10.1073/pnas.1608282113.
[53] D. S. Bassett, N. F. Wymbs, M. P. Rombach, M. A. Porter, P. J. Mucha, and S. T. Grafton, “Task-Based Core-Periphery Organization of Human Brain Dynamics,” *PLoS Computational Biology*, vol. 9, no. 9, p. e1003171, Apr. 2013, doi: 10.1371/journal.pcbi.1003171.
[54] J. M. Huntenburg, P. L. Bazin, and D. S. Margulies, “Large-Scale Gradients in Human Cortical Organization,” *Trends in Cognitive Sciences*, vol. 22, no. 1, pp. 21–31, Jan. 2018, doi: 10.1016/j.tics.2017.11.002.
[55] G. Northoff, *Unlocking the Brain*. 2014. doi: 10.1093/acprof:oso/9780199826995.001.0001.
[56] S. P. Borgatti and M. G. Everett, “Models of core/periphery structures,” *Social Networks*, 2000, doi: 10.1016/S0378-8733(99)00019-2.
[57] M. M. Mesulam, “From sensation to cognition,” *Brain*. 1998. doi: 10.1093/brain/121.6.1013.
[58] F. de Pasquale *et al.*, “A Cortical Core for Dynamic Integration of Functional Networks in the Resting Human Brain,” *Neuron*, vol. 74, no. 4, pp. 753–764, May 2012, doi: 10.1016/j.neuron.2012.03.031.
[59] F. de Pasquale, M. Corbetta, V. Betti, and S. Della Penna, “Cortical cores in network dynamics,” *NeuroImage*, vol. 180, no. Pt B, pp. 370–382, Oct. 2018, doi: 10.1016/j.neuroimage.2017.09.063.
[60] M. P. van den Heuvel and O. Sporns, “Network hubs in the human brain,” *Trends in Cognitive Sciences*, vol. 17, no. 12, pp. 683–696, Dec. 2013, doi: 10.1016/j.tics.2013.09.012.
[61] G. Tononi and G. M. Edelman, “Consciousness and complexity,” *Science*. 1998. doi: 10.1126/science.282.5395.1846.
[62] J. Chen, C. J. Honey, E. Simony, M. J. Arcaro, K. A. Norman, and U. Hasson, “Accessing Real-Life Episodic Information from Minutes versus Hours Earlier Modulates Hippocampal and High-Order Cortical Dynamics,” *Cerebral Cortex*, vol. 26, no. 8, pp. 3428–3441, Aug. 2016, doi: 10.1093/cercor/bhv155.
[63] U. Hasson, J. Chen, and C. J. Honey, “Hierarchical process memory: Memory as an integral component of information processing,” *Trends in Cognitive Sciences*, vol. 19, no. 6, pp. 304–313, Jun. 2015, doi: 10.1016/j.tics.2015.04.006.
[64] C. J. Honey *et al.*, “Slow Cortical Dynamics and the Accumulation of Information over Long Timescales,” *Neuron*, vol. 76, no. 3, p. 668, Oct. 2012, doi: 10.1016/j.neuron.2012.10.024.
[65] Y. Lerner, C. J. Honey, L. J. Silbert, and U. Hasson, “Topographic mapping of a hierarchy of temporal receptive windows using a narrated story,” *Journal of Neuroscience*, vol. 31, no. 8, pp. 2906–2915, Feb. 2011, doi: 10.1523/JNEUROSCI.3684-10.2011.
[66] R. Chaudhuri, B. J. He, and X. J. Wang, “Random recurrent networks near criticality capture the broadband power distribution of human ECoG dynamics,” *Cerebral Cortex*, vol. 28, no. 10, pp. 3610–3622, 2018, doi: 10.1093/cercor/bhx233.
[67] R. Chaudhuri, K. Knoblauch, M. A. Gariel, H. Kennedy, and X. J. Wang, “A Large-Scale Circuit Mechanism for Hierarchical Dynamical Processing in the Primate Cortex,” *Neuron*, vol. 88, no. 2, pp. 419–431, Oct. 2015, doi: 10.1016/j.neuron.2015.09.008.
[68] R. J. Murray, M. Debbané, P. T. Fox, D. Bzdok, and S. B. Eickhoff, “Functional connectivity mapping of regions associated with self- and other-processing,” *Human Brain Mapping*, vol. 36, no. 4, pp. 1304–1324, Apr. 2015, doi: 10.1002/hbm.22703.

[69] B. J. He, "Scale-free properties of the functional magnetic resonance imaging signal during rest and task," *Journal of Neuroscience*, vol. 31, no. 39, pp. 13786–13795, Sep. 2011, doi: 10.1523/JNEUROSCI.2111-11.2011.
[70] Z. Huang, N. Obara, H. H. Davis, J. Pokorny, and G. Northoff, "The temporal structure of resting-state brain activity in the medial prefrontal cortex predicts self-consciousness," *Neuropsychologia*, vol. 82, pp. 161–170, Feb. 2016, doi: 10.1016/j.neuropsychologia.2016.01.025.
[71] C. C. Hilgetag and A. Goulas, "'Hierarchy' in the organization of brain networks," *Phil. Trans. R. Soc. B*, vol. 375, no. 1796, p. 20190319, Apr. 2020, doi: 10.1098/rstb.2019.0319.
[72] T. Ito, L. J. Hearne, and M. W. Cole, "A cortical hierarchy of localized and distributed processes revealed via dissociation of task activations, connectivity changes, and intrinsic timescales," *NeuroImage*, 2020, doi: 10.1016/j.neuroimage.2020.117141.
[73] T. Watanabe, G. Rees, and N. Masuda, "Atypical intrinsic neural timescale in autism," *eLife*, vol. 8, Feb. 2019, doi: 10.7554/eLife.42256.
[74] R. V. Raut *et al.*, "Organization of Propagated Intrinsic Brain Activity in Individual Humans," *Cerebral cortex (New York, N.Y. : 1991)*, vol. 30, no. 3, pp. 1716–1734, 2020, doi: 10.1093/cercor/bhz198.
[75] J. D. Murray *et al.*, "A hierarchy of intrinsic timescales across primate cortex," *Nature neuroscience*, vol. 17, no. 12, p. 1661, 2014.
[76] S. E. Cavanagh, J. D. Wallis, S. W. Kennerley, and L. T. Hunt, "Autocorrelation structure at rest predicts value correlates of single neurons during reward-guided choice," *eLife*, 2016, doi: 10.7554/eLife.18937.
[77] J. Chen, U. Hasson, and C. J. Honey, "Processing Timescales as an Organizing Principle for Primate Cortex," *Neuron*. 2015. doi: 10.1016/j.neuron.2015.10.010.
[78] J. Chen, Y. C. Leong, C. J. Honey, C. H. Yong, K. A. Norman, and U. Hasson, "Shared memories reveal shared structure in neural activity across individuals," *Nature Neuroscience*, vol. 20, no. 1, pp. 115–125, Jan. 2017, doi: 10.1038/nn.4450.
[79] S. J. Kiebel, J. Daunizeau, and K. J. Friston, "A hierarchy of time-scales and the brain," *PLoS Computational Biology*, vol. 4, no. 11, p. e1000209, 2008, doi: 10.1371/journal.pcbi.1000209.
[80] G. J. Stephens, C. J. Honey, and U. Hasson, "A place for time: The spatiotemporal structure of neural dynamics during natural audition," *Journal of Neurophysiology*, vol. 110, no. 9, pp. 2019–2026, Nov. 2013, doi: 10.1152/jn.00268.2013.
[81] P. Wang *et al.*, "Inversion of a large-scale circuit model reveals a cortical hierarchy in the dynamic resting human brain," *Tropical and Subtropical Agroecosystems*, vol. 21, no. 3, 2019, doi: 10.1126/sciadv.aat7854.
[82] C. Murphy *et al.*, "Distant from input: Evidence of regions within the default mode network supporting perceptually-decoupled and conceptually-guided cognition," *NeuroImage*, vol. 171, pp. 393–401, May 2018, doi: 10.1016/j.neuroimage.2018.01.017.
[83] D. S. Bassett, E. Bullmore, B. A. Verchinski, V. S. Mattay, D. R. Weinberger, and A. Meyer-Lindenberg, "Hierarchical organization of human cortical networks in health and Schizophrenia," *Journal of Neuroscience*, 2008, doi: 10.1523/JNEUROSCI.1929-08.2008.
[84] J. M. Huntenburg, P. L. Bazin, A. Goulas, C. L. Tardif, A. Villringer, and D. S. Margulies, "A Systematic Relationship Between Functional Connectivity and Intracortical Myelin in the Human Cerebral Cortex," *Cerebral cortex (New York, N.Y. : 1991)*, 2017, doi: 10.1093/cercor/bhx030.
[85] K. Mahjoory, J. M. Schoffelen, A. Keitel, and J. Gross, "The frequency gradient of human resting-state brain oscillations follows cortical hierarchies," *eLife*, 2020, doi: 10.7554/ELIFE.53715.
[86] E. Tagliazucchi, M. Behrens, and H. Laufs, "Sleep neuroimaging and models of consciousness," *Frontiers in Psychology*, vol. 4, no. MAY, p. 256, May 2013, doi: 10.3389/fpsyg.2013.00256.
[87] G. Northoff and V. Lamme, "Neural signs and mechanisms of consciousness: Is there a potential convergence of theories of consciousness in sight?," *Neuroscience and Biobehavioral Reviews*. 2020. doi: 10.1016/j.neubiorev.2020.07.019.
[88] A. Bernacchia, H. Seo, D. Lee, and X.-J. J. Wang, "A reservoir of time constants for memory traces in cortical neurons," *Nature Neuroscience*, vol. 14, no. 3, pp. 366–372, Mar. 2011, doi: 10.1038/nn.2752.
[89] F. Zilio *et al.*, "Intrinsic neural time scales are related to sensory rather than motor processing – Evidence from abnormal behavioral states."
[90] Z. Huang *et al.*, "Is There a Nonadditive Interaction Between Spontaneous and Evoked Activity? Phase-Dependence and Its Relation to the Temporal Structure of Scale-Free Brain Activity," *Cerebral cortex (New York, N.Y. : 1991)*, vol. 27, no. 2, pp. 1037–1059, Dec. 2017, doi: 10.1093/cercor/bhv288.

[91] K. D. Himberger, H. Y. Chien, and C. J. Honey, "Principles of Temporal Processing Across the Cortical Hierarchy," *Neuroscience*, vol. 389. pp. 161–174, 2018. doi: 10.1016/j.neuroscience.2018.04.030.
[92] D. C. Van Essen, S. M. Smith, D. M. Barch, T. E. J. Behrens, E. Yacoub, and K. Ugurbil, "The WU-Minn Human Connectome Project: An overview," *NeuroImage*, vol. 80, pp. 62–79, Oct. 2013, doi: 10.1016/j.neuroimage.2013.05.041.
[93] L. J. Larson-Prior *et al.*, "Adding dynamics to the Human Connectome Project with MEG," *NeuroImage*, 2013, doi: 10.1016/j.neuroimage.2013.05.056.
[94] M. Demirtaş *et al.*, "Hierarchical Heterogeneity across Human Cortex Shapes Large-Scale Neural Dynamics," *Neuron*, vol. 101, no. 6, pp. 1181-1194.e13, Mar. 2019, doi: 10.1016/j.neuron.2019.01.017.
[95] A. Schaefer *et al.*, "Local-Global Parcellation of the Human Cerebral Cortex from Intrinsic Functional Connectivity MRI," *Cerebral Cortex*, 2018, doi: 10.1093/cercor/bhx179.
[96] J. L. Ji, M. Spronk, K. Kulkarni, G. Repovš, A. Anticevic, and M. W. Cole, "Mapping the human brain's cortical-subcortical functional network organization," *NeuroImage*, vol. 185, pp. 35–57, Jan. 2019, doi: 10.1016/j.neuroimage.2018.10.006.
[97] S. Seabold and J. Perktold, "Statsmodels: Econometric and Statistical Modeling with Python," 2010.
[98] B. C. Ross, "Mutual information between discrete and continuous data sets," *PLoS ONE*, 2014, doi: 10.1371/journal.pone.0087357.
[99] B. J. He, J. M. Zempel, A. Z. Snyder, and M. E. Raichle, "The temporal structures and functional significance of scale-free brain activity," *Neuron*, vol. 66, no. 3, pp. 353–369, May 2010, doi: 10.1016/j.neuron.2010.04.020.
[100] C. Tallon-Baudry, F. Campana, H.-D. Park, and M. Babo-Rebelo, "The neural monitoring of visceral inputs, rather than attention, accounts for first-person perspective in conscious vision," *Cortex*, vol. 102, pp. 139–149, May 2018, doi: 10.1016/j.cortex.2017.05.019.
[101] G. Northoff, P. Qin, and T. Nakao, "Rest-stimulus interaction in the brain: a review," *Trends in neurosciences*, vol. 33, no. 6, pp. 277–284, 2010.
[102] G. Northoff, "Spatiotemporal psychopathology I: No rest for the brain's resting state activity in depression? Spatiotemporal psychopathology of depressive symptoms," *Journal of Affective Disorders*, vol. 190, pp. 854–866, Jan. 2016, doi: 10.1016/j.jad.2015.05.007.
[103] A. Wolff *et al.*, "The temporal signature of self: Temporal measures of resting-state EEG predict self-consciousness," *Human Brain Mapping*, vol. 40, no. 3, pp. 789–803, Feb. 2019, doi: 10.1002/hbm.24412.
[104] I. R. Kolvoort, S. Wainio-Theberge, A. Wolff, and G. Northoff, "Temporal integration as 'common currency' of brain and self-scale-free activity in resting-state EEG correlates with temporal delay effects on self-relatedness," *Human Brain Mapping*, 2020, doi: 10.1002/hbm.25129.
[105] B. J. He and M. E. Raichle, "The fMRI signal, slow cortical potential and consciousness," *Trends in Cognitive Sciences*, vol. 13, no. 7, pp. 302–309, 2009, doi: 10.1016/j.tics.2009.04.004.
[106] M. Steriade, A. Nunez, and F. Amzica, "A novel slow (< 1 Hz) oscillation of neocortical neurons in vivo: Depolarizing and hyperpolarizing components," *Journal of Neuroscience*, vol. 13, no. 8, pp. 3252–3265, Aug. 1993, doi: 10.1523/jneurosci.13-08-03252.1993.
[107] A. T. Baria, B. Maniscalco, and B. J. He, "Initial-state-dependent, robust, transient neural dynamics encode conscious visual perception," *PLoS Computational Biology*, vol. 13, no. 11, p. e1005806, Nov. 2017, doi: 10.1371/journal.pcbi.1005806.
[108] Q. Li, Z. Hill, and B. J. He, "Spatiotemporal dissociation of brain activity underlying subjective awareness, objective performance and confidence," *Journal of Neuroscience*, 2014, doi: 10.1523/JNEUROSCI.1820-13.2014.
[109] P. Khader, T. Schicke, B. Röder, and F. Rösler, "On the relationship between slow cortical potentials and BOLD signal changes in humans," *International Journal of Psychophysiology*, 2008, doi: 10.1016/j.ijpsycho.2007.05.018.
[110] G. Northoff, "'Paradox of slow frequencies' – Are slow frequencies in upper cortical layers a neural predisposition of the level/state of consciousness (NPC)?," *Consciousness and Cognition*, vol. 54, pp. 20–35, Sep. 2017, doi: 10.1016/j.concog.2017.03.006.
[111] J. A. De Zwart *et al.*, "Temporal dynamics of the BOLD fMRI impulse response," *NeuroImage*, vol. 24, no. 3, pp. 667–677, Feb. 2005, doi: 10.1016/j.neuroimage.2004.09.013.
[112] C. J. Honey *et al.*, "Predicting human resting-state functional connectivity from structural connectivity," *Proceedings of the National Academy of Sciences of the United States of America*, vol. 106, no. 6, pp. 2035–2040, Feb. 2009, doi: 10.1073/pnas.0811168106.

[113] D. Gutierrez-Barragan, M. A. Basson, S. Panzeri, and A. Gozzi, "Infraslow State Fluctuations Govern Spontaneous fMRI Network Dynamics," *Current Biology*, vol. 29, no. 14, pp. 2295-2306.e5, Jul. 2019, doi: 10.1016/j.cub.2019.06.017.
[114] A. Mitra *et al.*, "Spontaneous Infra-slow Brain Activity Has Unique Spatiotemporal Dynamics and Laminar Structure," *Neuron*, vol. 98, no. 2, pp. 297-305.e6, Apr. 2018, doi: 10.1016/j.neuron.2018.03.015.
[115] B. J. He, A. Z. Snyder, J. M. Zempel, M. D. Smyth, and M. E. Raichle, "Electrophysiological correlates of the brain's intrinsic large-scale functional architecture," *Proceedings of the National Academy of Sciences of the United States of America*, vol. 105, no. 41. pp. 16039–16044, 2008. doi: 10.1073/pnas.0807010105.
[116] S. Palva and J. M. Palva, "Discovering oscillatory interaction networks with M/EEG: Challenges and breakthroughs," *Trends in Cognitive Sciences*, vol. 16, no. 4. pp. 219–230, 2012. doi: 10.1016/j.tics.2012.02.004.
[117] D. A. Leopold, Y. Murayama, and N. K. Logothetis, "Very slow activity fluctuations in monkey visual cortex: Implications for functional brain imaging," *Cerebral Cortex*, vol. 13, no. 4, pp. 422–433, Apr. 2003, doi: 10.1093/cercor/13.4.422.
[118] W.-J. Pan, G. J. Thompson, M. E. Magnuson, D. Jaeger, and S. Keilholz, "Infraslow {LFP} correlates to resting-state {fMRI} {BOLD} signals," *Neuroimage*, vol. 74, pp. 288–297, Jul. 2013.
[119] J. Turchi *et al.*, "The Basal Forebrain Regulates Global Resting-State fMRI Fluctuations," *Neuron*, vol. 97, no. 4, pp. 940-952.e4, Feb. 2018, doi: 10.1016/j.neuron.2018.01.032.
[120] S. Monto, S. Palva, J. Voipio, and J. M. Palva, "Very slow EEG fluctuations predict the dynamics of stimulus detection and oscillation amplitudes in humans," *Journal of Neuroscience*, vol. 28, no. 33, pp. 8268–8272, Aug. 2008, doi: 10.1523/JNEUROSCI.1910-08.2008.
[121] X. Liu, N. Zhang, C. Chang, and J. H. Duyn, "Co-activation patterns in resting-state fMRI signals," *NeuroImage*. 2018. doi: 10.1016/j.neuroimage.2018.01.041.
[122] N. K. Logothetis, J. Pauls, M. Augath, T. Trinath, and A. Oeltermann, "Neurophysiological investigation of the basis of the fMRI signal," *Nature*, vol. 412, no. 6843, pp. 150–157, Jul. 2001, doi: 10.1038/35084005.
[123] N. K. Logothetis, "What we can do and what we cannot do with fMRI," *Nature*, vol. 453, no. 7197. pp. 869–878, 2008. doi: 10.1038/nature06976.
[124] A. Kucyi, M. Esterman, C. S. Riley, and E. M. Valera, "Spontaneous default network activity reflects behavioral variability independent of mind-wandering," *Proceedings of the National Academy of Sciences of the United States of America*, vol. 113, no. 48, pp. 13899–13904, Nov. 2016, doi: 10.1073/pnas.1611743113.
[125] A. Kucyi *et al.*, "Anticorrelated inter-network electrophysiological activity varies dynamically with attentional performance and behavioral states," *bioRxiv*, p. 503193, 2018, doi: 10.1101/503193.
[126] A. M. Wohlschläger *et al.*, "Ongoing slow fluctuations in V1 impact on visual perception," *Frontiers in Human Neuroscience*, vol. 10, p. 13, Aug. 2016, doi: 10.3389/fnhum.2016.00411.
[127] M. W. Cole, T. Ito, D. S. Bassett, and D. H. Schultz, "Activity flow over resting-state networks shapes cognitive task activations," *Nature Neuroscience*, 2016, doi: 10.1038/nn.4406.
[128] M. W. Cole, J. R. Reynolds, J. D. Power, G. Repovs, A. Anticevic, and T. S. Braver, "Multi-task connectivity reveals flexible hubs for adaptive task control," *Nature neuroscience*, vol. 16, no. 9, p. 1348, 2013.
[129] M. W. Cole, D. S. Bassett, J. D. Power, T. S. Braver, and S. E. Petersen, "Intrinsic and task-evoked network architectures of the human brain," *Neuron*, 2014, doi: 10.1016/j.neuron.2014.05.014.
[130] Y. Bai, Z. Liang, and X. Li, "A permutation Lempel-Ziv complexity measure for EEG analysis," *Biomedical Signal Processing and Control*, 2015, doi: 10.1016/j.bspc.2015.04.002.
[131] D. Abásolo, R. Hornero, C. Gómez, M. García, and M. López, "Analysis of EEG background activity in Alzheimer's disease patients with Lempel-Ziv complexity and central tendency measure," *Medical Engineering and Physics*, vol. 28, no. 4, pp. 315–322, 2006, doi: 10.1016/j.medengphy.2005.07.004.
[132] A. J. Ibáñez-Molina, S. Iglesias-Parro, M. F. Soriano, and J. I. Aznarte, "Multiscale Lempel-Ziv complexity for EEG measures," *Clinical Neurophysiology*, 2015, doi: 10.1016/j.clinph.2014.07.012.
[133] A. Lempel and J. Ziv, "On the Complexity of Finite Sequences," *IEEE Transactions on Information Theory*, 1976, doi: 10.1109/TIT.1976.1055501.
[134] M. Aboy, R. Hornero, D. Abásolo, and D. Álvarez, "Interpretation of the Lempel-Ziv complexity measure in the context of biomedical signal analysis," *IEEE Transactions on Biomedical Engineering*, vol. 53, no. 11, pp. 2282–2288, Nov. 2006, doi: 10.1109/TBME.2006.883696.
[135] T. F. Varley *et al.*, "Consciousness & Brain Functional Complexity in Propofol Anaesthesia," *Scientific Reports*, vol. 10, no. 1, p. 1018, Dec. 2020, doi: 10.1038/s41598-020-57695-3.

[136] G. Deshpande, S. LaConte, S. Peltier, and X. Hu, "Tissue specificity of nonlinear dynamics in baseline fMRI," *Magnetic Resonance in Medicine*, vol. 55, no. 3, pp. 626–632, Mar. 2006, doi: 10.1002/mrm.20817.
[137] M. Boly *et al.*, "Stimulus set meaningfulness and neurophysiological differentiation: A functional magnetic resonance imaging study," *PLoS ONE*, vol. 10, no. 5, p. e0125337, May 2015, doi: 10.1371/journal.pone.0125337.
[138] A. G. Hudetz, X. Liu, S. Pillay, M. Boly, and G. Tononi, "Propofol anesthesia reduces Lempel-Ziv complexity of spontaneous brain activity in rats," *Neuroscience Letters*, vol. 628, pp. 132–135, Aug. 2016, doi: 10.1016/j.neulet.2016.06.017.
[139] C. Gómez, R. Hornero, D. Abásolo, A. Fernández, and J. Escudero, "Analysis of MEG background activity in Alzheimer's disease using nonlinear Methods and ANFIS," *Annals of Biomedical Engineering*, vol. 37, no. 3, pp. 586–594, Mar. 2009, doi: 10.1007/s10439-008-9633-6.
[140] A. Fernández *et al.*, "The correlation between white-matter microstructure and the complexity of spontaneous brain activity: A difussion tensor imaging-MEG study," *NeuroImage*, vol. 57, no. 4, pp. 1300–1307, Aug. 2011, doi: 10.1016/j.neuroimage.2011.05.079.
[141] Q. Luo *et al.*, "Complexity analysis of resting state magnetoencephalography activity in traumatic brain injury patients," *Journal of Neurotrauma*, vol. 30, no. 20, pp. 1702–1709, Oct. 2013, doi: 10.1089/neu.2012.2679.
[142] A. T. Baria, M. V. Centeno, M. E. Ghantous, P. C. Chang, D. Procissi, and A. V. Apkarian, "Bold temporal variability differentiates wakefulness from anesthesia-induced unconsciousness," *Journal of Neurophysiology*, vol. 119, no. 3, pp. 834–848, Mar. 2018, doi: 10.1152/jn.00714.2017.
[143] D. Abasólo, C. J. James, and R. Hornero, "Non-linear analysis of intracranial electroencephalogram recordings with approximate entropy and lempel-ziv complexity for epileptic seizure detection," in *Annual International Conference of the IEEE Engineering in Medicine and Biology - Proceedings*, Aug. 2007, vol. 6, pp. 1953–1956. doi: 10.1109/IEMBS.2007.4352700.
[144] M. Bachmann *et al.*, "Methods for classifying depression in single channel EEG using linear and nonlinear signal analysis," *Computer Methods and Programs in Biomedicine*, vol. 155, pp. 11–17, Mar. 2018, doi: 10.1016/j.cmpb.2017.11.023.
[145] A. J. Ibáñez-Molina, V. Lozano, M. F. Soriano, J. I. Aznarte, C. J. Gómez-Ariza, and M. T. Bajo, "EEG multiscale complexity in schizophrenia during picture naming," *Frontiers in Physiology*, vol. 9, no. SEP, p. 1213, Sep. 2018, doi: 10.3389/fphys.2018.01213.
[146] D. M. Mateos, R. Guevara Erra, R. Wennberg, and J. L. Perez Velazquez, "Measures of entropy and complexity in altered states of consciousness," *Cognitive Neurodynamics*, vol. 12, no. 1, pp. 73–84, Feb. 2018, doi: 10.1007/s11571-017-9459-8.
[147] J. Szczepański, J. M. Amigó, E. Wajnryb, and M. V. Sanchez-Vives, "Application of Lempel-Ziv complexity to the analysis of neural discharges," *Network: Computation in Neural Systems*, vol. 14, no. 2, pp. 335–350, Jan. 2003, doi: 10.1088/0954-898X_14_2_309.
[148] H. Schwilden, J. Schuttler, and H. Stoeckel, "Quantitation of the EEG and pharmacodynamic modelling of hypnotic drugs: etomidate as an example," *European Journal of Anaesthesiology*, vol. 2, no. 2, pp. 121–131, Jun. 1985.
[149] D. Schwender, M. Daunderer, S. Mulzer, S. Klasing, U. Finsterer, and K. Peter, "Spectral edge frequency of the electroencephalogram to monitor 'depth' of anaesthesia with isoflurane or propofol," *British Journal of Anaesthesia*, vol. 77, no. 2, pp. 179–184, 1996, doi: 10.1093/bja/77.2.179.
[150] T. McDonald, R. Berkowitz, and W. E. Hoffman, "Median eeg frequency is more sensitive to increases in sympathetic activity than bispectral index," *Journal of Neurosurgical Anesthesiology*, vol. 11, no. 4, pp. 255–259, 1999, doi: 10.1097/00008506-199910000-00005.
[151] A. Bachiller *et al.*, "Decreased entropy modulation of EEG response to novelty and relevance in schizophrenia during a P300 task," *European Archives of Psychiatry and Clinical Neuroscience*, vol. 265, no. 6, pp. 525–535, Sep. 2015, doi: 10.1007/s00406-014-0525-5.
[152] W. Verrusio, E. Ettorre, E. Vicenzini, N. Vanacore, M. Cacciafesta, and O. Mecarelli, "The Mozart Effect: A quantitative EEG study," *Consciousness and Cognition*, vol. 35, pp. 150–155, Sep. 2015, doi: 10.1016/j.concog.2015.05.005.
[153] I. Pappas, R. M. Adapa, D. K. Menon, and E. A. Stamatakis, "Brain network disintegration during sedation is mediated by the complexity of sparsely connected regions," *NeuroImage*, 2019, doi: 10.1016/j.neuroimage.2018.10.078.

[154] M. F. Glasser *et al.*, "The minimal preprocessing pipelines for the Human Connectome Project," *NeuroImage*, vol. 80, pp. 105–124, Oct. 2013, doi: 10.1016/j.neuroimage.2013.04.127.
[155] A. Thanh Vu *et al.*, "Tradeoffs in pushing the spatial resolution of fMRI for the 7T Human Connectome Project," *NeuroImage*, vol. 154, pp. 23–32, Jul. 2017, doi: 10.1016/j.neuroimage.2016.11.049.
[156] N. C. Benson *et al.*, "The Human Connectome Project 7 Tesla retinotopy dataset: Description and population receptive field analysis," *Journal of Vision*, vol. 18, no. 13, pp. 1–22, Dec. 2018, doi: 10.1167/18.13.23.
[157] G. Salimi-Khorshidi, G. Douaud, C. F. Beckmann, M. F. Glasser, L. Griffanti, and S. M. Smith, "Automatic denoising of functional MRI data: Combining independent component analysis and hierarchical fusion of classifiers," *NeuroImage*, vol. 90, pp. 449–468, Apr. 2014, doi: 10.1016/j.neuroimage.2013.11.046.
[158] M. M. Craig, A. E. Manktelow, B. J. Sahakian, D. K. Menon, and E. A. Stamatakis, "Spectral diversity in default mode network connectivity reflects behavioral state," *Journal of Cognitive Neuroscience*, 2018, doi: 10.1162/jocn_a_01213.
[159] R. Nagarajan, "Quantifying physiological data with Lempel-Ziv complexity - Certain issues," *IEEE Transactions on Biomedical Engineering*, vol. 49, no. 11, pp. 1371–1373, 2002, doi: 10.1109/TBME.2002.804582.
[160] P. D. Welch, "The Use of Fast Fourier Transform for the Estimation of Power Spectra: A Method Based on Time Averaging Over Short, Modified Periodograms," *IEEE Transactions on Audio and Electroacoustics*, vol. 15, no. 2, pp. 70–73, Jun. 1967, doi: 10.1109/TAU.1967.1161901.
[161] J. B. Burt *et al.*, "Hierarchy of transcriptomic specialization across human cortex captured by structural neuroimaging topography," *Nature Neuroscience*, 2018, doi: 10.1038/s41593-018-0195-0.
[162] D. Tingley, T. Yamamoto, K. Hirose, L. Keele, and K. Imai, "Mediation: R package for causal mediation analysis," *Journal of Statistical Software*, 2014, doi: 10.18637/jss.v059.i05.
[163] A. F. Hayes, "Beyond Baron and Kenny: Statistical mediation analysis in the new millennium," *Communication Monographs*, 2009, doi: 10.1080/03637750903310360.
[164] M. M. Schartner, R. L. Carhart-Harris, A. B. Barrett, A. K. Seth, and S. D. Muthukumaraswamy, "Increased spontaneous MEG signal diversity for psychoactive doses of ketamine, LSD and psilocybin," *Scientific Reports*, 2017, doi: 10.1038/srep46421.
[165] Y. Zhang *et al.*, "Altered functional networks in long-term unilateral hearing loss: A connectome analysis," *Brain and Behavior*, 2018, doi: 10.1002/brb3.912.
[166] C. Baldassano, J. Chen, A. Zadbood, J. W. Pillow, U. Hasson, and K. A. Norman, "Discovering Event Structure in Continuous Narrative Perception and Memory," *Neuron*, vol. 95, no. 3, pp. 709-721.e5, Aug. 2017, doi: 10.1016/j.neuron.2017.06.041.
[167] A. Huk, K. Bonnen, and B. J. He, "Beyond trial-based paradigms: Continuous behavior, ongoing neural activity, and natural stimuli," *Journal of Neuroscience*, vol. 38, no. 35, pp. 7551–7558, Aug. 2018, doi: 10.1523/JNEUROSCI.1920-17.2018.
[168] E. Tagliazucchi, R. Carhart-Harris, R. Leech, D. Nutt, and D. R. Chialvo, "Enhanced repertoire of brain dynamical states during the psychedelic experience," *Human Brain Mapping*, vol. 35, no. 11, pp. 5442–5456, Nov. 2014, doi: 10.1002/hbm.22562.
[169] G. Deco, J. Cruzat, and M. L. Kringelbach, "Brain songs framework used for discovering the relevant timescale of the human brain," *Nature Communications*, vol. 10, no. 1, 2019, doi: 10.1038/s41467-018-08186-7.
[170] F. Farzan *et al.*, "Brain temporal complexity in explaining the therapeutic and cognitive effects of seizure therapy," *Brain*, vol. 140, no. 4, pp. 1011–1025, Apr. 2017, doi: 10.1093/brain/awx030.
[171] R. Liégeois *et al.*, "Resting brain dynamics at different timescales capture distinct aspects of human behavior," *Nature Communications*, vol. 10, no. 1, 2019, doi: 10.1038/s41467-019-10317-7.
[172] D. F. Wasmuht, E. Spaak, T. J. Buschman, E. K. Miller, and M. G. Stokes, "Intrinsic neuronal dynamics predict distinct functional roles during working memory," *Nature Communications*, vol. 9, no. 1, p. 3499, Dec. 2018, doi: 10.1038/s41467-018-05961-4.
[173] Y. Yeshurun, M. Nguyen, and U. Hasson, "The default mode network: where the idiosyncratic self meets the shared social world," *Nature Reviews Neuroscience*, pp. 1–12, Jan. 2021, doi: 10.1038/s41583-020-00420-w.
[174] R. Chaudhuri, A. Bernacchia, and X.-J. Wang, "A diversity of localized timescales in network activity," *eLife*, 2014, doi: 10.7554/elife.01239.
[175] M. Golesorkhi, J. Gomez-Pilar, S. Tumati, M. Fraser, and G. Northoff, "Temporal hierarchy converges with spatial hierarchy: Intrinsic neural timescales follow core-periphery organization," *bioRxiv*, p. 2020.06.12.148866, Nov. 2020, doi: 10.1101/2020.06.12.148866.

[176] C. A. Runyan, E. Piasini, S. Panzeri, and C. D. Harvey, "Distinct timescales of population coding across cortex," *Nature*, 2017, doi: 10.1038/nature23020.
[177] G. Shafiei, R. Markello, R. V. de Wael, B. Bernhardt, B. Fulcher, and B. Misic, "Topographic gradients of intrinsic dynamics across neocortex," *bioRxiv*, Jul. 2020, doi: 10.1101/2020.07.03.186916.
[178] F. Zilio *et al.*, "Are intrinsic neural timescales related to sensory processing? Evidence from abnormal behavioral states," *NeuroImage*, vol. 226, p. 117579, Feb. 2021, doi: 10.1016/j.neuroimage.2020.117579.
[179] O. David and K. J. Friston, "A neural mass model for MEG/EEG:," *NeuroImage*, vol. 20, no. 3, pp. 1743–1755, Nov. 2003, doi: 10.1016/j.neuroimage.2003.07.015.
[180] B. H. Jansen and V. G. Rit, "Electroencephalogram and visual evoked potential generation in a mathematical model of coupled cortical columns," *Biological Cybernetics*, vol. 73, no. 4, pp. 357–366, Sep. 1995, doi: 10.1007/BF00199471.
[181] N. Y. Feng, D. J. Fergus, and A. H. Bass, "Neural transcriptome reveals molecular mechanisms for temporal control of vocalization across multiple timescales," *BMC Genomics*, vol. 16, no. 1, p. 408, Dec. 2015, doi: 10.1186/s12864-015-1577-2.
[182] H. S. Kaplan, O. Salazar Thula, N. Khoss, and M. Zimmer, "Nested Neuronal Dynamics Orchestrate a Behavioral Hierarchy across Timescales," *Neuron*, vol. 105, no. 3, pp. 562-576.e9, Feb. 2020, doi: 10.1016/j.neuron.2019.10.037.
[183] M. Beiran and S. Ostojic, "Contrasting the effects of adaptation and synaptic filtering on the timescales of dynamics in recurrent networks," *PLOS Computational Biology*, vol. 15, no. 3, p. e1006893, Mar. 2019, doi: 10.1371/journal.pcbi.1006893.
[184] J. Fallon *et al.*, "Timescales of spontaneous fMRI fluctuations relate to structural connectivity in the brain," *Network Neuroscience*, vol. 4, no. 3, pp. 788–806, Jan. 2020, doi: 10.1162/netn_a_00151.
[185] Y. Kaneoke, T. Donishi, J. Iwatani, S. Ukai, K. Shinosaki, and M. Terada, "Variance and Autocorrelation of the Spontaneous Slow Brain Activity," *PLoS ONE*, vol. 7, no. 5, p. e38131, May 2012, doi: 10.1371/journal.pone.0038131.
[186] T. Ogawa and H. Komatsu, "Differential Temporal Storage Capacity in the Baseline Activity of Neurons in Macaque Frontal Eye Field and Area V4," *Journal of Neurophysiology*, vol. 103, no. 5, pp. 2433–2445, May 2010, doi: 10.1152/jn.01066.2009.
[187] S. Sadaghiani and J. Wirsich, "Intrinsic connectome organization across temporal scales: New insights from cross-modal approaches," *Network Neuroscience*, vol. 4, no. 1, pp. 1–29, Jan. 2020, doi: 10.1162/netn_a_00114.
[188] T. Ito, L. Hearne, R. Mill, C. Cocuzza, and M. W. Cole, "Discovering the Computational Relevance of Brain Network Organization," *Trends in Cognitive Sciences*, vol. 24, no. 1, pp. 25–38, Jan. 2020, doi: 10.1016/j.tics.2019.10.005.
[189] A. T. Baria *et al.*, "Linking human brain local activity fluctuations to structural and functional network architectures," *NeuroImage*, 2013, doi: 10.1016/j.neuroimage.2013.01.072.
[190] H. Honari, A. S. Choe, J. J. Pekar, and M. A. Lindquist, "Investigating the impact of autocorrelation on time-varying connectivity," *NeuroImage*, vol. 197, pp. 37–48, Aug. 2019, doi: 10.1016/j.neuroimage.2019.04.042.
[191] A. Kucyi and K. D. Davis, "The dynamic pain connectome," *Trends in Neurosciences*, vol. 38, no. 2, pp. 86–95, Feb. 2015, doi: 10.1016/j.tins.2014.11.006.
[192] M. Menceloglu, M. Grabowecky, and S. Suzuki, "EEG state-trajectory instability and speed reveal global rules of intrinsic spatiotemporal neural dynamics," *PLOS ONE*, vol. 15, no. 8, p. e0235744, Aug. 2020, doi: 10.1371/journal.pone.0235744.
[193] R. Salvador *et al.*, "A simple view of the brain through a frequency-specific functional connectivity measure," *NeuroImage*, vol. 39, no. 1, pp. 279–289, Jan. 2008, doi: 10.1016/j.neuroimage.2007.08.018.
[194] M. Nguyen, T. Vanderwal, and U. Hasson, "Shared understanding of narratives is correlated with shared neural responses," *NeuroImage*, vol. 184, pp. 161–170, Jan. 2019, doi: 10.1016/j.neuroimage.2018.09.010.
[195] M. Regev, E. Simony, K. Lee, K. M. Tan, J. Chen, and U. Hasson, "Propagation of Information Along the Cortical Hierarchy as a Function of Attention while Reading and Listening to Stories," *Cerebral Cortex*, vol. 29, no. 10, pp. 4017–4034, Nov. 2019, doi: 10.1093/cercor/bhy282.
[196] Y. Yeshurun, M. Nguyen, and U. Hasson, "Amplification of local changes along the timescale processing hierarchy," *Proceedings of the National Academy of Sciences*, vol. 114, no. 35, pp. 9475–9480, Aug. 2017, doi: 10.1073/pnas.1701652114.
[197] T. Ito *et al.*, "Cognitive task information is transferred between brain regions via resting-state network topology," *Nature Communications*, vol. 8, no. 1, p. 1027, Dec. 2017, doi: 10.1038/s41467-017-01000-w.

[198] I. Tavor, O. P. Jones, R. B. Mars, S. M. Smith, T. E. Behrens, and S. Jbabdi, “Task-free MRI predicts individual differences in brain activity during task performance,” *Science*, vol. 352, no. 6282, pp. 216–220, Apr. 2016, doi: 10.1126/science.aad8127.
[199] G. Northoff, N. W. Duncan, and D. J. Hayes, “The brain and its resting state activity—Experimental and methodological implications,” *Progress in Neurobiology*, vol. 92, no. 4, pp. 593–600, Dec. 2010, doi: 10.1016/j.pneurobio.2010.09.002.
[200] A. Sarracino, O. Arviv, O. Shriki, and L. de Arcangelis, “Predicting brain evoked response to external stimuli from temporal correlations of spontaneous activity,” *Physical Review Research*, vol. 2, no. 3, p. 033355, Sep. 2020, doi: 10.1103/PhysRevResearch.2.033355.
[201] S. Wainio-Theberge, A. Wolff, and G. Northoff, “Bridging the gap – Spontaneous fluctuations shape stimulus-evoked spectral power,” *bioRxiv*, Jun. 2020, doi: 10.1101/2020.06.23.166058.
[202] L. L. Gollo, “Exploring atypical timescales in the brain,” *eLife*, vol. 8, Feb. 2019, doi: 10.7554/eLife.45089.
[203] G. Northoff and J. Gomez-Pilar, “Overcoming Rest–Task Divide—Abnormal Temporospatial Dynamics and Its Cognition in Schizophrenia,” *Schizophrenia Bulletin*, 2020, doi: 10.1093/schbul/sbaa178.
[204] R. Cirillo, V. Fascianelli, L. Ferrucci, and A. Genovesio, “Neural Intrinsic Timescales in the Macaque Dorsal Premotor Cortex Predict the Strength of Spatial Response Coding,” *iScience*, vol. 10, pp. 203–210, Dec. 2018, doi: 10.1016/j.isci.2018.11.033.
[205] Z. Huang, X. Liu, G. A. Mashour, and A. G. Hudetz, “Timescales of intrinsic BOLD signal dynamics and functional connectivity in pharmacologic and neuropathologic states of unconsciousness,” *Journal of Neuroscience*, vol. 38, no. 9, pp. 2304–2317, Feb. 2018, doi: 10.1523/JNEUROSCI.2545-17.2018.
[206] K. Sugimura *et al.*, “Association between long-range temporal correlations in intrinsic EEG activity and subjective sense of identity,” *Scientific Reports*, 2021, doi: 10.1038/s41598-020-79444-2.
[207] E. Déli, A. Tozzi, and J. F. Peters, “Relationships between short and fast brain timescales,” *Cognitive Neurodynamics*, vol. 11, no. 6, pp. 539–552, Dec. 2017, doi: 10.1007/s11571-017-9450-4.
[208] F. Ventriglia, “Random dispersion in excitatory synapse response,” *Cognitive Neurodynamics*, vol. 8, no. 4, pp. 327–334, Aug. 2014, doi: 10.1007/s11571-014-9285-1.
[209] T. Andrillon and S. Kouider, “The vigilant sleeper: neural mechanisms of sensory (de)coupling during sleep,” *Current Opinion in Physiology*, vol. 15, pp. 47–59, Jun. 2020, doi: 10.1016/j.cophys.2019.12.002.
[210] K. W. Fischer, U. Goswami, and J. Geake, “The Future of Educational Neuroscience,” *Mind, Brain, and Education*, vol. 4, no. 2, pp. 68–80, Jun. 2010, doi: 10.1111/j.1751-228X.2010.01086.x.
[211] F. Pistoia *et al.*, “Contribution of Interoceptive Information to Emotional Processing: Evidence from Individuals with Spinal Cord Injury,” *Journal of Neurotrauma*, vol. 32, no. 24, pp. 1981–1986, Dec. 2015, doi: 10.1089/neu.2015.3897.
[212] N. D. Schiff, T. Nauvel, and J. D. Victor, “Large-scale brain dynamics in disorders of consciousness,” *Current Opinion in Neurobiology*, vol. 25, pp. 7–14, Apr. 2014, doi: 10.1016/j.conb.2013.10.007.
[213] K. K. Sellers, D. V. Bennett, A. Hutt, J. H. Williams, and F. Fröhlich, “Awake vs. anesthetized: layer-specific sensory processing in visual cortex and functional connectivity between cortical areas,” *Journal of Neurophysiology*, vol. 113, no. 10, pp. 3798–3815, Jun. 2015, doi: 10.1152/jn.00923.2014.
[214] G. Northoff, “Gene, brains, and environment—genetic neuroimaging of depression,” *Current Opinion in Neurobiology*, vol. 23, no. 1, pp. 133–142, Feb. 2013, doi: 10.1016/j.conb.2012.08.004.
[215] G. Northoff and W.-D. Heiss, “Why Is the Distinction Between Neural Predispositions, Prerequisites, and Correlates of the Level of Consciousness Clinically Relevant?,” *Stroke*, vol. 46, no. 4, pp. 1147–1151, Apr. 2015, doi: 10.1161/STROKEAHA.114.007969.
[216] Y. Mochizuki *et al.*, “Similarity in Neuronal Firing Regimes across Mammalian Species,” *Journal of Neuroscience*, vol. 36, no. 21, pp. 5736–5747, May 2016, doi: 10.1523/JNEUROSCI.0230-16.2016.
[217] S. Shinomoto *et al.*, “Relating Neuronal Firing Patterns to Functional Differentiation of Cerebral Cortex,” *PLoS Computational Biology*, vol. 5, no. 7, p. e1000433, Jul. 2009, doi: 10.1371/journal.pcbi.1000433.
[218] G. Buzsáki, N. Logothetis, and W. Singer, “Scaling Brain Size, Keeping Timing: Evolutionary Preservation of Brain Rhythms,” *Neuron*, vol. 80, no. 3, pp. 751–764, Oct. 2013, doi: 10.1016/j.neuron.2013.10.002.
[219] B. D. Fulcher, J. D. Murray, V. Zerbi, and X.-J. Wang, “Multimodal gradients across mouse cortex,” *Proceedings of the National Academy of Sciences*, vol. 116, no. 10, pp. 4689–4695, Mar. 2019, doi: 10.1073/pnas.1814144116.
[220] Y. S. Zhang and A. A. Ghazanfar, “A Hierarchy of Autonomous Systems for Vocal Production,” *Trends in Neurosciences*, vol. 43, no. 2, pp. 115–126, Feb. 2020, doi: 10.1016/j.tins.2019.12.006.

[221] D. Henao, M. Navarrete, M. Valderrama, and M. Le Van Quyen, “Entrainment and synchronization of brain oscillations to auditory stimulations,” *Neuroscience Research*, vol. 156, pp. 271–278, Jul. 2020, doi: 10.1016/j.neures.2020.03.004.
[222] P. Lakatos, J. Gross, and G. Thut, “A New Unifying Account of the Roles of Neuronal Entrainment,” *Current Biology*, vol. 29, no. 18, pp. R890–R905, Sep. 2019, doi: 10.1016/j.cub.2019.07.075.
[223] X. Teng, X. Tian, J. Rowland, and D. Poeppel, “Concurrent temporal channels for auditory processing: Oscillatory neural entrainment reveals segregation of function at different scales,” *PLOS Biology*, vol. 15, no. 11, p. e2000812, Nov. 2017, doi: 10.1371/journal.pbio.2000812.
[224] S. E. Cavanagh, L. T. Hunt, and S. W. Kennerley, “A Diversity of Intrinsic Timescales Underlie Neural Computations,” *Frontiers in Neural Circuits*. 2020. doi: 10.3389/fncir.2020.615626.
[225] K. Müsch, K. Himberger, K. M. Tan, T. A. Valiante, and C. J. Honey, “Transformation of speech sequences in human sensorimotor circuits,” *Proceedings of the National Academy of Sciences*, vol. 117, no. 6, pp. 3203–3213, Feb. 2020, doi: 10.1073/pnas.1910939117.
[226] B. Gauthier, E. Eger, G. Hesselmann, A.-L. Giraud, and A. Kleinschmidt, “Temporal Tuning Properties along the Human Ventral Visual Stream,” *Journal of Neuroscience*, vol. 32, no. 41, pp. 14433–14441, Oct. 2012, doi: 10.1523/JNEUROSCI.2467-12.2012.
[227] U. Hasson, O. Furman, D. Clark, Y. Dudai, and L. Davachi, “Enhanced Intersubject Correlations during Movie Viewing Correlate with Successful Episodic Encoding,” *Neuron*, vol. 57, no. 3, pp. 452–462, Feb. 2008, doi: 10.1016/j.neuron.2007.12.009.
[228] G. Buzsáki, *Rhythms of the Brain*. 2009. doi: 10.1093/acprof:oso/9780195301069.001.0001.
[229] G. Buzsáki, “The Brain from Inside Out,” *The Brain from Inside Out*. 2019. doi: 10.1093/oso/9780190905385.001.0001.
[230] A. V Oppenheim, *Signals, Systems and Interference*. 2016.
[231] K. Wengler, A. T. Goldberg, G. Chahine, and G. Horga, “Distinct hierarchical alterations of intrinsic neural timescales account for different manifestations of psychosis,” *eLife*, 2020, doi: 10.7554/eLife.56151.
[232] C. E. Shannon, “Communication in the Presence of Noise,” *Proceedings of the IRE*, 1949, doi: 10.1109/JRPROC.1949.232969.
[233] M. Golesorkhi, S. Tumati, J. Gomez-Pilar, E. A. Stamatakis, and G. Northoff, “The interplay between information flux and temporal dynamics in infraslow frequencies,” *bioRxiv*, 2020.
[234] M. V. Sanchez-Vives, M. Massimini, and M. Mattia, “Shaping the Default Activity Pattern of the Cortical Network,” *Neuron*, vol. 94, no. 5, pp. 993–1001, Jun. 2017, doi: 10.1016/j.neuron.2017.05.015.
[235] M. V. Sanchez-Vives and M. Mattia, “Slow wave activity as the default mode of the cerebral cortex,” *Archives Italiennes de Biologie*, vol. 152, no. 2–3, pp. 147–155, Jun. 2014, doi: 10.12871/000298292014239.
[236] A. Vanhaudenhuyse *et al.*, “Two distinct neuronal networks mediate the awareness of environment and of self,” *Journal of Cognitive Neuroscience*, 2011, doi: 10.1162/jocn.2010.21488.
[237] G. Deco and M. L. Kringelbach, “Hierarchy of Information Processing in the Brain: A Novel ‘Intrinsic Ignition’ Framework,” *Neuron*. 2017. doi: 10.1016/j.neuron.2017.03.028.
[238] J. Hohwy, “The Self-Evidencing Brain,” *Noûs*, vol. 50, no. 2, pp. 259–285, Jun. 2016, doi: 10.1111/nous.12062.
[239] D. Benrimoh, T. Parr, P. Vincent, R. A. Adams, and K. Friston, “Active Inference and Auditory Hallucinations,” *Computational Psychiatry*, vol. 2, pp. 183–204, Dec. 2018, doi: 10.1162/cpsy_a_00022.
[240] A. Scalabrini, C. Mucci, R. Esposito, S. Damiani, and G. Northoff, “Dissociation as a disorder of integration – On the footsteps of Pierre Janet,” *Progress in Neuro-Psychopharmacology and Biological Psychiatry*, vol. 101, p. 109928, Jul. 2020, doi: 10.1016/j.pnpbp.2020.109928.
[241] G. Northoff, “Anxiety Disorders and the Brain’s Resting State Networks: From Altered Spatiotemporal Synchronization to Psychopathological Symptoms,” in *Advances in Experimental Medicine and Biology*, vol. 1191, Springer, 2020, pp. 71–90. doi: 10.1007/978-981-32-9705-0_5.
[242] G. Northoff, K. E. Sandsten, J. Nordgaard, T. W. Kjaer, and J. Parnas, “The Self and Its Prolonged Intrinsic Neural Timescale in Schizophrenia,” *Schizophrenia Bulletin*, Jul. 2020, doi: 10.1093/schbul/sbaa083.
[243] S. Gallagher and A. Daly, “Dynamical Relations in the Self-Pattern,” *Frontiers in Psychology*, vol. 9, no. MAY, May 2018, doi: 10.3389/fpsyg.2018.00664.
[244] A. K. Seth and M. Tsakiris, “Being a Beast Machine: The Somatic Basis of Selfhood,” *Trends in Cognitive Sciences*, vol. 22, no. 11. Elsevier Ltd, pp. 969–981, Nov. 01, 2018. doi: 10.1016/j.tics.2018.08.008.
[245] A. K. Seth, “Presence, objecthood, and the phenomenology of predictive perception,” *Cognitive Neuroscience*, vol. 6, no. 2–3, pp. 111–117, Jul. 2015, doi: 10.1080/17588928.2015.1026888.

[246] K. J. Friston, R. Rosch, T. Parr, C. Price, and H. Bowman, "Deep temporal models and active inference," *Neuroscience & Biobehavioral Reviews*, vol. 77, pp. 388–402, Jun. 2017, doi: 10.1016/j.neubiorev.2017.04.009.
[247] J. E. Clark, S. Watson, and K. J. Friston, "What is mood? A computational perspective," *Psychological Medicine*, vol. 48, no. 14, pp. 2277–2284, Oct. 2018, doi: 10.1017/S0033291718000430.
[248] X. Gu, P. R. Hof, K. J. Friston, and J. Fan, "Anterior insular cortex and emotional awareness," *Journal of Comparative Neurology*, vol. 521, no. 15, pp. 3371–3388, Oct. 2013, doi: 10.1002/cne.23368.
[249] A. K. Seth and K. J. Friston, "Active interoceptive inference and the emotional brain," *Philosophical Transactions of the Royal Society B: Biological Sciences*, vol. 371, no. 1708, p. 20160007, Nov. 2016, doi: 10.1098/rstb.2016.0007.
[250] R. Smith, R. D. Lane, T. Parr, and K. J. Friston, "Neurocomputational mechanisms underlying emotional awareness: Insights afforded by deep active inference and their potential clinical relevance," *Neuroscience & Biobehavioral Reviews*, vol. 107, pp. 473–491, Dec. 2019, doi: 10.1016/j.neubiorev.2019.09.002.
[251] R. Smith, T. Parr, and K. J. Friston, "Simulating Emotions: An Active Inference Model of Emotional State Inference and Emotion Concept Learning," *Frontiers in Psychology*, vol. 10, Dec. 2019, doi: 10.3389/fpsyg.2019.02844.
[252] G. Northoff, "The brain's spontaneous activity and its psychopathological symptoms – 'Spatiotemporal binding and integration,'" *Progress in Neuro-Psychopharmacology and Biological Psychiatry*, vol. 80, no. Pt B. Elsevier Inc., pp. 81–90, Jan. 03, 2018. doi: 10.1016/j.pnpbp.2017.03.019.
[253] S. Damiani, A. Scalabrini, J. Gomez-Pilar, N. Brondino, and G. Northoff, "Increased scale-free dynamics in salience network in adult high-functioning autism," *NeuroImage: Clinical*, vol. 21, p. 101634, 2019, doi: 10.1016/j.nicl.2018.101634.
[254] M. Spronk *et al.*, "A Whole-Brain and Cross-Diagnostic Perspective on Functional Brain Network Dysfunction," *Cerebral Cortex*, vol. 31, no. 1, pp. 547–561, Jan. 2021, doi: 10.1093/cercor/bhaa242.
[255] B. Voytek and R. T. Knight, "Dynamic Network Communication as a Unifying Neural Basis for Cognition, Development, Aging, and Disease," *Biological Psychiatry*, vol. 77, no. 12, pp. 1089–1097, Jun. 2015, doi: 10.1016/j.biopsych.2015.04.016.
[256] K. Friston, "Active inference and free energy," *Behavioral and Brain Sciences*, vol. 36, no. 3, pp. 212–213, Jun. 2013, doi: 10.1017/S0140525X12002142.
[257] E. D. Fagerholm *et al.*, "Conservation laws by virtue of scale symmetries in neural systems," *PLOS Computational Biology*, vol. 16, no. 5, p. e1007865, May 2020, doi: 10.1371/journal.pcbi.1007865.
[258] J. Bruineberg, A. Chemero, and E. Rietveld, "General ecological information supports engagement with affordances for 'higher' cognition," *Synthese*, vol. 196, no. 12, pp. 5231–5251, Dec. 2019, doi: 10.1007/s11229-018-1716-9.
[259] Y. Yamashita and J. Tani, "Emergence of functional hierarchy in a multiple timescale neural network model: A humanoid robot experiment," *PLoS Computational Biology*, vol. 6, no. 10, Oct. 2008, doi: 10.1371/journal.pcbi.1000220.
[260] M. Choi and J. Tani, "Predictive Coding for Dynamic Visual Processing: Development of Functional Hierarchy in a Multiple Spatiotemporal Scales RNN Model," *Neural Computation*, vol. 30, no. 1, pp. 237–270, Jan. 2018, doi: 10.1162/neco_a_01026.
[261] R. W. Paine and J. Tani, "Motor primitive and sequence self-organization in a hierarchical recurrent neural network," *Neural Networks*, vol. 17, no. 8–9, pp. 1291–1309, Oct. 2004, doi: 10.1016/j.neunet.2004.08.005.
[262] J. Tani, "Model-based learning for mobile robot navigation from the dynamical systems perspective," *IEEE Transactions on Systems, Man, and Cybernetics, Part B (Cybernetics)*, vol. 26, no. 3, pp. 421–436, Jun. 1996, doi: 10.1109/3477.499793.
[263] J. Tani, "On the interactions between top-down anticipation and bottom-up regression," *Frontiers in Neurorobotics*, vol. 1, no. NOV, 2007, doi: 10.3389/neuro.12.002.2007.